LONGITUDINAL POLARIZATION OF THE Λ IN DEEP INELASTIC SCATTERING OF POLARIZED POSITRONS FROM NUCLEONS

BY

GUNAR SCHNELL, M.S.

A Dissertation submitted to the Graduate School

in partial fulfillment of the requirements

for the Degree

Doctor of Philosophy

Subject: Physics

New Mexico State University

Las Cruces, New Mexico

May 1999

" Longitudinal Polarization of the Λ Particle in Deep Inelastic Scattering of Polarized Positrons from Nucleons," a dissertation prepared by Gunar Schnell in partial fulfillment of the requirements for the degree, Doctor of Philosophy, has been approved and accepted by the following:

Timothy J. Pettibone
Dean of the Graduate School

Stephen F. Pate
Chair of the Examining Committee

Date

Committee in charge:

Dr. Stephen F. Pate, Chair

Dr. Matthias Burkardt

Dr. James Pommersheim

Dr. Vladimir M. Shalaev

"Daß ich erkenne, was die Welt

Im Innersten zusammenhält."

(J. W. von Goethe, Faust I)

ACKNOWLEDGMENTS

It seems impossible to me to list all the people I want to thank for their support, their contribution and friendship. Hence, please do not curse me if your name does not explicitly appear here. First of all, I want to thank my parents and my sister for their life-long support. Without them I surely would not be where I am now. Their constant encouragement always helped me on my way through life, their support enabled me to proceed with my education and writing this thesis. I would also like to express my gratitude to my advisor Dr. Stephen Pate. He guided me through my research and always had time for tea and chocolate, making life in the physics department much more enjoyable. Thanks also to the whole nuclear group at NMSU, in particular to Dr. Gary Kyle, who paid me faithfully, and to Dr. Matthias Burkardt, who encouraged me to study nuclear physics in the first place and always had time to answer those tricky theory questions. This work also would not have been possible without my friends, fellow students and colleagues here at NMSU and at DESY, who made my years both at NMSU and at DESY pleasant and enjoyable. I, in particular, appreciated the friendship of Fayez Assaf and Hala El-Khozondar who always had time to share their thoughts and to help me. I want to thank the Λ group, in particular Dr. Pamela Chumney, Mark Sutter and Stefan Bernreuther for many fruitful discussions. Last but not least I want to thank the whole HERMES collaboration which provided me with the opportunity to work in this field.

VITA

November 4, 1971–Born in Schönebeck, GERMANY

1990–Graduated from Erweiterte Oberschule “Otto Grotewohl”, Schönebeck

1992–Vordiplom, Friedrich Schiller Universität Jena

1995–M.S., University of Massachusetts Dartmouth

1999–Ph.D., New Mexico State University

PUBLICATIONS

K. Ackerstaff *et al.* [HERMES Collaboration], “Observation of a coherence length effect in exclusive ρ^0 electroproduction,” Phys. Rev. Lett. **82**, 3025 (1999).

K. Ackerstaff et al. [HERMES Collaboration], “Determination of the deep inelastic contribution to the generalized Gerasimov-Drell-Hearn integral for the proton and neutron,” Phys. Lett. **B444**, 531 (1998).

A. Airapetian et al. [HERMES Collaboration], “Measurement of the proton spin structure function g1(p) with a pure hydrogen target,” Phys. Lett. **B442**, 484 (1998).

K. Ackerstaff et al. [HERMES Collaboration], “The Flavor asymmetry of the light quark sea from semi-inclusive deep inelastic scattering,” Phys. Rev. Lett. **81**, 5519 (1998).

K. Ackerstaff et al. [HERMES Collaboration], “The HERMES spectrometer,” Nucl. Instrum. Meth. **A417**, 230 (1998).

K. Ackerstaff et al. [HERMES Collaboration], “Beam induced nuclear depolarization in a gaseous polarized hydrogen target,” Phys. Rev. Lett. **82**, 1164 (1999).

FIELD OF STUDY

Major Field: Physics

ABSTRACT

LONGITUDINAL POLARIZATION OF THE Λ IN DEEP INELASTIC SCATTERING OF POLARIZED POSITRONS FROM NUCLEONS

BY

GUNAR SCHNELL, M.S.

Doctor of Philosophy in Physics

New Mexico State University

Las Cruces, New Mexico, 1999

Dr. Stephen Pate, Chair

The spin transfer from a polarized quark fragmenting into a Λ is measured using the longitudinally polarized positron beam at HERA scattering off unpolarized nucleons into the HERMES spectrometer. A polarization consistent with zero has been measured in current fragmentation at an average fractional Λ energy of $z = 0.45$. The result is in agreement with predictions based on the assumption of quark helicity conservation in fragmentation and using the naïve parton model or the SU(3) flavor symmetry predictions for the spin structure of the Λ.

CONTENTS

LIST OF TABLES

LIST OF FIGURES

CHAPTER 1

INTRODUCTION

1.1 A Short Journey Through the History of Particle Physics

Simplicity has always been the goal of physicists: Complex phenomena should be derivable from general principles. All the different appearances of matter should go back to simple building blocks – elementary particles. The idea of the world being built of small building blocks is not new. In ancient Greece, Democritus introduced the *atomon*. But in some sense his ideas came too early. It took two millenia in order to really change the picture about the structure of matter. In the beginning of the twentieth century Rutherford, Geiger and Marsden showed [Ruth] that space is mostly made of "nothing." When shooting α particles at a thin gold foil only a few of them were deflected. Most of the α particles went through the foil as if there were nothing in their way and, sometimes, very large deflections were observed, practically bouncing back off the foil. The explanation for this was that most of the charge (and mass) was concentrated in an almost point-like nucleus. Not only did this contradict the then common view of a more or less uniform positive charge distribution with the electrons embedded, it also opened the door to a new field: nuclear and particle physics. However, the "paradise of simplicity" had not been reached. Beside the electron and proton new particles were found or predicted which destroyed the hope for a simple picture. The main problem was the vast number of the so-called strongly interacting hadrons. It took until the sixties to bring order into the "zoo of particles." Gell-Mann and Zweig [GZ] independently proposed an underlying symmetry, SU(3), leading to the known meson and hadron spectra. All hadrons were built of constituents called quarks.[1] Feynman [Feyn] associated partons as the generators for this symmetry which led to the quark-parton-model (QPM). Baryons (mesons) were made up of three (two) quarks from a pool of three different quark flavors: u (up), d (down) and s (strange) which were assumed to be fundamental (elementary) particles. Together with the known family of leptons, which do not interact strongly, they formed the basic set of particles making up the world. In the following years more particles have been discovered leading to a more complete set described in the *Standard Model* (SM).

What is the main idea of the Standard Model? The fundamental constituents of matter are the quarks and leptons which are classified in three generations (see also table 1.1). In addition, there are four fundamental forces: the strong, the

[1] One should mention that originally quarks were only assumed to be abstract objects of the model and not real fundamental constituents. This is true in particular for Gell-Mann who,ironically, later got the Nobel prize for his work.

electro-magnetic, the weak and the gravitational force. The latter plays no role in the studies of nuclear and particle physics due to its rather weak coupling. It will, hence, be ignored in this description. Each of these interactions is described by a field theory where the forces are mediated by gauge bosons.

The best understood interaction is the electro-magnetic interaction described by Quantum-Electrodynamics (QED). The gauge boson is the photon (γ). The weak interaction got its name from the fact that it is far weaker than the electro-magnetic and strong interaction. The gauge bosons are the Z and the W, the first one being electrically neutral and the latter one being charged. The electro-magnetic and weak interactions have been combined to the Glashow-Weinberg-Salam theory of electroweak interactions [GWS].

Table 1.1: Quarks and Leptons in the Standard Model

Charge	1. Generation	2. Generation	3. Generation
$\frac{2}{3}$	u (up)	c (charm)	t (top)
$-\frac{1}{3}$	d (down)	s (strange)	b (bottom)
0	ν_e	ν_μ	ν_τ
-1	e^-	μ^-	τ^-

The strong interaction is described by Quantum Chromodynamics (QCD) based on SU(3). The associated charges are called color, of which there are three. Quarks are color triplets and gluons (the gauge bosons) form the octet representation. All other known particles are color singlets and, therefore, do not experience strong interactions. So far, no single quarks or colored objects have been observed, leading to the notion of confinement. The strong coupling constant is small at small distances (large momentum transfers) but large at large distances (small momentum transfer) explaining asymptotic freedom (quarks can be considered "free" when scattered with high momentum transfer). In that region perturbative methods can be applied for calculations but not at low momentum transfers where the coupling is large.

1.2 Spin physics

In the last twenty years – especially after EMC published its results on the proton spin structure [EMC 88] – high energy spin physics became an ever-growing field of research activities. QCD provides the theoretical framework for understanding polarization effects as long as one deals with perturbative QCD. However, many puzzles are so far still unsolved when going to the non-perturbative regime.

A fundamental relation derived by Bjørken relates the difference between the integral over the proton spin-structure function and the neutron spin-structure function to the weak neutron decay [Bjør]. This sum rule has been experimentally verified, and, nowadays, newer results are used to extract α_s – the strong coupling constant. A less successful prediction for the integrals itself were presented by Ellis and Jaffe [EJ] and its failure to comply with the experimental values led to the so-called "spin crisis":

- Not all the spin of the nucleon is due to the quarks[2]

- The strange sea in the proton/neutron is polarized.

Experiments are now taking data to measure the missing contribution to the nucleon spin coming from gluons.

There are other interesting aspects in spin physics. One example is the large hyperon polarizations observed in hadron-hadron collisions which will be discussed in section 1.3. Another example is the question to what extent parton helicities are preserved in the fragmentation process. The latter will be addressed in this thesis by studying the polarized fragmentation functions and the longitudinal polarization of the Λ hyperon.[3]

1.3 The Λ Particle as a Member of the Hyperon Octet

When Gell-Mann and Zweig proposed an underlying SU(3) symmetry only hadrons were known which were built from the three light quarks u, d, and s. They formed a spin-$\frac{1}{2}$ octet and a spin-$\frac{3}{2}$ decuplet. After the discovery of the c quark, the SU(3) octet and decuplet became part of two SU(4) 20-plets (figure 1.1). The octet takes a unique position since its members are relatively stable baryons. This comes from the fact that they can only decay via weak decays (with the exception of the Σ^0 which decays electro-magnetically into a Λ). The most stable baryon (and also

[2]in fact, the contribution coming from the quarks is almost negligible

[3]as will be seen later polarization and polarized fragmentation are just two sides of the same coin

the lightest one), the proton, has yet to be seen to decay, a decay which would violate the SM since the baryon number is supposed to be conserved and no lighter baryon is known to which the proton could decay. The baryons in this octet are the hyperons and are the subject of many experiments for the following reasons (among others):

- Long lifetimes – relatively easy to study experimentally
- Parity violating decay allows to reconstruct their polarization
- Weak decay amplitudes are related to the spin structure of the hyperons

All three of the above items are of importance for this thesis. The main subject will be the polarization of the Λ produced in Deep Inelastic Scattering (DIS). The long lifetime is necessary to identify the Λ without diluting the signal by too much background. The polarization can be extracted through the parity-violating weak decay which results in an asymmetric decay distribution:

$$\frac{d\sigma}{d\Theta} = \sigma_0(1 + \beta P \cos\Theta), \tag{1.1}$$

where P is the polarization of the decaying hyperon, β is the *weak decay parameter* and Θ the angle between the spin 3-vector and the momentum vector of the spin-$\frac{1}{2}$ daughter particle in the center of momentum (c.m.) frame of the decaying hyperon, i.e., the Λ.

Some of the models predicting the Λ polarization in DIS use the spin structure of the Λ. The connection of the spin structure of the hyperons and the semi-

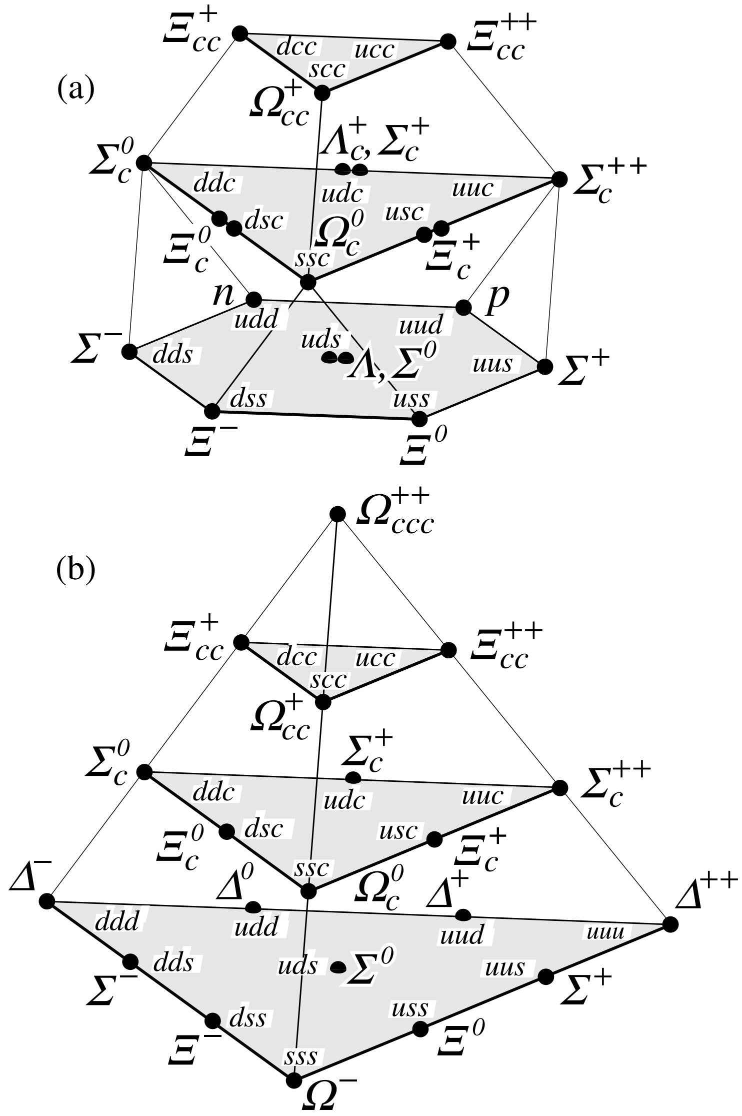

Figure 1.1: The SU(4) multiplets of baryons made of u, d, s and c quarks. (a) The 20-plet of spin-$\frac{1}{2}$ baryons including the hyperon octet (lowest sheet). (b) The 20-plet of spin-$\frac{3}{2}$ baryons. The lowest sheet is the SU(3) decuplet. (taken from [PDG])

leptonic hyperon decay amplitudes will be discussed in Appendix C. It turns out that this approach will give significantly different results then naïvely expected.

The Λ is the lightest of the strange baryons and consists of a u, a d and an s quark. Since its main decay channel is the decay into a pion and a proton, both easy-to-detect particles, and since its decay asymmetry due to its polarization is reasonably high ($\beta = 0.642$) it has been subject of many theses and publications. The polarization of Λ's has been studied extensively in hadron-hadron collisions. Interactions at those processes are, however, hard to describe in a theoretical framework except in a phenomenological way. Nevertheless, the experimental results are very interesting in that the Λ usually is produced polarized. As yet there is no model which is consistent with all the data. More recently, the polarization of Λ's produced at the Z^0 pole in e^+e^- collision has been measured [OPAL, ALEPH]. And last but not least – and subject of this thesis – the polarization of Λ's produced in DIS is under investigation.

In this thesis I will address the formalism of DIS and fragmentation. I will discuss various models of Λ polarization, describe the experimental setup of HERMES which is used to measure the Λ polarization in DIS, report on the analysis done as well as on the result. I finally will discuss implications, especially when combining the HERMES result with results from e^+e^- collisions.

CHAPTER 2

PHYSICS

2.1 Deep Inelastic Scattering

Scattering experiments have been a tool for physicists for a long time. In the early stages of nuclear physics Rutherford [Ruth] bombarded a thin gold foil with α particles to come to the conclusion that atoms are made of mainly space with the mass concentrated at an (almost) point-like nucleus. Nowadays, smaller, more fundamental, particles (i.e., leptons) are used to bombard nucleons in order to study their structure. Structure here not only means spatial structure, i.e., how extended is the nucleon, but also the spin structure, i.e., what contributes to the spin of a nucleon, as it is done at the HERMES experiment [Düren].

In elastic scattering the cross section can be expressed as a function of one variable. In classical mechanics, for instance, the scattering angle merely depends on the impact parameter; in nuclear physics one describes the cross section in terms of the 4-momentum transfer Q. In inelastic scattering, i.e., in DIS where one scatters leptons (with mass m) off nucleons (with mass M) (illustrated in

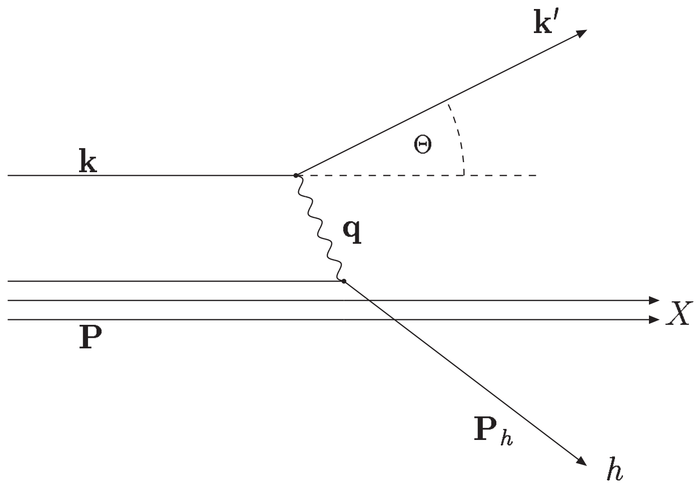

Figure 2.1: Schematic view of a DIS event.

figure 2.1), one also has to consider the energy loss of the scattered particle:

$$\begin{aligned} \mathbf{q}^2 &= (\mathbf{k} - \mathbf{k}')^2 \\ &= 2m^2 + 2(kk' \cos\Theta - EE') \end{aligned} \tag{2.1}$$

In the relativistic limit $(m \ll E)$ $E \cong k$ and thus

$$Q^2 \equiv -\mathbf{q}^2 \tag{2.2}$$

$$\begin{aligned} &\cong 2EE'(\cos\Theta - 1) \\ &\cong 2EE' \sin^2 \frac{\Theta}{2} \end{aligned} \tag{2.3}$$

Hence, in general, one expects the scattering cross section to be a function of two variables (i.e., $\Theta = f(Q^2, E')$).

2.1.1 Elastic Scattering

A special case in scattering theory is the case of elastic scattering. Here, the interacting particles do not change identities but only their kinematics:

$$\mathbf{k}^2 = m^2 = \mathbf{k}'^2 \tag{2.4}$$

$$\mathbf{P}^2 = M^2 = \mathbf{P}'^2 \tag{2.5}$$

One can see readily that now Q^2 and E' are not independent anymore:

$$\begin{aligned} M^2 &= \mathbf{P}'^2 \\ &= (\mathbf{P} + \mathbf{q})^2 \\ &= M^2 - Q^2 + 2\mathbf{P}\cdot\mathbf{q}, \end{aligned} \tag{2.6}$$

$\mathbf{P}\cdot\mathbf{q}$ being a Lorentz invariant, one can calculate it in the target rest frame where $\mathbf{P}$=(M,0,0,0). Hence, Q^2 depends on E' as

$$Q^2 = 2M(E - E'). \tag{2.7}$$

Other useful Lorentz invariant are the photon energy in the target rest frame, ν, the invariant mass of the final hadronic state, W^2, and the Bjørken scaling variable, x:

$$\nu = \frac{\mathbf{P}\cdot\mathbf{q}}{\sqrt{\mathbf{P}^2}} \tag{2.8}$$

$$\stackrel{lab}{=} E - E' \tag{2.9}$$

$$W^2 = \mathbf{P}'^2 \tag{2.10}$$

$$x = \frac{Q^2}{2M\nu}. \qquad (2.11)$$

In elastic scattering, x is equal one (cf., equ. 2.7). The final hadronic mass is equal to the initial hadronic mass (the involved particles stay the same in elastic scattering): $W^2 = M^2$. In inelastic scattering, x gives a measure of the inelasticity of the process and is smaller than one. In that case the final hadronic mass is larger than the initial mass.[1] In experiment, the elastic peak is not a sharp peak at $x = 1$ but the peak has a finite width. But more interestingly, if one, for instance, scatters off a ^{4}He nucleus one observes the following behavior: At increasing Q^2 a second peak emerges at around $x = 0.25$. Now, what one sees is not elastic scattering from the ^{4}He nucleus but rather from its constituents (nucleons) which have a mass of about 1/4 of the ^{4}He nucleus mass:

$$1 = x_{nucleon} = \frac{Q^2}{2m_n\nu} \qquad (2.12)$$

for elastic scattering, hence

$$x_{He} = \frac{Q^2}{2 \cdot 4m_n\nu} = \frac{1}{4}x_{nucleon} = \frac{1}{4} \qquad (2.13)$$

This has been seen already in the 1950s. Later, a similar effect has been observed when scattering off protons – a peak around $x = \frac{1}{3}$ emerged which was one more hint for the existence of partons.

[1]From equ. 2.10, using $\mathbf{P}'=\mathbf{P}+\mathbf{q}$ and equ. (2.11), one obtains $W^2 = M^2 + Q^2(\frac{1}{x} - 1)$, which, for $x < 1$, gives $W^2 > M^2$.

2.1.2 Electro-magnetic Scattering

Rutherford derived a relation between the differential cross section and the scattering angle for α particles scattering off Au nuclei:

$$\left(\frac{d\sigma}{d\Omega}\right) = \frac{\alpha^2}{4E^2 \sin^4 \frac{\Theta}{2}} \tag{2.14}$$

This is a valid formula for the case of an infinitely heavy target and spin-less particles. If one includes the target's recoil and the spin of the scattered lepton one obtains:

$$\left(\frac{d\sigma}{d\Omega}\right)_{Mott} = \frac{\alpha^2}{4E^2 \sin^4 \frac{\Theta}{2}} \frac{E'}{E} \cos^2 \frac{\Theta}{2} \tag{2.15}$$

which is valid for scattering of leptons from point-like spin-less particles. Including the spin of the target particle one finally arrives at an expression valid for scattering Dirac particles from Dirac particles (i.e., $e^-\mu^- \longrightarrow e^-\mu^-$):

$$\begin{aligned} \left(\frac{d\sigma}{d\Omega}\right) &= \frac{\alpha^2}{4E^2 \sin^4 \frac{\Theta}{2}} \frac{E'}{E} \cos^2 \frac{\Theta}{2} \left(1 + \frac{Q^2}{2M^2} \tan^2 \frac{\Theta}{2}\right) \\ &= \left(\frac{d\sigma}{d\Omega}\right)_{Mott} \left(1 + \frac{Q^2}{2M^2} \tan^2 \frac{\Theta}{2}\right) \end{aligned} \tag{2.16}$$

2.1.3 Unpolarized Structure Functions

As noted before (2.16) is only valid for scattering from point-like particles. For extended objects, i.e., nucleons, (2.16) is not applicable. However, the differential cross section can be written in terms of polarized and unpolarized structure functions. For the unpolarized case[2], the scattering cross section for charged leptons can be expressed, after consideration of Lorentz invariance, parity and current conservation, in terms of only two structure functions. The cross section can be written as

$$\frac{d\sigma}{dE'd\Omega} = \left(\frac{d\sigma}{d\Omega}\right)_{Mott} \left(W_2(\nu, Q^2) + 2W_1(\nu, Q^2)\tan^2\frac{\Theta}{2}\right). \tag{2.17}$$

Compared with (2.16) (before integrating it over E')

$$\frac{d\sigma}{dE'd\Omega} = \left(\frac{d\sigma}{d\Omega}\right)_{Mott} \left(1 + \frac{Q^2}{2M^2}\tan^2\frac{\Theta}{2}\right)\delta\left(\nu - \frac{Q^2}{2M}\right) \tag{2.18}$$

one finds the structure functions for a Dirac particle:

$$2W_1 = \frac{Q^2}{2M^2}\delta\left(\nu - \frac{Q^2}{2M}\right) \tag{2.19}$$

$$W_2 = \delta\left(\nu - \frac{Q^2}{2M}\right), \tag{2.20}$$

Using the relation $\delta(x/\nu) = \nu\delta(x)$ one can rewrite above expressions as

$$2MW_1 = \frac{Q^2}{2M\nu}\delta\left(1 - \frac{Q^2}{2M\nu}\right) \tag{2.21}$$

$$\nu W_2 = \delta\left(1 - \frac{Q^2}{2M\nu}\right), \tag{2.22}$$

Apparently, the right-hand-sides only depend on $x = \frac{Q^2}{2M\nu}$, which is also known as scaling, emphasizing the elastic character of this process. In the Bjørken limit

[2]As will become clear later (section 2.1.4), in order to measure the polarized structure functions, one needs to have both a polarized target and a polarized lepton beam. All other cases involve only the unpolarized structure functions.

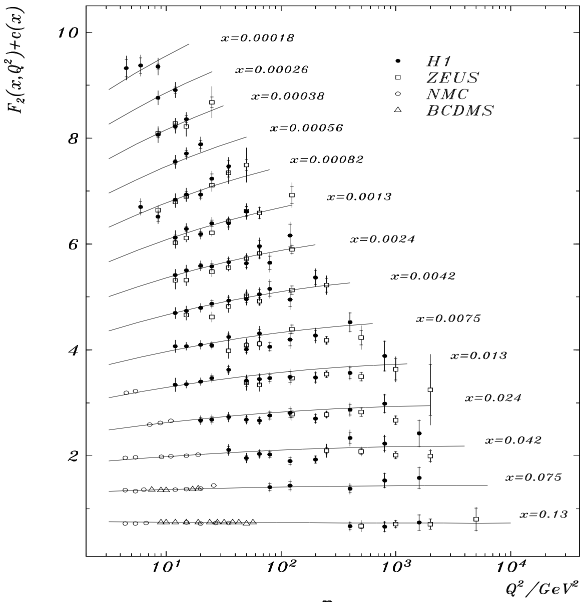

Figure 2.2: The structure function F_2^p for the proton as a function of Q^2 for different values of x. The F_2^p's are plotted adding a constant term $c(x) = 0.6(i_x - 0.4)$ to F_2^p for display purposes where i_x is the x-bin number starting at $i_x = 1$ for $x = 0.13$. The curves represent a phenomenological fit to the data. (Taken from [H1]). The scaling of F_2^p is apparent for large x, at lower x higher order QCD corrections introduce a more significant Q^2 dependence

$Q^2 \to \infty$, keeping x fixed, $W_{1/2}$ go over to the structure functions $F_{1/2}$:

$$\lim_{Q^2 \to \infty,\ x \text{ fixed}} MW_1(\nu, Q^2) = F_1(x) \tag{2.23}$$

$$\lim_{Q^2 \to \infty,\ x \text{ fixed}} \nu W_2(\nu, Q^2) = F_2(x) \tag{2.24}$$

Interesting enough, scaling has also been observed for scattering from protons (fig. 2.2). This suggests a substructure of point-like partons. The structure functions $F_{1/2}$ have simple interpretations in the naïve parton model which will be discussed in section 2.2.

2.1.4 Polarized Structure Functions

Scattering experiments have not only been done using unpolarized targets, where one can average over helicity states, but also scattering of polarized leptons from polarized targets has been examined. In order to measure the polarized structure functions it is necessary to have both the target and the beam polarized, though this is not true in general when studying spin physics. In the very general case, the lepton-nucleon scattering cross-section can be calculated by contracting the leptonic tensor $L^{\mu\nu}$ with the hadronic tensor $W^{\mu\nu}$:[3]

$$\frac{d^2\sigma}{dxdQ^2} = \frac{e^4}{8\pi Q^4}\frac{y^2}{Q^2}L^{\mu\nu}W_{\mu\nu}. \tag{2.25}$$

The leptonic tensor can be calculated exactly in QED. However, the hadronic tensor is only known in its general structure, containing the structure functions[4] F_1, F_2, G_1 and G_2. All the spin dependence is carried by the antisymmetric parts of $L^{\mu\nu}$ and $W^{\mu\nu}$. Only the contraction of either the symmetric parts or the antisymmetric parts will lead to a non-vanishing contribution to the cross section. Hence, only by requiring both the target and the beam to be polarized, one can get access to the spin-dependent (polarized) structure functions. This has been exploited in many (more or less) recent experiments [EMC 88, E142, E143, E154, HER 97, HER 98a, SMC]. Contracting the symmetric parts will result in the

[3] $L^{\mu\nu}$ and $W^{\mu\nu}$, which are not of interest in this thesis, can be found, *f.i.*, in [AEL].

[4] in case of ν scattering, or in general in the case of a weak current, there will be a third spin independent structure function F_3.

unpolarized cross section[5]

$$\frac{d^2\sigma}{d\Omega dE'} = \left(\frac{d\sigma}{d\Omega}\right)_{Mott} \left(\frac{2}{M}\tan^2\frac{\Theta}{2}F_1(x,Q^2) + \frac{F_2(x,Q^2)}{\nu}\right). \tag{2.26}$$

In the case of longitudinally polarized beam and target the spin dependent part of the cross-section can be written as [Bass]

$$\frac{d^2\Delta\sigma}{d\Omega dE'} = \frac{4\alpha^2}{Q^2\nu}\frac{E'}{E}\left(g_1(x,Q^2)(E+E'\cos\Theta) - 2xMg_2(x,Q^2)\right). \tag{2.27}$$

where $\Delta\sigma$ stands for the difference in the cross sections for the case of the target being polarized parallel to the beam and anti-parallel:

$$\Delta\sigma = \sigma\upuparrows - \sigma\updownarrow. \tag{2.28}$$

Whereas the unpolarized structure functions have a simple interpretation in the naïve QPM (see 2.2), the polarized structure functions do not always live up to this expectation (leading e.g., to the "Spin Crisis" mentioned in sections 1.2 and 2.4). At the moment there are three main approaches, of varying level of sophistication, to the theoretical treatment of structure functions [AEL]:

- The naïve Quark-Parton Model (QPM) – the nucleon is viewed as an ensemble of free, parallel moving quarks. The structure functions are obtained as the sum of parton distribution functions which give the probability to find a parton (in a certain helicity state in case of polarized scattering) with a

[5] Q^2-dependence of $F_{1/2}$ is included here to account for the weak scaling violation observed and predicted by QCD (see also section 2.3).

momentum fraction x of the nucleon's momentum.

- The QCD Improved Parton Model – Q^2 evolution of the structure functions is controlled by QCD-based splitting functions [AP].
- Field Theoretic Models – predictions are done starting from general principles. The problem is that a full treatment from general principles is not possible. One has to sub-divide the calculation into a hard part which can be treated with perturbative methods and a soft part where one has to make some (reasonable) assumption in producing a model.

The first two points will be discussed later in this thesis.

2.1.5 Semi-Inclusive DIS

Up to now we only concentrated on the scattered lepton, i.e., all possible final hadronic states were included. The opposite to the inclusive case is the exclusive case where only certain final states are considered. This is rather hard to realize if no 4π detector is available since all final particles have to be detected. One can, however, also look at specific classes of final states, e.g., states which have a Λ present. Then, one speaks about semi-inclusive DIS.

It is obvious that the number of observables increases. Hence, the information about the structure of the target available also increases. Looking at certain particles formed in the jet of the struck parton might give hints about the nature of the struck parton. It is common to look for $\pi^{\pm}$ in order to probe the u and d

quark content of the nucleon assuming that the outgoing π tags the struck quark. Furthermore, from studying strange mesons like K's one might get insight to the strange sea of the nucleon.

Figure 2.1 presents a basic picture of a semi-inclusive measurement. The struck quark has to pick up either an anti-quark or at least two more quarks in order to form a color singlet final hadronic state. It is assumed that this process, *fragmentation*, is independent from the scattering process itself, i.e., the scattering (emission and absorption of a virtual photon) and fragmentation (breakup of the color field between struck quark and target remnant and forming of final hadronic states) are independent from each other; they *factorize*.

The struck quark carries most of the energy of the photon and the fractional energy of the resulting hadron h is denoted by z

$$z = \frac{E_h}{\nu} \tag{2.29}$$

which, in fragmentation, holds a similar meaning to x in the nucleon structure. The fragmentation functions $\hat{q}^h(z, Q^2)$ are the probabilities for a quark q to fragment into a hadron h with energy fraction z.

A summary of variables used in inclusive and semi-inclusive DIS is given in table 2.1.

Table 2.1: Definition of inclusive and semi-inclusive variables. All vectors are measured in the lab frame, definitions are given in terms of quantities in the lab frame

Variable	Definition	Name
$\mathbf{k}$	$(E, \vec{k})$	4-Momentum of incoming lepton
$\mathbf{k}'$	$(E', \vec{k}')$	4-Momentum of outgoing lepton
$\mathbf{P}$	$(M, 0, 0, 0)$	4-Momentum of target nucleon
$\mathbf{P}_h$	$(E_h, \vec{p}_h)$	4-Momentum of outgoing hadron
Θ	$\sphericalangle(\vec{k}', \vec{k})$	Scattering angle of lepton
$\mathbf{q}$	$\mathbf{k}$-$\mathbf{k}'$	4-Momentum of virtual photon
Q^2	$-\mathbf{q}^2 \overset{lab}{\cong} 4EE' \sin^2 \frac{\Theta}{2}$	negative squared 4-momentum transfer
ν	$\frac{\mathbf{P}\cdot\mathbf{q}}{\sqrt{\mathbf{P}^2}} \overset{lab}{=} E - E'$	Energy transfer
y	$\frac{\mathbf{P}\cdot\mathbf{q}}{\mathbf{P}\cdot\mathbf{k}} \overset{lab}{=} \frac{\nu}{E}$	Relative Energy transfer
x	$\frac{Q^2}{2\mathbf{P}\cdot\mathbf{q}} \overset{lab}{=} \frac{Q^2}{2M\nu}$	Bjørken scaling variable
W^2	$M^2 + Q^2(\frac{1}{x} - 1)$	Invariant mass of final hadronic state
$p_{\vert\vert}$	$\frac{\vec{p}_h\cdot\vec{q}}{q}$	Parallel momentum of hadron
x_f	$\frac{p_{\vert\vert}}{p_{\vert\vert}^{max}}$	Feynman's scaling variable
z	$\frac{\mathbf{P}\cdot\mathbf{P}_h}{\mathbf{P}\cdot\mathbf{q}} \overset{lab}{=} \frac{E_h}{\nu}$	Fractional hadron energy

2.2 Quark Parton Model

As mentioned before many observed effects can be described by introducing a partonic sub-structure to the nucleons. Already the baryon and meson spectra evoked the idea of the nucleon being made up of three quarks and mesons being made up of a quark and an anti-quark [GZ]. Furthermore, scaling effects in the structure functions of the proton suggested that leptons scattering from nucleons inelastically are actually scattering from point-like constituents (partons [Feyn]) in an elastic way. For high momentum transfer the photon "sees" a "free" parton (at least for the time of interaction). Making the connection between Gell-Mann's quarks and Feynman's partons led to the naïve quark parton model (QPM).

Let us consider a frame where the transverse components of all the partons are negligible and, thus, the momentum of a parton is parallel to the momentum of the nucleon (*infinite momentum frame*). Let ξ be the momentum fraction of the nucleon carried by the struck parton/quark: $\mathbf{p}=\xi\mathbf{P}$. After the absorption of the photon the quark's 4-momentum squared will be:

$$\begin{aligned} m_q^2 &= (\xi\mathbf{P}+\mathbf{q})^2 \\ &= \xi^2\mathbf{P}^2 + 2\xi\mathbf{P}\cdot\mathbf{q} + \mathbf{q}^2 \\ &\approx 2\xi\mathbf{P}\cdot\mathbf{q} - Q^2 \end{aligned} \tag{2.30}$$

and therefore

$$\xi = \frac{Q^2 + m_q^2}{2\mathbf{P}\cdot\mathbf{q}}. \tag{2.31}$$

For the light quarks d, u and s one can certainly neglect the quark mass and it turns out that Bjørken's scaling variable can be interpreted as the momentum fraction of the nucleon carried by the quark in the infinite momentum frame:

$$\xi \approx \frac{Q^2}{2\mathbf{P}\cdot\mathbf{q}} \equiv x. \tag{2.32}$$

In the QPM scattering from the proton is just the incoherent sum of scattering from the quarks in the proton. The quarks can be considered *asymptotically free*; there is no further interaction between the quarks. Furthermore, quarks are point-like spin-1/2 particles. The structure functions can be written in terms of the quark distribution functions $q(x)$ which are the probabilities to find a quark q with the momentum fraction x. For the unpolarized case one has:

$$F_1(x) = \frac{1}{2}\sum_q e_q^2 q(x) \tag{2.33}$$

$$F_2(x) = \sum_q e_q^2 x q(x). \tag{2.34}$$

From (2.33) and (2.34) one can see that F_1 and F_2 are not independent but are related to each other through the *Callan-Gross-Relation*[6]

$$F_2(x) = 2xF_1(x) \tag{2.35}$$

which has been verified well in experiment.

The spin-dependent structure functions can also be expressed as sums over the different quark distribution functions. Contrary to the unpolarized case the

[6]see also Appendix A

helicities of the quarks have to be taken into account. Doing so, the explicit expressions for the polarized structure functions can be written as

$$g_1(x) = \frac{1}{2}\sum_q e_q^2 \Delta q(x) \qquad (2.36)$$

$$g_2(x) = 0, \qquad (2.37)$$

where Δq denotes the difference of the distribution functions with quark spin parallel and anti-parallel to the nucleon spin. g_2 vanishes in the naïve QPM since it is either related to the transverse momentum of the quarks or interaction terms, both of which are neglected in the naïve QPM.

2.3 Nucleon Structure in QCD

The simple picture of nucleons made of three quarks can be further extended using QCD. The introduction of QCD became necessary when conflicts occurred describing the structure of e.g., the $\Delta^{++} = u\uparrow u\uparrow u\uparrow$ which is symmetric in space, flavor and spin. This clearly violates the Pauli principle, making necessary a new quantum number: *color*. QCD was born. With the introduction of QCD, every quark became also carrier of a color charge of which one needs at least three. Moreover, forces were mediated through a gauge boson, the *gluon*, which itself carries color. QCD also explains the weak scaling violation of the structure functions by introducing a logarithmic Q^2 dependence through the *Altarelli-Parisi-Evolution-Equations*[7] [AP]. The main idea here is that the virtual photon not only "sees"

[7] also known as DGLAP (Dokshitzer-Gribov-Lipatov-Altarelli-Parisi) formalism

the *constituent* or *valence* quarks but also quarks from the $q\bar{q}$ *sea*, and that the measured momentum fraction x is actually not the true momentum fraction due to emission or absorption of a gluon around the time of interaction. Evidence for gluons can be found when looking at the total momentum fraction carried by the quarks. In the naïve QPM all the momentum of the proton is carried by the quarks:

$$\sum_q \int_0^1 dx\, x q(x) \overset{QPM}{=} 1. \tag{2.38}$$

However, experiments show that only about 50% of the proton's momentum is carried by quarks and the remaining part can be accounted for by the gluons. For a short period of time those gluons can split into a $q\bar{q}$-pair which naturally only carry a small fraction of the proton's momentum (small x). The probability to see such a quark increases with Q^2 of the virtual photon. This explains a part of the Q^2 dependence of the structure function. As already mentioned before, a second contribution comes from the fact that a quark with momentum fraction ξ can emit a gluon with momentum fraction ζ changing its "true" momentum fraction from ξ to $\xi - \zeta$ (*gluon radiation*). Again, the probability to see this effect increases with Q^2.

2.4 Spin Structure of Nucleons

With the introduction of the parton model not only the wide spectrum of mesons and baryons could be explained but also other spin effects, i.e., the magnetic moments of nucleons, leading to predictions not only of the parton structure but also of the spin structure. In the non-relativistic parton model the spin wave function of the proton can be written as (cf., Appendix B)

$$\begin{aligned}
\Phi &= \frac{1}{\sqrt{18}}(2u\uparrow u\uparrow d\downarrow + 2d\downarrow u\uparrow u\uparrow + 2u\uparrow d\downarrow u\uparrow \\
& -u\downarrow d\uparrow u\uparrow - u\uparrow u\downarrow d\uparrow - u\downarrow u\uparrow d\uparrow \\
& -d\uparrow u\downarrow u\uparrow - u\uparrow d\uparrow u\downarrow - d\uparrow u\uparrow u\downarrow). \qquad (2.39)
\end{aligned}$$

It explains quite well some static properties of nucleons, e.g., the ratio of the magnetic moments of the proton and the neutron

$$\mu = \mu_u + \mu_d = \mu_u \sigma_u + \mu_d \sigma_d \qquad (2.40)$$

where

$$\mu_q = \frac{e_q h}{2m_q} \qquad (2.41)$$

thus,

$$\begin{aligned}
\mu_p &= <\Phi_p|\mu|\Phi_p> \\
&= \frac{4}{3}\mu_u - \frac{1}{3}\mu_d \\
&= \frac{eh}{2m} \qquad (2.42) \\
\mu_n &= <\Phi_n|\mu|\Phi_n> \\
&= \frac{4}{3}\mu_d - \frac{1}{3}\mu_u \\
&= -\frac{2}{3}\frac{eh}{2m} \qquad (2.43)
\end{aligned}$$

where the quark masses are assumed to be equal ($m_u = m_d = m$), resulting in

$$\frac{\mu_n}{\mu_p} = -\frac{2}{3}. \tag{2.44}$$

However, it fails to predict the right value for the quark polarizations:

$$\begin{aligned}
\Delta u &= u\uparrow - u\downarrow = <\Phi_p|\sigma_u|\Phi_p> & (2.45)\\
&= \frac{4}{3} & (2.46)\\
\Delta d &= d\uparrow - d\downarrow = <\Phi_p|\sigma_d|\Phi_p> & (2.47)\\
&= -\frac{1}{3} & (2.48)
\end{aligned}$$

which agree with the sign of the measured values but not with the values themselves (cf., table 2.2).

When EMC [EMC 88] published its results for the proton's spin structure function g_1^p it became clear that the naïve QPM was not sufficient to describe the spin structure of the proton. Other experiments followed [E142, E143, E154, HER 97, HER 98a, SMC] verifying the then so-called "Spin Crisis." Table 2.2

Table 2.2: Polarized quark distributions of the proton (measured values are at $Q^2 = 10.7 GeV^2$ [Che 96])

Δu		Δd		Δs	
naïve QPM	measured	naïve QPM	measured	naïve QPM	measured
$\frac{4}{3}$	0.77 ± 0.06	$-\frac{1}{3}$	-0.49 ± 0.06	0	-0.15 ± 0.06

summarizes the latest measurements of the quark polarizations for the proton, including the prediction from the naïve QPM.

Facing the dilemma of the quarks not carrying all the nucleon's spin ($\Delta\Sigma = \Delta u + \Delta d + \Delta s \neq 1$) one has to look for other contributions. Gluons have to be considered as well as angular momentum of the quarks and gluons. The total spin of the proton can be written as a sum of all the three contributions:

$$S_z^P = \frac{1}{2}\Delta\Sigma + \Delta G + L_z = \frac{1}{2}. \tag{2.49}$$

A lot of effort is currently dedicated to experiments promising to measure ΔG. However, this will not be the focus of this thesis.

In the same way the naïve QPM fails for the prediction of the polarized quark distributions in the proton it probably fails for the Λ as well. Thus, it is unlikely that the prediction of the Λ spin being entirely due to its s quark actually holds. In contrary, using the present nucleon data and applying SU(3) (cf., Appendix C) will result in a contribution from u and d quarks as well (table 2.3).

Table 2.3: Polarized quark distributions of the Λ (predictions by the QPM and by Burkardt and Jaffe [BJ] applying SU(3) to present nucleon data)

Δu		Δd		Δs	
naïve QPM	BJ	naïve QPM	BJ	naïve QPM	BJ
0	-0.23 ± 0.06	0	-0.23 ± 0.06	1	0.58 ± 0.07

2.5 Fragmentation

It is difficult if not impossible at the moment to derive parton distribution functions from general principles in QCD. The same holds for fragmentation functions; even more, it is hard to tackle the entire problem from mere theoretical grounds, considering the fact that free quarks fragmenting into hadrons is a notion hostile to confinement. A main problem arising is that perturbative methods can not be applied since the coupling constant becomes too large. The subject of fragmentation is, nevertheless, often studied both in experiment, where a large amount of data is available from e^+e^- collision, and in theory, where different models have been proposed (though they are seldom able to describe the whole range of experimental results). Despite the fundamental problems encountered in the calculation of fragmentation functions there exists a theoretical framework which can be used in most descriptions. Perturbative QCD supports the idea of factorization, the ability to separate the hard scattering process (which can be treated with perturbative methods) from the fragmentation process. For the fragmentation process itself there are models which will be discussed in more detail later on. Most of them make use of Monte Carlo techniques. Similar to the case of parton distribution functions, fragmentation functions are subject to Q^2 evolution described by the DGLAP formalism and exhibit scaling behavior.

The "cleanest" process from which one can extract fragmentation functions is e^+e^- collision. Here, the underlying $e^+e^- \to q\bar{q}$ scattering cross section can be calculated in electro-weak theory. The probability of producing a certain quark flavor is thus calculable in contrast to the case of DIS where one needs to know the parton distribution functions. In the particular case of polarized fragmentation functions this is a big advantage since quarks produced at the Z^0 pole are naturally strongly polarized[8] and in DIS the polarized parton distribution functions are so far not too well known, hence flavor tagging in polarized DIS is much more difficult than in e^+e^- collision.

Symbolically, one can write down the cross section for a certain semi-inclusive process like $e^+ + e^- \to \Lambda + X$ as a convolution of the sub-processes:

$$\sigma = \text{annihilation} \otimes \text{quark production} \otimes \text{fragmentation} \tag{2.50}$$

or, concentrating only on the fragmentation part

$$\frac{d\sigma}{dz} = \sigma_0 \sum_q e_q^2 \hat{q}^\Lambda(z, Q^2), \tag{2.51}$$

where all the calculable quantities are buried in σ_0[9]. Hence, the extraction of the fragmentation functions $\hat{q}^\Lambda(z, Q^2)$ is relatively straight-forward.

If one, in contrast, looks at DIS (i.e., $e + p \to e + \Lambda + X$) one has to convolute the parton distributions as well:

$$\sigma = \text{pdf} \otimes \text{hard scatter} \otimes \text{fragmentation} \tag{2.52}$$

[8]cf., table 2.4

[9]Strictly speaking this is only true if the leptons annihilate into a photon. In case of the weak coupling the charges e_q are not the electric charges anymore.

resulting in a sum over both the parton distribution functions and the fragmentation functions:

$$\frac{d\sigma}{dzdx} = \sigma_0 \sum_q e_q^2 q^p(x,Q^2)\hat{q}^\Lambda(z,Q^2). \tag{2.53}$$

Obviously, this makes it harder to extract the fragmentation functions.

Before discussing some (phenomenological) models it should be emphasized that the fragmentation function $\hat{q}^h$ is the probability of a quark q to fragment into a hadron h. It is not necessary for the quark to directly form hadron h (which would be anyway hard to measure). All strong processes which lead to hadron h are included in the fragmentation functions. As an example consider the case of an s quark fragmenting into a Λ: The s quark can "pick up" a u quark and a d quark forming a uds Λ. However, it can also first form a hyperon resonance (i.e., a Σ^*), decaying strongly into a Λ. In contrast to this, weak or electro-magnetic decays are not included, thus the reaction $\Sigma^0 \to \gamma\Lambda$ does not formally contribute to the Λ fragmentation but often is included in the measured Λ fragmentation functions[10].

Furthermore, it should be noted that one usually distinguishes polarized and unpolarized fragmentation functions. If one defines $\hat{q}^h_{\uparrow\uparrow}$ to be the probability for a quark q with given helicity to fragment into a hadron h with the same helicity, and, vice versa, if one defines $\hat{q}^h_{\uparrow\downarrow}$ to be the probability to produce a hadron with

[10] As pointed out by [BJ] Λ's produced by a decaying Σ^0 can be vetoed when looking at prompt photons. Unfortunately, this is not possible at HERMES due to its limited acceptance and the insufficient energy resolution of the electro-magnetic calorimeter at low energies.

opposite helicity, then the polarized fragmentation function can be written as

$$\Delta \hat{q}^h = \hat{q}^h_{\uparrow\uparrow} - \hat{q}^h_{\uparrow\downarrow}. \tag{2.54}$$

The unpolarized fragmentation function will just be

$$\hat{q}^h = \hat{q}^h_{\uparrow\uparrow} + \hat{q}^h_{\uparrow\downarrow}. \tag{2.55}$$

Thus, the polarized fragmentation functions are constraint by the unpolarized fragmentation functions:

$$|\Delta \hat{q}^h| \leq \hat{q}^h. \tag{2.56}$$

2.5.1 General Fragmentation Models

Currently one can classify three main groups of fragmentation or hadronization models: Independent fragmentation (IF), string fragmentation and cluster fragmentation (CF). The independent fragmentation model developed by Field and Feynman [FF] was the first widely used phenomenological fragmentation model. It was not intended to present a realistic picture of hadronization, but rather, to parameterize the available data on jet production. The model is based on the assumption that all partons hadronize independently. The calculation is a recursive process where the leading quark q_0 picks up an anti-quark $\bar{q}_1$ from a $q\bar{q}$ pair leaving behind the quark q_1 with an energy $(1 - z_0)$ Here, z_0 is the energy of the primary meson. The left-over quark q_1 will, again, pick up an anti-quark $\bar{q}_2$ leaving behind a quark q_2 with energy $(1 - z_0 - z_1)$ etc.. This iterative process continues until a certain cut-off energy is reached. Both the energy fraction z_i and the transverse momentum are chosen from probability functions which can be adjusted to fit the data. The energy distribution function $f(z)$ allows scaling and the transversity is based on a Gaussian distribution.

Although successful in describing the initial data the IF model has many weak spots. From a theoretical point of view one problem is that it is not invariant under Lorentz transformations. It also fails to describe newer data and is rather unsuitable for baryon production.

The best-known model of string fragmentation is the LUND string model of hadronization [LUND]. It is based on the QCD prediction of confinement. The force between quarks and anti-quarks[11] is contained in a narrow flux tube or string. For low (transverse) momentum, quarks just oscillate around a common center due to the string. When the energy is high enough the string can break by creating quark-antiquark pairs (or diquark-antidiquark pairs) at the position where the string breaks. One interesting feature (which actually increases the baryon production rate) is the so-called "popcorn" mechanism: When the string breaks one does not have to create color singlets right away. It could also happen that the color of the produced quark-antiquark pair does not match the color of the initial quarks – the color indices can not be saturated. Hence there will still be a string which will break forming more quark-antiquark pairs; those pairs

[11] one should better say color and anti-color, i.e., in the case of the struck quark in DIS and the remnant nucleon.

will continue to "pop out" from the vacuum. Since diquark-antidiquark pair production is suppressed due to the higher mass of diquarks compared to quarks, baryon production is suppressed outside the "popcorn" mechanism (though not prohibited). This leads to the above-mentioned enhancement of baryon production when including the "popcorn" mechanism. It should also be noted that production of heavy quarks is generally suppressed. Also the probability to create an $s\bar{s}$ pair is suppressed in the LUND model compared to the production of $u\bar{u}$ and $d\bar{d}$ pairs[12]:

$$u\bar{u} : d\bar{d} : s\bar{s} = 1 : 1 : 0.3 \tag{2.57}$$

Those flavor production ratios are parameters going into the model and can be changed to accommodate measured cross-sections. The same is true for the relative strength of the "popcorn" mechanism and other parameters.

Although the LUND model uses an iterative mechanism as it is the case in IF, it features (among others) one important difference: The treatment is Lorentz invariant which also makes the ordering of the produced hadrons irrelevant – the fastest hadrons in one frame are not necessarily the fastest hadrons in a different frame. The LUND model has now become a standard model used for most Monte Carlo models of fragmentation.

The cluster model takes a completely different way. It uses a perturbative QCD prediction to generate highly virtual colorless clusters which are then allowed

[12]This indicates SU(3) flavor symmetry breaking in fragmentation.

to decay to hadrons. These decays are based on phase space considerations or on a parameterization of the low energy particle production data. Practically, hadronization is achieved by first allowing the primary quarks to radiate gluons which radiate more quarks and gluons according to perturbative QCD. After the invariant mass of the $q\bar{q}$ system reaches a certain cut off scale the partons are "pre-confined" into clusters. Heavy quarks usually already decay weakly within the cluster before the cluster decays into light hadrons. The beauty of this model is that it does not need many parameters as in the other models. Only the QCD scale parameter $\Lambda_{\rm QCD}$, the parton masses and the maximal cluster mass are adjustable. One criticism of CF, however, is the use of perturbative QCD at relatively low momentum transfer, where, strictly speaking, it is not anymore applicable. The CF model is incorporated into the HERWIG [HERWIG] Monte Carlo generator.

2.5.2 Polarized Λ Fragmentation

As mentioned in the previous section there is currently no way known to calculate fragmentation functions. This is the same dilemma as encountered in the case of structure functions. In fact, the formalisms in both cases are very similar. The Λ fragmentation functions are not an exception to this. Hence, all the above mentioned is still true. There exist, however, a few models[13] explicitly dealing with the polarized Λ fragmentation functions.[14]

[13] I will not discuss polarized Λ production in hadron collisions which is a vast field but hard to include in this work. (see also footnote 26)

[14] The formalism involved usually could also be applied to other particles besides the Λ.

Table 2.4: Polarization of quarks created in e^+e^- collision at the Z^0-pole

Quark Flavor	Quark Polarization
d	-93.5%
u	-66.4%
s	-93.5%

In principle, the polarized quark fragmentation functions could be extracted from looking at the helicity asymmetry of Λ's produced in e^+e^- collisions. The Λ helicity asymmetry involves different linear combinations of the polarized fragmentation functions. For quarks produced via the process $e^+e^- \to \gamma \to q\bar{q}$ one needs at least one of the lepton beams to be polarized. For quarks produced at the Z^0-pole this is not anymore true since those quarks are naturally polarized through the parity violating $Z^0 q\bar{q}$ coupling (table 2.4). A more detailed discussion can be found in [BJ]. Additionally, one can include data from DIS which, once again, will provide a further linear combination of the polarized fragmentation functions.

Formally, there are 6 quarks and 6 anti-quarks leading to 12 quark fragmentation functions for the Λ. Isospin symmetry reduces this number to 10. If one neglects contributions from heavy quark flavors (c, b and t) one ends up with 4 independent polarized fragmentation functions[15]:

$$\begin{aligned}
\Delta\hat{u}^{\Lambda}(z) &= \Delta\hat{d}^{\Lambda}(z) \\
\Delta\hat{\bar{u}}^{\Lambda}(z) &= \Delta\hat{\bar{d}}^{\Lambda}(z) \\
&\Delta\hat{s}^{\Lambda}(z) \\
&\Delta\hat{\bar{s}}^{\Lambda}(z)
\end{aligned}$$

In most cases one can even neglect the unfavored fragmentation functions, i.e., fragmentation functions of quarks which are not valence quarks in the Λ, since they are usually suppressed. Then, only 2 independent fragmentation functions, $\Delta\hat{u}^{\Lambda}(z)$ and $\Delta\hat{s}^{\Lambda}(z)$, are left to be measured.

The model proposed by Burkardt and Jaffe [BJ] assumes that the fragmentation process preserves the helicity of the struck quark. In this model polarized quarks leading to a polarized Λ have to be polarized inside the Λ as well. In other words, the polarized fragmentation functions are related to the polarized quark distributions. This is a strong statement, especially when considering the fact that there is no formal connection between those two quantities, the fragmentation and the structure functions. However, it is appealing as well as it would give the possibility to measure the polarized quark distributions in the Λ. Using SU(3) arguments those could then be compared to the polarized quark distributions in

[15]For a full QCD treatment, i.e., Q^2 evolution, one also has to include the gluon contribution. An attempt to do so has been made in [deFlo].

the proton[16] (see appendix C). Two comments should be made regarding this model: As mentioned before the assumption of conserving the quark helicity has no direct theoretical basis in non-perturbative QCD. Moreover, the simple picture of a quark directly fragmenting into a Λ is not as simple as suggested. The fragmentation functions include also strong decays into a Λ, i.e., decays from hyperon excitations. Those processes, however, make it harder to believe that the helicity of the struck quark is indeed preserved and still the same in the resulting Λ.

In [deFlo], fits to the available Λ production and polarization data from e^+e^- collider experiments are used to make predictions for other experiments. This is done by evolving the obtained fragmentation functions according to the DGLAP formalism. Since the individual fragmentation functions are not known so far different scenarios are examined. The basic ansatz for the polarized fragmentation functions $\Delta\hat{q}^{\Lambda}(z)$ is[17]

$$\Delta\hat{u}^{\Lambda}(z) = \Delta\hat{d}^{\Lambda}(z) = N_u \Delta\hat{s}^{\Lambda}(z) \tag{2.58}$$

$$\Delta\hat{s}^{\Lambda}(z) = z^{\alpha}\hat{s}^{\Lambda}(z). \tag{2.59}$$

N_u is a parameter describing the contribution of the u and d quarks to the polarized fragmentation which depends on the scenario, and α is a fit parameter. One should mention that the unpolarized fragmentation functions $\hat{q}^{\Lambda}(z)$ are assumed

[16]The model, in which the Λ spin structure is obained from the proton spin structure through SU(3), will be referred to as the BJ model.

[17]Q^2 dependence is implicitly assumed.

to be equal for the light quark flavors u, d and s. They are described through the ansatz

$$\hat{q}^{\Lambda}(z) = N z^{\alpha_q}(1-z)^{\beta_q}, \tag{2.60}$$

where q denotes the quark flavor, and α_q as well as β_q are parameters obtained by fits to the available cross section data.

Three different scenarios are considered, each using a different u-quark contribution, N_u in equ. 2.58, to the polarized fragmentation. The first two follow the assumption of helicity conservation in fragmentation but use different polarized quark distributions of the Λ. In the last scenario all quarks are assumed to contribute the same. In more detail the scenarios are:

- $N_u = 0$ - only s quarks contribute to a polarized Λ. This corresponds to the naïve QPM where only polarized s quarks can produce a polarized Λ.

- $N_u = -0.20$ - u and d quarks contribute to the polarized Λ as well. The value is taken according to the BJ model assuming the polarization of the u and d quarks in the Λ is about -20%. However, the contribution from polarized s quarks has not been changed, despite the fact that their polarization is only 58% in the BJ model.

- $N_u = 1$ - all the polarized fragmentation functions are assumed to be equal. The justification of this (rather extreme) model is the fact that Λ's could

Table 2.5: Leading order fit parameter for deFlorian's Ansatz for the polarized Λ fragmentation functions [deFlo]

	Leading Order Fit		
Parameter	Scenario 1	Scenario 2	Scenario 3
N_u	0	-0.2	1.0
α	0.62	0.27	1.66

come from the strong (or even electro-magnetic and weak[18]) decay of heavier hyperons allowing the u and d quarks to contribute considerably more than expected from the previous two scenarios.

The results of these fits are summarized in table 2.5. The predictions for the HERMES experiment will be discussed in section 2.6.

A less predictive model (because of missing data) is based on SU(3) arguments. The same way the polarized quark distributions in the hyperon octet are related to each other, the polarized quark fragmentation functions for the baryons in the hyperon octet are related to each other.[19] The polarized fragmentation function can be written down as a linear combination of a singlet term and two octet terms. This is in analogy to the spin structure functions which also can be expressed in terms of a singlet term and two octet terms. Keeping the notation

[18]There is, of course, no theoretical justification for this, but as pointed out in the paper, even including the Σ^0 decay the data is modeled successfully (within the errors, author)

[19]The same is true for the unpolarized fragmentation functions and a treatment in this manner can be found in [IMR].

Table 2.6: Polarized quark fragmentation functions in the SU(3) model

Baryon	$\Delta\hat{u}^B$	$\Delta\hat{d}^B$	$\Delta\hat{s}^B$
p	$\frac{1}{3}(\hat{\Sigma}+\hat{D}+3\hat{F})$	$\frac{1}{3}(\hat{\Sigma}-2\hat{D})$	$\frac{1}{3}(\hat{\Sigma}+\hat{D}-3\hat{F})$
n	$\frac{1}{3}(\hat{\Sigma}-2\hat{D})$	$\frac{1}{3}(\hat{\Sigma}+\hat{D}+3\hat{F})$	$\frac{1}{3}(\hat{\Sigma}+\hat{D}-3\hat{F})$
Σ^+	$\frac{1}{3}(\hat{\Sigma}+\hat{D}+3\hat{F})$	$\frac{1}{3}(\hat{\Sigma}+\hat{D}-3\hat{F})$	$\frac{1}{3}(\hat{\Sigma}-2\hat{D})$
Σ^0	$\frac{1}{3}(\hat{\Sigma}+\hat{D})$	$\frac{1}{3}(\hat{\Sigma}+\hat{D})$	$\frac{1}{3}(\hat{\Sigma}-2\hat{D})$
Σ^-	$\frac{1}{3}(\hat{\Sigma}+\hat{D}-3\hat{F})$	$\frac{1}{3}(\hat{\Sigma}+\hat{D}+3\hat{F})$	$\frac{1}{3}(\hat{\Sigma}-2\hat{D})$
Λ	$\frac{1}{3}(\hat{\Sigma}-\hat{D})$	$\frac{1}{3}(\hat{\Sigma}-\hat{D})$	$\frac{1}{3}(\hat{\Sigma}+2\hat{D})$
Ξ^0	$\frac{1}{3}(\hat{\Sigma}-2\hat{D})$	$\frac{1}{3}(\hat{\Sigma}+\hat{D}-3\hat{F})$	$\frac{1}{3}(\hat{\Sigma}+\hat{D}+3\hat{F})$
Ξ^-	$\frac{1}{3}(\hat{\Sigma}+\hat{D}-3\hat{F})$	$\frac{1}{3}(\hat{\Sigma}-2\hat{D})$	$\frac{1}{3}(\hat{\Sigma}+\hat{D}+3\hat{F})$

of Appendix C one can write down the polarized quark fragmentation functions in terms of[20] $\hat{\Sigma}$, $\hat{F}$ and $\hat{D}$ (table 2.6). Of course, $\hat{\Sigma}$, $\hat{F}$ and $\hat{D}$ have nothing to do with the $\Delta\Sigma$, F and D in the case of polarized quark distributions. Hence, their values have to be determined from experiment by measuring different linear combinations of them. Once one knows the values of $\hat{\Sigma}$, $\hat{F}$ and $\hat{D}$ one can construct all the polarized quark fragmentation functions for the hyperon octet.[21]

2.6 Λ Polarization

As mentioned before, the Λ polarization is closely related to the polarized Λ fragmentation functions. In fact, if one neglected any contributions to the Λ production from electro-magnetic or weak decays, the Λ polarization would have its

[20]To distinguish the polarized quark distributions from the polarized quark fragmentations, the latter will be denoted by a hat.

[21]Care should be taken, though, since SU(3) flavor is not an exact symmetry.

origin solely in the polarized Λ fragmentation. The complete expressions for the longitudinal polarization[22] and transverse polarization in the current fragmentation region[23] of an DIS event can be found in [MT]. For the special case of a polarized lepton beam and an unpolarized target one obtains [Jaffe]:

$$\mathcal{P}_\Lambda = \mathcal{P}_b D(y) \frac{\sum_q e_q^2 q^N(x,Q^2) \Delta\hat{q}^\Lambda(z,Q^2)}{\sum_q e_q^2 q^N(x,Q^2) \hat{q}^\Lambda(z,Q^2)} \tag{2.61}$$

where P_b is the polarization of the beam (incoming lepton),

$$D(y) = \frac{1-(1-y)^2}{1+(1-y)^2} \tag{2.62}$$

is the longitudinal depolarization factor of the virtual photon, e_q is the fractional charge of quark q, $q^N(x,Q^2)$ are the quark distributions in the nucleon and $\hat{q}^\Lambda(z,Q^2)$ and $\Delta\hat{q}^\Lambda(z,Q^2)$ are the unpolarized and polarized quark fragmentation functions in the Λ, respectively.

Eq. (2.61) becomes intuitively clear when comparing to the polarization transfer from a polarized lepton to an unpolarized quark (Dirac particle)

$$\mathcal{P}_q = \mathcal{P}_b D(y). \tag{2.63}$$

[22]along the Λ momentum direction

[23]So far no distinction has been made between current and target fragmentation region. In semi-inclusive DIS one can form hadrons from the struck quark (current fragmentation region) and/or from the target remnants (target fragmentation region). Strictly speaking the notion of quark fragmentation has only meaning in the current fragmentation region where one quark – the struck quark – forms a hadron. In the target fragmentation region one already starts with an ensemble of quarks – the idea of quark fragmentation is not anymore defendable. In order to distinguish between the two regions in the experiment, one usually considers the forwardness of the emerging hadron in the gamma-nucleon c.m.. This is accomplished by applying a cut on x_f, where $x_f > 0$ denotes the current fragmentation and $x_f < 0$ denotes the target fragmentation region.

The number of unpolarized quarks is described by the quark distribution in the nucleon. The final Λ polarization depends on the probability that a polarized quark then fragments into a polarized Λ. For normalization reasons one has to divide by the unpolarized fragmentation.

It might be more useful to introduce a different quantity which will be denoted as the *spin transfer* coefficient $\hat{Q}$. When looking at eq. (2.61) one notices that the Λ polarization depends, as expected, on the experimental conditions like the beam polarization and the lepton kinematics. In order to compare to different experiments (or to later results from HERMES which might have seen better beam polarizations), those dependencies are factored out:

$$\hat{Q}(z) = \frac{\mathcal{P}_\Lambda}{\mathcal{P}_B D(y)} \tag{2.64}$$

$$= \frac{\sum_q e_q^2 q^N(x,Q^2)\Delta\hat{q}^\Lambda(z,Q^2)}{\sum_q e_q^2 q^N(x,Q^2)\hat{q}^\Lambda(z,Q^2)}. \tag{2.65}$$

Eq. (2.61) reduces to

$$\mathcal{P}_\Lambda = \mathcal{P}_b D(y)\hat{Q}. \tag{2.66}$$

In the case of e^+e^- collision quarks are naturally polarized when produced at the Z^0-pole. This is due to the parity-violating electro-weak $q\bar{q}Z^0$ coupling (see Appendix G). The polarization of the light quarks produced at the Z^0-pole can be found in table 2.4. As already mentioned, studying the Λ polarization for Λ's produced in e^+e^- collision gives easier access to the polarized fragmentation functions since the parton distributions of the nucleon do not have to been known.

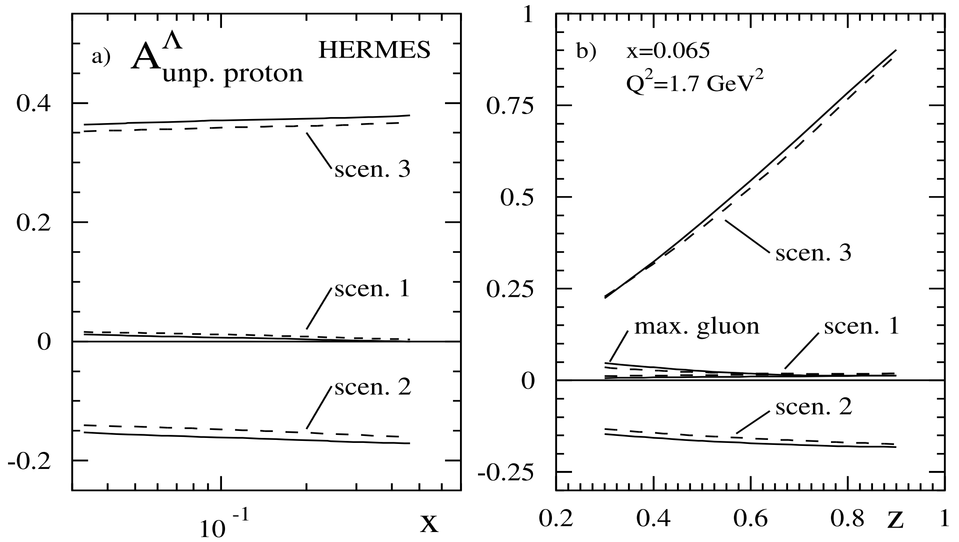

Figure 2.3: The Spin transfer according to [deFlo]. The different scenarios refer to the spin transfer modeled according to the naïve QPM (1), the BJ model (2) and an equal distribution to the Λ polarization by all the quark flavors (3). Also included is the case of maximal gluon contribution (for scenario 1) - gluons contributiong to the Λ fragmentation. The underlying proton parton distributions are the ones in [GRV].(Taken from [deFlo])

There are two recent numerical predictions for the Λ polarization. Both of them are based on the assumption that the quark helicity is preserved in the fragmentation process. One of them [deFlo], described in section 2.5.2, uses the available Λ polarization and production data in e^+e^--collision. Using the Q^2-evolved polarized fragmentation functions and a parametrization for the quark distributions in the target proton, different predictions for the spin transfer for HERMES kinematics are made. These predictions for the different scenarios are shown in figure 2.3.

Another approach [KBH] uses the LEPTO and JETSET [MCG] Monte Carlo generators to produce Λ's. Under the assumption of helicity conservation, the polarized fragmentation functions are related to the Λ spin structure. Two scenarios for the polarized quark distributions in the Λ are considered:

- Non-relativistic QPM – Only the s quark directly produces polarized Λ's. Other sources of Λ polarization come from decays of heavier particles[24].

- BJ Model – The spin transfer is proportional to the quark polarization in the Λ which is derived from the proton data on polarized DIS using SU(3). The u-quark and the d-quark polarizations are -20% and the s-quark polarization is 58%. One weakness in this scenario in that no contribution from decays were included[25].

The prediction for HERMES kinematics is shown in figure 2.6. Note that in the original paper the polarization is quoted and not the spin transfer. The change to $\hat{Q}$ has been done not only for presentation reasons but also to avoid confusion: [KBH] uses different values for the beam polarization and the average photon depolarization than actually present at HERMES.

Jaffe pointed out that for HERMES kinematics Λ production will be dominated by the u quark [Jaffe]. Thus, a sizable Λ polarization points to a non-zero polarized u quark fragmentation. Within errors HERMES would therefore mea-

[24]Not only strong decays are considered but also the decay from Σ^0. Besides the Σ^0 the Ξ and the $\Sigma(1385)$ contribute to the Λ polarization

[25]In the experiment those will, however, contribute.

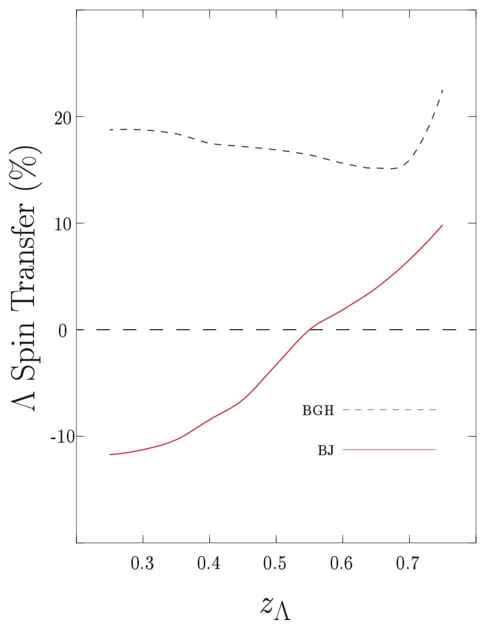

Figure 2.4: Spin transfer $\hat{Q}$ as predicted by [KBH]

sure the polarized u quark fragmentation:

$$\mathcal{P}_\Lambda = \mathcal{P}_b D(y) \frac{\Delta \hat{u}^\Lambda}{\hat{u}^\Lambda}. \tag{2.67}$$

It should be noted that there exists also a prediction for Λ polarization in the target fragmentation region [EKK]. Although an interesting subject to study it will not be considered here since at the present stage HERMES is not able to probe the target fragmentation region. Detector upgrades, which will facilitate tracking of low momentum particles, might change this situation in the future.

At last a few comments about decaying particles. As mentioned, heavier particles can contribute via decay to the polarization of the Λ. It is known that

Table 2.7: Polarization inherited from the decay of heavier particles [GH, Dukes, PDG]

Parent particle	Decay channel	Branching ratio	Interaction	Resulting $\mathcal{P}_\Lambda$
Σ^0	$\Lambda\gamma$	100%	electro-magnetic	$-\frac{1}{3}\mathcal{P}_{\Sigma^0}$
$\Sigma(1385)$	$\Lambda\pi$	$88 \pm 2\%$	strong	$\mathcal{P}_{\Sigma(1385)}$
Ξ	$\Lambda\pi$	$\approx 100\%$	weak	$\approx 0.9\mathcal{P}_\Xi$
$\Xi(1530)$	$\Xi\pi \to \Lambda\pi\pi$	$\approx 100\%$	weak	$\approx 0.9\mathcal{P}_{\Xi(1530)}$

hyperons are produced polarized in hadron-hadron collisions[26] and polarizations in lepto productions would not be surprising. The same way the Λ might get its polarization (i.e., quark helicity conservation), one would expect the other hyperons to be produced polarized. Also using SU(3) arguments they should be polarized if the Λ is polarized. Those polarizations can be carried over when decaying into a Λ. The most prominent candidates are summarized in table 2.7. Other decays like the ones from the Ω^- or the weak decay of the $\Sigma(1385)$ give only very small contributions and – certainly in the limit of the statistical error – can be neglected here.

Technically, all the contributions from strong decay's are included in the fragmentation functions although they are not necessarily considered in the Monte Carlo predictions previously mentioned. The other contributions have to be ex-

[26] For a summary on this topic see e.g., [Heller].

cluded from the Λ sample which is analyzed (i.e., by vetoing events with a prompt photon in case of the Σ^0) or otherwise have to be dealt with in the analysis and interpretation of the result. For the HERMES experiment only the Σ^0 really contributes without being part of the Λ fragmentation process.

CHAPTER 3

THE HERMES EXPERIMENT

HERMES (HERa MEasurement of Spin) was designed to study the spin structure of the nucleon. It follows the footsteps of EMC, SMC and SLAC – complementing their measurements but also providing data on semi-inclusive DIS, which allows quark flavor tagging[1]. HERMES was commissioned in 1995, when it took data on polarized positron scattering from polarized ^{3}He (effectively a polarized neutron target). In 1996 and 1997 ^{3}He was replaced by hydrogen. Since 1998, HERMES is taking data on polarized deuterium. It is an internal gas target experiment utilizing the polarized lepton[2] beam at HERA.

Complimentary to the polarized target, data with unpolarized targets (H, D, ^{3}He and ^{14}N) has been taken providing high statistics data on related topics like nuclear effects or Λ polarization.

An extensive description of the detector can be found in reference [HERMES]. In this chapter I will briefly describe the main components of the experiment.

[1]Although SMC was able to study semi-inclusive asymmetries they did not have the capabilities of distinguishing different hadrons as it is the case at HERMES.

[2]Although electrons or positrons can be used, subsequently I will address the lepton beam as the electron beam.

3.1 HERA

HERA (Hadron-Electron Ring Accelerator) is a collider housing a storage ring for protons and a storage ring for positrons or electrons. The diameter of the ring is about 1.2 km. The maximum electron energy is about 30 GeV whereas the energy of the protons, using super-conducting magnets in order to bend the beam, is currently 900 GeV. Four experimental halls give access to the beam, two of them, North and South, utilize both of the beams in a collider mode. The two experiments, H1 and ZEUS, measure the unpolarized[3] structure functions of the proton. The third experiment at HERA is the HERMES experiment, making use of the polarized electron beam. A new experiment in the West hall is near completion: HERA B, studying CP violation in the B system, uses only the proton beam.

Both the electrons and the protons come in bunches 96 ns apart. Furthermore, there are three gaps in the bunch structure allowing systematic studies to be done while there is no beam crossing the detector. The typical current of the electron beam after injection is about 30 mA but higher currents (up to 45 mA) have been achieved. The electron beam is highly focused with an elliptical cross section of 0.31 mm (horizontally) times 0.07 mm (vertically). The bunch length is 27 ps which corresponds to 5.4 mm [HER 98b].

[3]Unlike the electron beam the proton beam is not polarized. However, plans for polarized protons are discussed, opening a new kinematic region in polarized DIS.

The HERMES experiment makes use of the fact that electrons in a storage ring are naturally polarized. This is due to the Sokolov-Ternov effect [ST] yielding transversely polarized electrons. In order to obtain a longitudinally polarized electron beam, spin rotators have been installed before and after the HERMES experiment. These also allow to have the helicity of the beam reversed. In 1996 data was taken with positive beam helicity and in 1997 the beam helicity was negative. Maximum polarization of 70-80% has been achieved[4], however, the average beam polarization is between 35% and 65%.

Two beam polarimeters measure the polarization of the electron beam. The transverse polarimeter (TPOL) measures the (transverse) polarization just behind the West hall (which houses HERA-B). In 1997, the longitudinal polarimeter (LPOL) was installed behind the HERMES experiment measuring the there longitudinal polarization of the beam. It thus provides complimentary data to the information from the TPOL. This is especially useful in the case when one of the polarimeters is malfunctioning.

Both polarimeters exploit the spin dependence of the Compton cross section. Left and right circularly polarized laser light is scattered off the electron beam. In the case of a transversely polarized electron beam a top-bottom asymmetry in the distribution of the back scattered photons arises. This is measured in a calorimeter which is then used to determine the beam polarization. The LPOL measures the

[4]The maximum theoretical value is 92.4% [Düren].

asymmetry in the integrated energy of the back scattered light which is caused by flipping the helicity of the laser light. Since the electron beam is longitudinally polarized the intensity of the back scattered light depends on whether the spins of the photon and the electron are parallel or anti-parallel.

The polarization of the electron beam is assumed to be the same everywhere in the ring. The two polarimeters thus give two independent measurements of the same quantity which reduces the systematic uncertainty in the beam polarization value.

3.2 The internal gas target

HERMES uses a fixed target in the form of a windowless internal gas target. The 40-cm-long storage cell is installed in the electron ring and can provide either a polarized target (fed by an atomic beam source) or an unpolarized target (usually hydrogen, deuterium, helium-3 or nitrogen, though other gases are possible as well). For the polarized physics program at HERMES an atomic beam source provides a polarized proton (hydrogen) target. In 1995, an optically pumped ^{3}He cell provided a polarized neutron target [He3]. For the data analyzed in this thesis only the unpolarized gas system was used. The luminosity was $(1-5)\times 10^{32}$ cm^{-2}s^{-1}. Higher luminosities are possible but have a rather large effect on the beam lifetime.

An injection pipe, situated at the center of the cell, feeds the gas into the target cell. Pumps close to the end of the cell continuously pump out the target gas creating a triangular shaped density distribution. The cell itself has an elliptic cross section and is 9.8 mm high and 29.0 mm wide. It is protected from synchrotron radiation by a set of collimators in front of the target region. The collimator closest to the target cell (C2) is fixed in size whereas the size of the collimator in front of C2 (C1) can be adjusted. This allows an easy beam injection procedure by opening C1 and a safe running during data taking where one closes the collimator to the necessary size.

3.3 The HERMES detector

The HERMES detector is a forward acceptance spectrometer. Its rather complicated acceptance, especially for decaying particles, is due to the fact that it has been designed to measure spin asymmetries in which acceptance effects ought to cancel out. The HERMES detector can be divided up into a front region, mainly used for tracking, the spectrometer magnet and the back region, which is used for tracking and particle identification. Other parts of the detector are trigger scintillators, luminosity monitors and various beam tune monitors. Since both the electron pipe and the proton pipe, separated by 72 cm, go through the apparatus, the detector consists of two equal halves, the top and the bottom detector. They cover an angular acceptance of about

$$40\text{mrad} < |\Theta_{vert}| < 140\text{mrad} \tag{3.1}$$

$$|\Theta_{horiz}| < 170\text{mrad}. \tag{3.2}$$

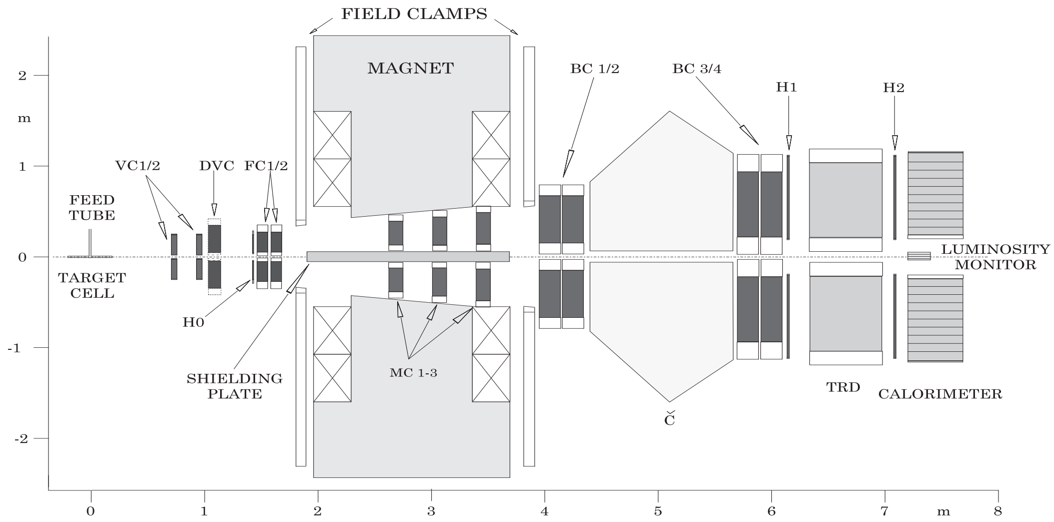

Figure 3.1: Systematic view of the HERMES detector.

A systematic view of the detector can be found in figure 3.1.

3.3.1 Tracking System

HERMES uses several tracking detectors for track reconstruction. In the front region, originally only the vertex chamber (VC) and the front chamber (FC) provided information for track reconstruction. In the first year of data taking, track reconstruction was burdened by low efficiencies of the VC's. In order to increase redundancy in the front region drift vertex chambers (DVC's) were installed in 1997. In the back region the back chambers (BC's) provide tracking information to reconstruct the event and relate particle identification (PID) detector hits with a track. Within the spectrometer magnet, proportional wire chambers track the particle while traversing the magnet. These magnet chambers (MC's) are of particular interest for reconstructing low momentum particles which were deflected too much to be tracked by the BC's. In such a case the MC's are used to reconstruct the bending angle and thus to determine the particle's momentum.

The VC's were designed to give accurate information about the tracks in the target region. The scattering angle, for inclusive measurements, as well as decay vertex positions, for the semi-inclusive program, are major concerns in the reconstruction. In order to provide high precision tracking information the VC consists of two micro-strip gas counters with 24,800 channels in six planes. The resolution per plane is about 65 μm.

The DVC's and FC's as well as the BC's are conventional drift chambers. They consist of six planes[5]; two in the $\hat{x}$ direction, two in the $\hat{u}$ direction and two in the $\hat{v}$ direction. Here, $\hat{x}$ measures the x position of the track (thus the wires are arranged vertically). The $\hat{u}$ and $\hat{v}$ directions are rotated by $\pm 30°$ w.r.t. the $\hat{x}$ direction.

There are three proportional wire chambers which reside inside the magnet. They were intended to disentangle multiple track events. It turned out that the multiplicities are not very high and the MC's are not required for track reconstruction. This, however, is only true for tracks which will be deflected into the back region of the detector. There the BC's provide sufficient data to reconstruct the track. For low momentum particles, i.e., the decay products of the Λ, the BC's often can not be used because the particle will be bent out of the detector

[5]There are two sets of BC's – one before and one after the Cherenkov detector. This gives a total of 12 planes.

acceptance by the spectrometer magnet. Together with the front tracking, the MC's provide the necessary information to reconstruct these events.

3.3.2 Particle Identification

A major part of the detector is dedicated to particle identification (PID). This was necessary not only to detect electrons but also to discriminate between different hadrons, important for the semi-inclusive physics program. There are several different types of detectors involved, each of them providing additional information about the particle.

The main task of the spectrometer magnet is the determination of the particle's momentum. A dipole magnet provides a deflecting power of up to $\int Bdl = 1.5$ Tm. The two beam pipes go through the whole detector and, therefore, also through the spectrometer magnet. In order to shield the beams from the magnetic field, a massive iron plate, the septum plate, is inserted in the symmetry plane of the magnet. In addition, a correction coil is accommodated within the shielding of the electron beam pipe. There are also field clamps in front and behind the magnet in order to reduce the magnetic fields in the adjacent drift chambers.

The Cherenkov detector relies on the principle that particles which fly through a medium faster than the speed of light in that particular medium will radiate light. Together with the momentum information from the spectrometer magnet one can thus discriminate particles by their mass, or more specific by their $\beta = \frac{v}{c}$. For the first three years a threshold gas Cherenkov counter was in use. In 1995 pure nitrogen was used and in 1996 as well as in 1997 a mixture of 70% nitrogen and 30% perfluorobutane, C_4F_{10}, was used, yielding different thresholds on β of the particle. One disadvantage of a threshold detector is that after passing the threshold no discrimination between particles with $\beta < \beta_{thresh}$ or, vice versa, no discrimination between particles with $\beta > \beta_{thresh}$ can be provided by the detector. Information from other PID detectors are necessary to clearly identify the particle. To illustrate this take pions and kaons as an example. From table 3.1 one can see that in 1996-97 the threshold momentum to fire the Cherenkov counter was 3.8 GeV in the case of pions and 13.6 GeV for kaons. Electrons in the momentum acceptance of the HERMES detector will always fire the Cherenkov counter. Thus, below 3.8 GeV only electrons could be identified. Between 3.8 GeV and 13.6 GeV a signal in the Cherenkov counter could come from either electrons or pions but not kaons. By including electron identifying detectors like the transition radiation detector (TRD) and/or the electro-magnetic calorimeter, one can establish a rather clean pion identification in the momentum range 3.8-13.6 GeV. Above 13.6 GeV a distinction between pions and kaons is no longer possible; both will fire the Cherenkov counter.

Since 1998 HERMES is running with a Ring Imaging Cherenkov (RICH) which also measures the opening angle of the Cherenkov light. One, therefore, can distinguish particles with $\beta > \beta_{thresh}$ since the opening angle still depends on β. The HERMES RICH consists of two radiators of different index of refraction

Table 3.1: Threshold momenta for pions, kaons and protons in the Cherenkov detector [HERMES]

Year	Gas Mixture	Threshold Momentum [GeV]		
		Pion	Kaons	Proton
1995	Nitrogen	5.6	19.8	37.6
1996/97	70% N_2, 30% C_4F_{10}	3.8	13.6	25.8

enhancing the discrimination of particles (see figure 3.2). This will provide a much cleaner hadron PID, particularly in the case of decaying hadrons.[6]

The trigger hodoscopes H1 and H2 can also, in principle, be used for PID. For low momentum particles the time of flight from the target to the hodoscopes depends on the mass of the particle (when comparing particles with the same momentum). Unfortunately, the TDC and ADC information were not always reliable. Therefore, time of flight information were not used for the final result though their potential will be addressed in section 4.1.

Due to the lead foil in front (c.f. 3.3.3) of H2[7], it can also be used as a PID detector. Photons as well as electrons shower in the extra radiator. This causes a larger energy deposit in H2 than that of heavier particles, i.e., hadrons, which only deposit minimum ionizing energy.

[6]In this analysis a clean pion/proton discrimination would have reduced the background coming from the K_s^0, which decays into two pions, considerably for momenta of the positive hadron below 4 GeV.

[7]Subsequently also addressed as the pre-shower detector

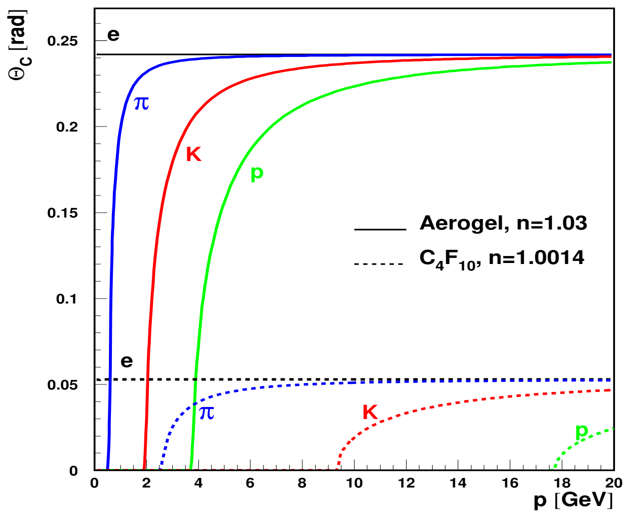

Figure 3.2: The opening angle of the Cherenkov light for different particles as a function of their momenta.

Similar to the pre-shower, the electro-magnetic calorimeter utilizes the fact that photons as well as electrons shower and lose all their energy in the lead glass blocks of the calorimeter. The ratio of the energy deposited in the calorimeter and the momentum of the particle (E_{calo}/p) will be about one for electrons. The energy deposit of hadrons (as well as of heavier leptons, i.e., muons) will (in first approximation) not be related to their momentum. A cut on E_{calo}/p thus can be used to discriminate electrons from other particles. The pion suppression factor is ≥ 100 [HERMES].

The calorimeter consists of 420 lead glass blocks in each the top and bottom halves. There are 42 columns with 10 blocks each. The blocks are 50 cm long and have an area of 9×9 cm^2. For the analysis arrays of 3×3 counters are used to determine the energy deposit. Also bremsstrahlung clusters are detected which allow a better determination of the energy of the particle.

The TRD is another detector to distinguish electrons from hadrons, in particular pions. Its design is based on the fact that highly relativistic particles will radiate when crossing boundaries between two dielectric media. The TRD consists of 6 modules in either half of the detector. Polypropylene/polyethylene fibers are used as radiator and the radiated X-rays are detected by proportional wire chambers. The analysis of all the six chambers results in an energy-averaged pion suppression factor of about 150.

By means of the PID detectors an efficient electron/hadron discrimination can be achieved. One way, the simplest way, is to apply hard cuts on the responses of all the PID detectors. However, this might unnecessarily decrease the accepted electron sample, i.e., when one of the detectors is inefficient in one particular event. A more sophisticated method is based on a probability analysis. The responses of the Cherenkov counter, the pre-shower and the electro-magnetic calorimeter are combined to form the $PID3$:

$$PID3 = \log_{10}\left(\frac{P^e_{Cher}P^e_{Pre}P^e_{Calo}}{P^h_{Cher}P^h_{Pre}P^h_{Calo}}\right), \tag{3.3}$$

where P^i_j is the probability that a particle of type i produces the measured detector response in detector j. In general, one can introduce *logarithmic likelihoods* Γ_j for

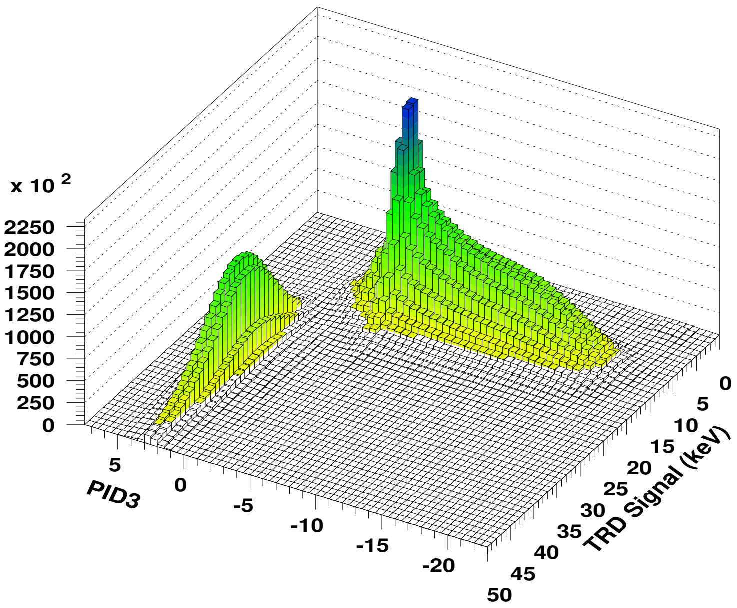

Figure 3.3: $PID3$ versus the TRD response. Clearly visible are the electron peak on the left side and the hadron peak on the right side (taken from [HERMES]).

all PID detectors:

$$\Gamma_j = \log_{10} \frac{P_j^e}{P_j^h}. \tag{3.4}$$

$PID3$ is the sum over the logarithmic likelihoods for the Cherenkov counter, the pre-shower and the electro-magnetic calorimeter. Clearly, the larger the value of $PID3$ is the more likely it is an electron that has been detected. Different extensions to above approach are possible. In particular, the TRD should be included in order to achieve an even larger pion/hadron suppression. This would lead to electron efficiencies of above 98% with hadron contamination smaller 1%. In figure 3.3 a 3D plot of the PID3-TRD space is shown. Clearly visible are the electron peak and the hadron peak. A detailed discussion of the different PID schemes can be found in [Kaiser].

In addition to the RICH another new detector has been installed in 1998 as part of the "Charm[8] upgrade." The so-called Muon Hodoscopes (HM's) are located behind the calorimeter shielded by an iron wall. The main purpose of the HM's is to identify muons. Other particles will be stopped latest inside the iron wall. One can therefore reduce the background for charm particles like the J/Ψ or the D which involve decays into at least one muon.

3.3.3 Trigger Detectors

The main physics goal of the HERMES experiment is to measure (semi)inclusive spin-dependent electron scattering asymmetries. In accordance with this goal the main trigger was designed to trigger on the scattered electron, provided its energy is larger than 3.5 GeV (which corresponds to $y < 0.85$, keeping radiative corrections small). For this trigger a coincidence of hits in the three trigger scintillators H0, H1 and H2 is required. One should note that top and bottom are treated separately such that a hit in H0 top can not form a coincidence with hits in H1 bottom etc. The required minimum energy will be established by demanding the minimum energy deposit in two adjacent columns of the calorimeter to be larger than 3.5 GeV. The corresponding pulse height of the signal is 55 mV. In the case of the scintillators the discriminator threshold is below minimum ionizing.

H0 is the only trigger detector in the front region of the HERMES detector. It was introduced a year after the commission of HERMES, the main reason being

[8]The upgrade aims to increase the acceptance for charm particles.

triggers caused by backward flying showers coming from the proton beam. The spatial (and thus the timing) separation of the hodoscopes H1 and H2 was not sufficient to discriminate between these "fake" events and "real" events coming from the HERMES target. Each half of H0 consists of one scintillator paddle covering the whole acceptance of the corresponding half of the HERMES acceptance, two photo multiplier tubes (PMT's) and light guides which connect the tubes to the scintillating paddles. The PMT signals are amplified. Afterwards the summed signal is fanned out and discriminated at different pulse heights. For the DIS trigger a threshold below minimum ionizing energy is used, allowing for a highly efficient trigger.

Both H1 and H2 are in the back region and consist of 42 paddles in each half. Each signal from all the paddles is discriminated separately allowing not only differentiation between top and bottom tracks but also an estimation of the track multiplicity of the event. This becomes of particular interest in the case of multi hadron triggers. In addition to the scintillator hodoscopes, a 11 mm thick lead foil is placed in front of H2 causing electrons (and photons) to shower and deposit more energy in H2 than the minimum ionizing energy. This could, in principle, be used to further distinguish hadrons (minimum ionizing particles) and electrons in the first level trigger.

The electro-magnetic calorimeter is used to provide a fast energy determination of the particle. For the trigger, it is important to have a signal which can be used to select 3.5 GeV electrons. It has been shown that over 95% of the particle energy is contained within two out of the 42 columns of the calorimeter. Summing the individual signals of two columns thus gives a good measure of the particle energy. Care has to be taken that the gain of all the PMT's stays constant over time. The gain monitoring system (see section 3.3.4) measures relative gain changes during running to avoid large fluctuation in the gain. Nevertheless, the gain might still drift over a longer period of time. This can be seen in figure 3.4 where the relative correction to the measured energy deposit in a calorimeter block is plotted. It has been determined by demanding that an electron's energy deposit in the calorimeter is in average equal the energy (momentum) of the electron ($\langle E_{calo}/p \rangle = 1$, see also section 3.3.2). The correction factor can be used in software to calibrate the calorimeter response, however, the trigger uses a hard cut on the signal height - gain changes will directly change the effective trigger threshold. If one plots the trigger efficiency vs. the electron energy, the trigger threshold becomes clearly visible (figure 3.5). It is apparent that for real events the threshold region is much broader than what is seen in the Monte Carlo simulation where all the gains are equal.

Besides the DIS program, the photo-production program is of large interest at HERMES. One of the reasons for this is the believe that it will give access to the gluon polarization ΔG of the nucleon. Unlike an DIS event, a photo-production event usually is not accompanied by a relativistic electron in the HERMES ac-

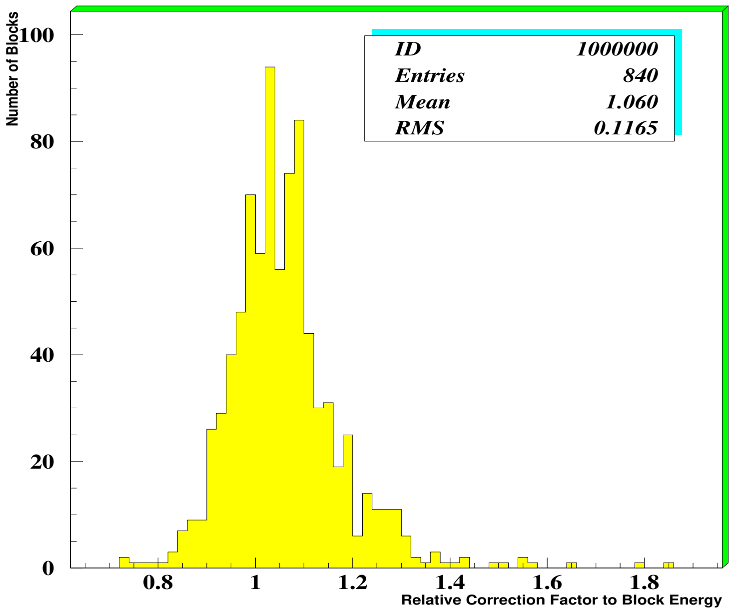

Figure 3.4: The relative correction factor to the measured energy deposit in the calorimeter. Shown are the corrections based on the 1997 data.

ceptance. Since all other particles will deposit considerably less energy in the calorimeter, they will not cause the DIS trigger to fire. An additional set of triggers is provided to fulfill the different requirements of the photo-production program. Most of the interesting channels involve production and subsequent decays of charmed[9] particles. Decay products of interest (since they can be identified) are μ's, π's and K's. Unfortunately, π's are also produced plentiful when the electron beam scatters off the collimators or the beam pipe. One, therefore, has to be more restrictive when selecting events. One class of events involves the reconstruction of the charmed particle by calculating the invariant mass of the

[9]The charm quark is not believed to be abundant in the nucleon. The production of charmed particles will, therefore, very often involve a photon-gluon-fusion kind of process, providing access to the gluon distribution and polarization.

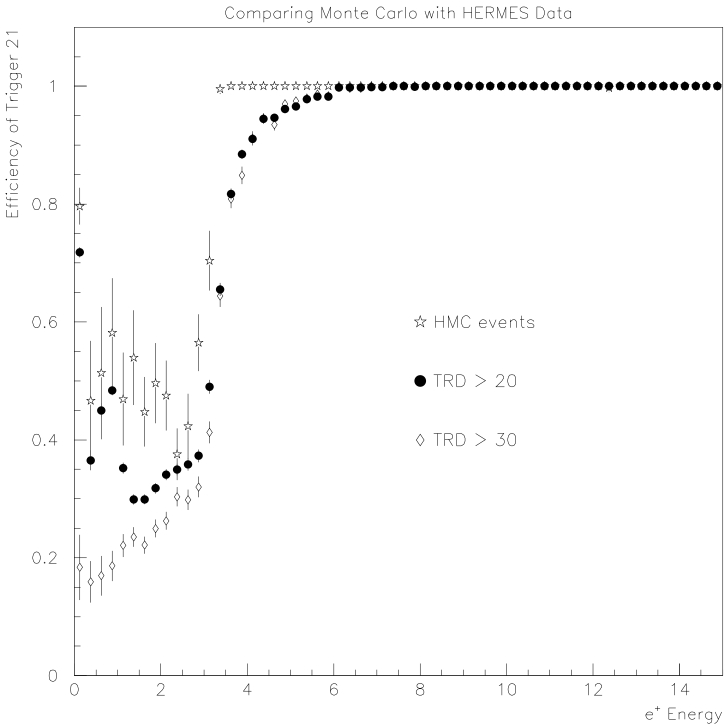

Figure 3.5: The trigger efficiency for electrons vs. the energy deposit of the scattered positron in the calorimeter. Shown are simulated events, using the Hermes Monte Carlo (HMC) program, as well as real events, applying hard cuts on the Transition Radiator Detector response in order to tag electrons. The set trigger threshold is 3.5 GeV. The stretching of the threshold region due to gain mismatch is apparent. (Taken from [Assaf])

decay products. At least two hadrons[10] have to be in the HERMES acceptance, hence triggering on two charged tracks is required. Two combinations are possible: Both the tracks are in one of the two halves of the detector (subsequently labeled as TR27) or either halve will have one track (noted as a TR28 event). Since the trigger is divided into a top and a bottom part this has important consequences for the trigger logic involved. Before the implementation in 1996, an extensive analysis has been done on the 1995 data which showed that most of the bad events, triggering the single hadron trigger, came from showers traveling down the beam pipe. The drift chambers BC1 and BC2 are located just behind the magnet and thus are shielded from most of the showers. They also have a smaller acceptance compared to the hodoscopes, in particular close to the beam pipe where most of the bad events were coming from. In order to include the BC's in the trigger, fast signals have to be provided. Custom made cards are used which produce an analog OR of 16 adjacent wires of the x planes of BC1. This provides enough granularity to distinguish multiple tracks. The cards are installed near the BC's and the OR output is sent via air-foam cable to the trigger electronics. The signals are then discriminated. The sum of the discriminated signals gives a measure of the hit multiplicity. In general, one expects to get two hits from one track: One hit from the x plane and another hit from the x' plane. Since the

[10]Though μ's are not hadrons they leave a similar signature as hadrons. In fact, only by installing an absorbing iron wall, which will stop mainly everything but μ's, a μ identification could be established.

efficiency of the BC's is not 100% this is not always true. Hence, tracks with only a hit in one of the two planes are possible and not uncommon. It is therefore desirable to not require two hits per track for the trigger in order to achieve a higher trigger efficiency. This has been done for TR28 where only one track per halve is required. In the case of TR27, where one requires two tracks in one half, demanding only one hit per track will unnecessarily increase the one-track sample in this trigger. To see this one should remember that only the total multiplicity of hits per halve is available. Assuming that there is at least one hit per track but possibly, and in most cases, even two hits per track, the sum of two tracks can produce a hit multiplicity of two, three or four. Since a single track can produce a hit multiplicity of two, only by requiring at least three hits one can exclude single track events. In addition to the BC multiplicity information, multiplicity information from the hodoscopes are used to isolate multi-track events. Furthermore, events with an excessive front region track multiplicity (an upper threshold on the H0 is placed) are vetoed, since they most likely originate from showers. It turned out that the rate of TR27 still was too high. The fast PCOS OR's of the magnet chamber read out system are used to further clean up the event sample. The MC's are even better shielded because of the septum plate, helping to veto showers.

Another class of events involves the detection of μ's specifically. As mentioned before, the muon wall will shield the HM's from other particles. A hit in the HM's in coincidence with hits in the other trigger detectors, thus, suggests the presence of a μ. Different combinations of triggers are provided involving single and multi track events.

The heart of the trigger is the trigger logic. Different combinations of coincidences (trigger logics) are made possible by the use of programmable logic units (PLU's). The fact that one can program different logics without changing any electronics make them an important and very flexible tool. This is even more true for the case of HERMES where new and different trigger logics are installed almost every year. The PLU's provide any combination of AND, OR and NOT applied to the 8 input signals – thus any 8-fold logic is readily realized. For triggers involving more inputs, two 8-fold logic outputs are used, together with an AND or OR, to provide a quasi-16-fold logic. The strobed coincidence mode is used. This means that a strobe is provided to determine the time to look for a certain trigger logic. The most natural choice for this strobe is the hera clock (HC) signal. It comes directly from HERA and is synchronized with the electron bunch crossing. Before a trigger decision can be made, however, all the signals have to be provided. CAMAC discriminators and programmable delays are used to form the input bus of ECL signals and to establish a well defined timing relation between the different detector signals.[11]

[11]One should keep in mind that at the coincidence unit (PLU) all the signals belonging to one track should overlap. In principle, any (fixed) timing relation between different detectors are possible because of their location within the detector (time of flight will "delay" signals from the back region in comparison to front region detectors) and the different electronics (including signal path, mainly cable length) involved for each detector component.

After a logic decision is made one obtains the raw trigger rate. Not all triggers might be of same importance or interest. In fact, some triggers are only monitoring triggers or even just tests for future trigger and/or detector upgrades. Therefore, single trigger types can be pre-scaled or vetoed by programmable VME pre-scalers. An OR of all (pre-scaled) trigger types is performed (not before the information about the trigger types is secured in latches) and, depending on the status of the data acquisition system, a trigger signal is sent to all the read out modules and the data acquisition system. Before that, however, the signal will be retimed, i.e., synchronized, with the HC signal to, once again, ensure a fixed timing relation between the bunch crossing and the trigger signal.

3.3.4 Monitoring devices

Besides the detectors described above, various components which have mainly monitoring purposes are part of the detector. Here the luminosity monitor (LUMI), the tuning scintillators, as well as the gain monitoring system (GMS) will be described briefly.

The LUMI consists of two calorimeters to the right and the left of the electron beam pipe. They cover an angular acceptance of 4.5 to 8.2 mrad [Benisch]. Luminosity is determined by measuring symmetric scattering, which is due to Møller or Bhabha scattering from the electrons of the target atoms. It can also be used to detect the electron of a low-Q^2 event where the electron scatters at a very low angle.

The tuning scintillator consists of two sets of scintillators, one in front of the FC's and one behind the LUMI. Each set has 2 layers of 4 paddles, the second layer being wrapped with 3 mm of lead, shielding them from synchrotron radiation. (Anti)coincidences between the two layers help to monitor the relative beam position and the amount of synchrotron radiation. This information can be used to tune the beam.

All PMT's at the HERMES experiment are subject to aging. In order to monitor their gain the GMS has been installed. A dye laser sends light pulses of different intensities through glass fibers to every PMT of H2, the calorimeter, the LUMI and to a reference photo diode. By comparing the signals coming from the PMT's to the signal from the reference diode relative gain changes can be detected. The different light intensities is controlled by a filter wheel in front of the laser, which houses different attenuating filters.

3.4 The Data Acquisition System

The main purpose of the data acquisition system is to collect the data of the detectors and convert them into a format which can be used for further analysis. The raw signals from the detectors are digitized using analog-to-digital converters (ADC's) and time-to-digital converters (TDC's). FASTBUS as well as VME modules are used at HERMES. Several FASTBUS crates are equipped with digital signal processors (DSP's) which allow preprocessing of the incoming data. As an example, DSP's could be used for a second level trigger using the ADC information of the hodoscopes. The FASTBUS and VME crates are interconnected. The event builder collects all the digitized data in case a positive trigger decision has been made. The data is then sent via an optical link from the electronics trailer to the DEC/ALPHA computer cluster in the HERMES control room. Hard disks are used as a buffer before writing the data to tape locally (EXABYTE or DLT) and sending it to the HERMES SGI on the DESY main side via a FDDI link. There they are stored again on disk as well as on tape. Parallel to single event information, slow control data is written to disk and tape. Parts of the slow control data are all information which are not specific for one event, i.e., scaler rates, detector status, HERA status and target information. In the off-line analysis, both the slow control information and the event data have to be merged.

Data taking is divided into fills (the length of an electron fill), runs (about 50k events), bursts (time between scaler readout – usually 10 s) and events (each accepted trigger). Scaler rates, as well as most other slow control information, are read out every burst, or, in case of a polarized target, every time the spin state of the target changes. Events are read out immediately. Not every event can be read out since the read out time is about 600 μs during which no trigger can be accepted. This leads to a dead time which increases with increasing trigger rate. The event size is typically about 10 kBytes. Data is transferred and stored in EPIO format.

3.5 The HERMES Event Reconstruction

In the off-line analysis the digitized detector information is used to reconstruct the event. The first step is to decode all the data reading the EPIO files and filling ADAMO [ADAMO] tables with the detector specific information. The decoder is responsible to assign the signals from the hardware channels to the corresponding detectors. In the second step ADC and TDC channel numbers are converted into physical quantities like energies or the position of the track in the tracking chambers. For this step calibration data is provided by servers.

The back-bone of the off-line analysis is the track reconstruction software (HRC – HERMES reconstruction program [Wander]). HRC uses the decoded hits in the tracking chambers to separately construct partial tracks in the front and back region. Afterwards HRC looks for complete tracks by matching the partial tracks at the center of the magnet. In order not to track each particle in the magnet, momentum lookup tables are generated once using the field map of the spectrometer magnet. The particle's momentum will be determined by matching the positions and directions of the partial tracks to the entries in the momentum lookup tables. This reduces the time to reconstruct the event significantly. A special class of tracks are short tracks, named so because there is usually no back track to match the front partial track. This is most likely the case when the particle's momentum is insufficient to travel through the magnet and still be in the acceptance of the back detector. After reconstructing a complete track, PID information are assigned to this track. This is done by tracking the particle through the PID detectors and checking their response of the appropriate module/wire etc. Since all the PID detectors are located in the back region of the HERMES detector, short tracks will not have any PID information. Moreover, since there is not a back track to match with the front track, the MC's are used to track the particle in the magnet and to determine its momentum.

3.6 The HERMES Monte Carlo

The HERMES Monte Carlo program (HMC) is not a direct part of the experimental apparatus or the immediate data analysis. Nevertheless, it is a crucial part of the experiment. It was used to design the experiment and is now used to model detector responses, to calculate acceptance functions and efficiencies, and by using different physics generators one can make predictions about the expected signals and measurements at HERMES.

HMC usually works in two stages: Various event generators, suitable for the physics of interest, will randomly, but weighted by their probability coming from parameterizations of the cross sections, pick scattering kinematics. Afterwards they generate the 4-momenta of the involved particles and, if one is interested, use different fragmentation models (see also 2.5.1) to produce the final set of hadrons. This whole stage is also called event generation. In the second stage one can track the generated particles through a model description of the HERMES detector. The particle interaction with the detector material is simulated using GEANT

[BHHL]. Digitization routines convert the energy loss described by GEANT into signals equivalent to what is obtained from the real detector. The digitization data has the same structure as the output of the decoder for real data, hence HRC can be used to reconstruct the events allowing an equivalent treatment of real and Monte Carlo data.

CHAPTER 4

DATA ANALYSIS

The Λ decays weakly into a pion and a nucleon. The decay $\Lambda \to p\pi$ is the prominent decay channel occurring about 64 % of the time. Fortunately, this is also the most favored decay channel from the experimenter's point of view: both the pion and the proton are charged particles and thus easy to detect and to identify. The analysis presented in this thesis only considers the above decay channel.

The parity-violating decay of the Λ results in an asymmetric angular decay distribution. In the Λ c.m. frame the proton preferably flies in the direction of the spin of the Λ:

$$\frac{d\sigma}{d\Theta_{p\vec{P}_\Lambda}} = \sigma_0(1 + \beta \cos \Theta_{p\vec{P}_\Lambda}) \tag{4.1}$$

$\vec{P}_\Lambda$ is the Λ polarization vector, proportional to the spin vector $\vec{s}_\Lambda$ of the Λ and normalized to unity. $\Theta_{p\vec{P}_\Lambda}$ is the angle between $\vec{P}_\Lambda$ and $\vec{e}_p$, the unit vector in the momentum direction of the outgoing proton (see also figure 4.1). The parity-violating coefficient β has been measured to be 0.642 ± 0.013 [PDG].

If one is only interested in the longitudinal polarization (projection of $\vec{P}_\Lambda$ on

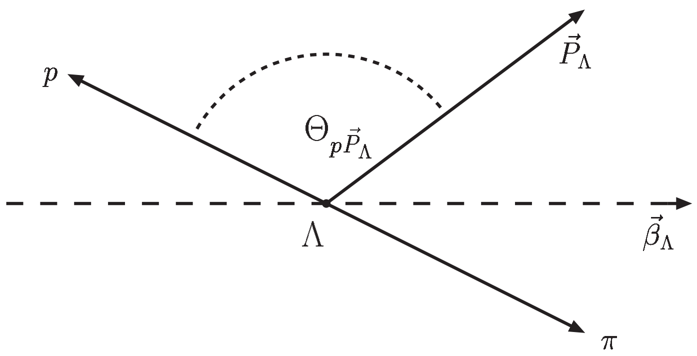

Figure 4.1: Schematics of the Λ decay in the Λ c.m. frame.

the Λ momentum or boost direction $\vec{\beta}_\Lambda$) equ. (4.1) can be written as

$$\frac{d\sigma}{d\Theta_{p\Lambda}} = \sigma_0(1 + \beta P_\Lambda^{||} \cos\Theta_{p\Lambda}). \tag{4.2}$$

$\Theta_{p\Lambda}$ is the angle between the proton and the Λ momentum directions. Since only the longitudinal polarization $P_\Lambda^{||}$ of the Λ is considered in this analysis it will from now on be denoted P_Λ.

It seems to be straight-forward to extract the polarization by just fitting a straight line to the angular distribution. As can be seen in figure 4.2 this does not apply for HERMES. Due to its limited acceptance the angular distribution is highly asymmetric, particularly in the case when all the decay particles have full tracks through the entire detector.[1]

In the laboratory frame the momentum of the proton coming from a Λ will be larger than the momentum of the pion.[2] If the pion and the proton go through

[1]Events, in which all the three required particles (electron, proton and pion) have full tracks, will subsequently be called long tracks. If the pion track is a short track, i.e., does not have a matching back track due to its low momentum, the event will be called a short track event.

[2]This is true as long as the momentum of the Λ is larger than 0.28 GeV which for an detected

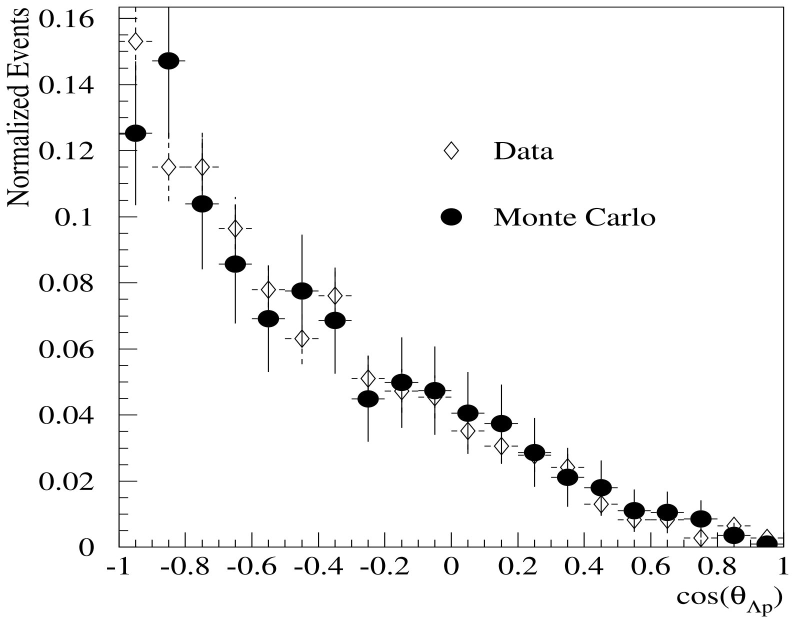

Figure 4.2: The angular decay distribution of the proton in the c.m. frame of the Λ. Data and Monte Carlo points are shown for long tracks. The distribution is highly asymmetric due to the acceptance of the detector (Λ's in HMC are unpolarized).

the whole detector it is more likely that the pion originally (in the Λ c.m. frame) went in the forward direction in order to have enough momentum to get through the magnet without being deflected out of the acceptance of the rear detector. Hence, the proton most likely went backward in the Λ c.m. frame leading to the large asymmetry in the angular distribution.

There are different approaches possible to extract the Λ polarization. One approach is to model the acceptance for Λ's by using HMC. Afterwards one can correct the measured angular distribution, hopefully leading to the real angular distribution due to the polarization of the Λ. Since the Λ is a decaying particle,

event at HERMES is always the case.

its acceptance is rather complicated. Moreover, the hadron responses of the detector is not yet modeled reliably. In order to keep the systematic error on the Λ polarization as small as possible, a large number of generated and reconstructed HMC Λ's is required.

A different approach, which is used in this analysis, is to not be interested in acceptance itself. One rather tries to cancel out the acceptance, i.e., by forming an asymmetry. The advantage of this method is that one does not need to know the exact shape of the acceptance, hence no extensive Monte Carlo studies are necessary to correct the data. The disadvantage is that one relies much more on the stability of the acceptance over time. It is assumed that the acceptance is constant during data taking. Changes in the acceptance can not be corrected for easily and thus contribute to the systematic uncertainty.

The main difference between the two approaches lies in the use of a reliable Monte Carlo simulation of the detector, which (given enough computing power) can reduce the systematic error due to the acceptance to a negligible value in the acceptance correction approach. The assumption that the acceptance stays the same over the whole period of data taking is also not required in the acceptance correction approach as long as one knows how the acceptance changes. For all its beauty this method lacks the practicality at HERMES. The acceptance is hard to model reliably; there is yet to be a sufficiently realistic Monte Carlo model of the detector.

Coming back to the approach of canceling out the acceptance, there are different ways to do so. Both the methods discussed here require the polarization of the Λ to be reversed which is established by reversing the beam helicity.[3] One method is based on count rates in the different $\cos\Theta_{p\Lambda}$ bins and forming an asymmetry. Since the acceptance function cancels out directly this method is also referred to as the method of direct elimination of the acceptance function. Another method uses different moments of the $\cos\Theta_{p\Lambda}$ distributions which will eliminate acceptance effects. Latter method requires a helicity-balanced data set, meaning the integrated luminosity weighted by the (magnitude of the) beam polarization must be the same for the two data sets. It, therefore, will be referred to as the helicity balance method. Both methods are described in more detail in Appendix F.

4.1 Data Selection

In this analysis only data from the two dedicated unpolarized run periods were used. During this time the beam helicity (and thus the source for any Λ polarization in current fragmentation) has been reversed: the 1996 running period used positive beam helicity and the 1997 running period used negative beam helicity.

[3] It is assumed that the only longitudinal polarization arises from the polarization transfer from the beam to the produced Λ.

4.1.1 Overview of applied cuts

General data quality cuts (see Appendix E) are applied to the data before being processed any further. This is done on a burst level analysis. After this each event is examined for the presence of possible Λ candidates in conjunction with a DIS electron. Oppositely charged hadron[4] tracks are used to reconstruct the invariant mass of the assumed parent particle. In case of the parent being a $\overset{(-)}{\Lambda}$, the particle with the higher momentum is assumed to be the (anti)proton. The other hadron is assumed to be the pion.[5]

Following kinematic and geometric cuts on the electron track are applied:

$$24 > Q^2 > 1 \tag{4.3}$$

$$W^2 > 4 \tag{4.4}$$

$$y < 0.85 \tag{4.5}$$

The first two of these cuts (Q^2 and W^2) insure a DIS positron while the y cut avoids a region where excessive radiative corrections would be necessary. To avoid fluctuations of the trigger threshold a hard cut on the energy deposit in the calorimeter is applied:

$$E_{calo}^{backtrack} > 4.0 \tag{4.6}$$

[4]The HERMES PID scheme is used to discriminate between hadrons ($PID3 + PID5 < 0$) and electrons ($PID3 + PID5 > 0$).

[5]The decision about the parent being a Λ or a $\bar{\Lambda}$ is made using the charges of the daughter particles: If the hadron with the larger momentum is positive the parent is a Λ candidate and vice versa. In the case of the K_s^0 analysis both hadrons are assumed to be pions.

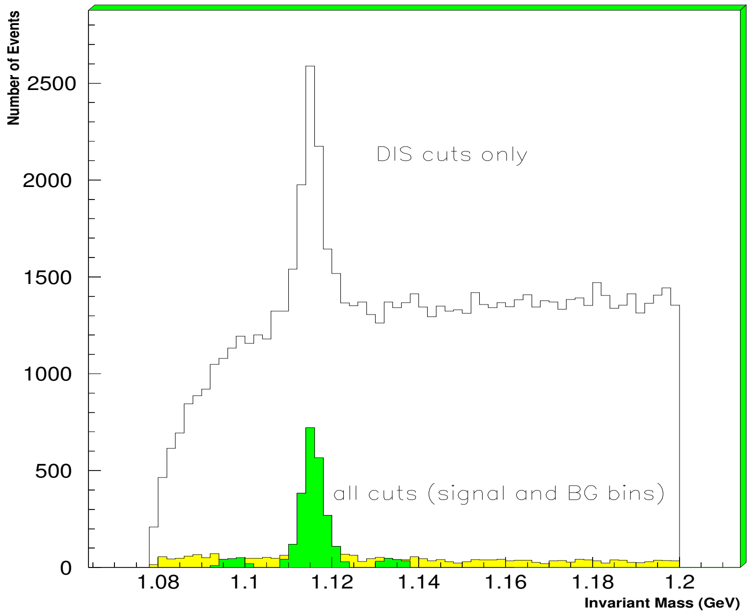

Figure 4.3: Mass spectrum for the 1997 data before and after background reducing cuts. Also indicated are the regions used for the calculation and BG subtraction.

Furthermore, to assure that the scattered electron comes from the target cell and not from collimators or other sources a cut on the z_{vtx} position is applied:

$$-20\text{cm} < z_{vtx} < 20\text{cm}, \qquad (4.7)$$

where the z_{vtx} position denotes the point of closest approach of the electron track to the beam line.

The resulting mass distribution (upper curve in figure 4.3) shows a clear Λ peak over a considerable background. In order to reduce this background several other cuts, both on track kinematics and PID detector responses, are applied to the data.

The only further PID cut on the hadrons is a cut on the Cherenkov counter response. Protons will not fire the Cherenkov counter (c.f. table 3.1). Therefore, a cut is placed on the Cherenkov response[6]:

$$\text{Cherenkov} < 0.3. \tag{4.8}$$

In principle, time of flight (TOF) information could also be used to discriminate different hadrons. This would be of particular interest since a pion/proton discrimination by means of the Cherenkov counter is only possible for hadrons with momenta bigger than about 4 GeV. Time of flight would give information for lower momenta particles (< 2 GeV). However, most protons have already a larger momentum than that, at least after applying an x_f cut. Moreover, problems with the reliability of the TDC information during some periods of data taking questioned the assumption of a steady acceptance when applying a TOF cut. The slight gain in the statistical uncertainty did not justify the involved systematic uncertainty. Nevertheless, there does not seem to be a reason why the TOF information can not be used for future data taking, in particular when there will be access to the target fragmentation due to the installation of the Λ wheels, a new detector designed to track low momentum pions. Those events will also have lower momentum protons making TOF a good PID. The effect of the Cherenkov and TOF cut on the mass spectrum can be seen in figure 4.4.

[6]The cut is placed such it is above pedestal but below the one photo-electron peak (see also figure 4.4).

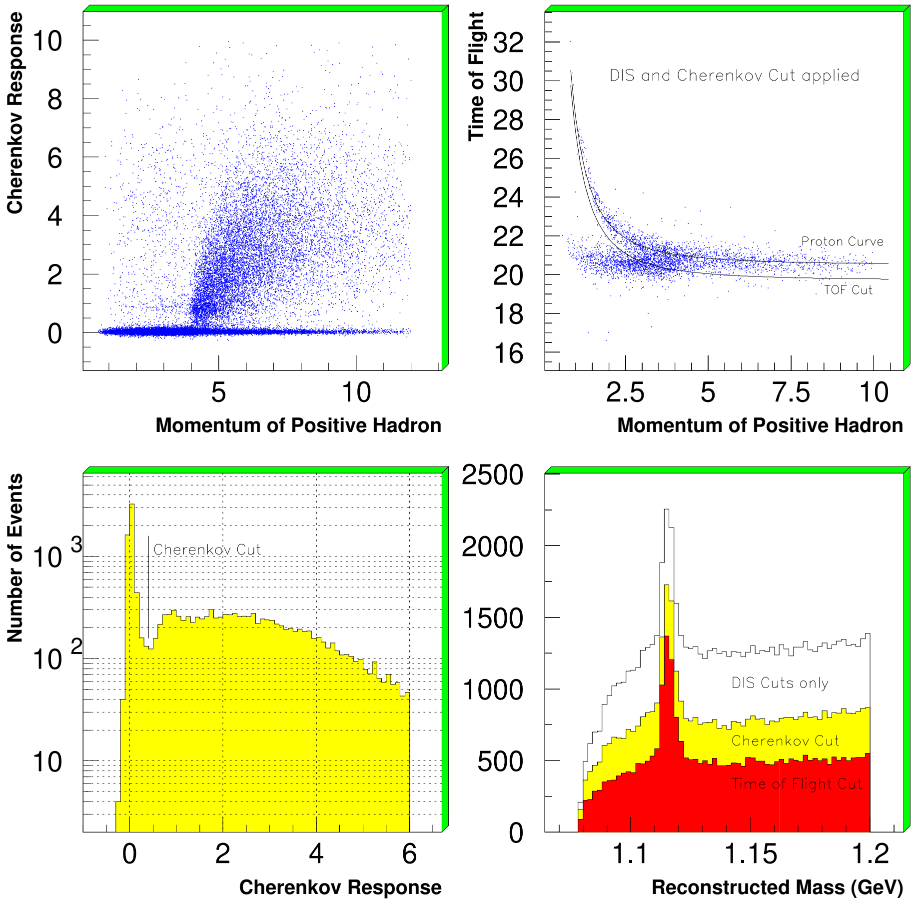

Figure 4.4: Proton Identification by using the Cherenkov and Time of Flight Detectors. The Cherenkov response is used to discriminate between protons and pions for momenta greater than 4 GeV (left pictures). The Time of Flight information is used for low momentum protons (upper right picture. The effect on the mass spectrum can be seen in the lower right picture.

Further cuts have to be applied to reduce the background. In order to come from a decaying Λ, the pion track as well as the proton track have to come from a common point in space: the decay vertex of the Λ. Due to the finite tracking resolution this will never be the case for the reconstructed tracks. A cut is placed on the distance d at closest approach of the two hadron tracks:

$$d < 1.5\text{cm} \tag{4.9}$$

The closest approach is used to define the Λ decay vertex, also called the secondary vertex. There are a few possibilities to define the secondary vertex: being on the proton track, being on the pion track, using the mid point between proton and pion track or using the error on the track parameterization to find a weighted mid point. For simplicity, the mid point between the two tracks is used, though studies showed that any of above definitions would be fine and will give similar results. The primary vertex, also called the interaction point or the Λ production vertex, is defined through the closest approach of the scattered electron track and the beam line. Same arguments as before apply for the choice of the actual vertex. A cut is applied on the smallest distance t_{vtx} between the scattered electron track and the beam line:

$$t_{vtx} < 0.75\text{cm}. \tag{4.10}$$

The Λ track can be defined in two ways: One can either add the momenta of the two hadrons which should be the Λ momentum $\vec{p}$ if the two hadrons are the decay products of the Λ, or one uses the vector $\vec{x}$ connecting the two vertices, the production vertex and the decay vertex. If the Λ hypothesis is correct both the methods should give tracks with the same direction. A cut can therefore be placed on their collinearity:

$$\frac{\vec{p} \cdot \vec{x}}{|p||x|} > 0.9995 \tag{4.11}$$

Another cut is placed on the separation of the two vertices. Since the Λ is a relatively stable particle, its $c\tau$ is 7.89 cm, it will travel through the detector and decay later than most other hadrons.[7] Demanding that the vertex separation is larger than 10 cm will thus eliminate most of the short-living hadrons. This cut is also applied to avoid problems with the limited resolution as will be discussed in section 4.3.

In order to select the current fragmentation region a cut on the forwardness of the Λ in the $p\gamma$ c.m. frame is applied:

$$x_f > 0. \tag{4.12}$$

After all those cuts a well defined Λ peak is visible with a low background contaminating the signal (lower curve in figure 4.3). For the event selection we apply a cut on the Λ mass which is wide enough to account for the different widths of the distributions in the different years and from the different reconstruction

[7]Except the K_s^0 with a $c\tau$ of 2.68 cm. It is also produced sufficiently often in order to contribute to the background.

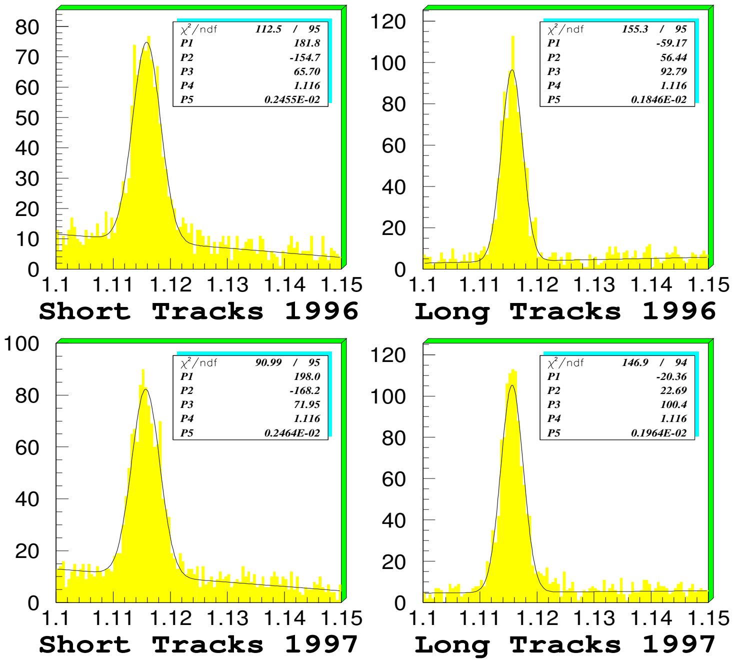

Figure 4.5: Reconstructed mass of $p\pi$-system after DIS cuts, cuts on vertex and track separation, cherenkov response as well as on collinearity.

methods, but also avoiding a high contamination from the background[8]:

$$|m_{p\pi} - 1.1157| < 0.007. \tag{4.13}$$

In figure 4.5 the resulting peaks for the different years and the different track types can be seen.

For the background subtraction following mass bins are used to calculate the contribution form the background to the Λ polarization value:

$$0.01 < |m_{p\pi} - 1.1157| < 0.035 \tag{4.14}$$

[8]Averaged over all tracks and both years the mass cut is equivalent to a 3σ cut using a Gaussian fit of the reconstructed mass peak.

4.1.2 Helicity Balanced Run List

In order to use the helicity balance method to eliminate acceptance effects one needs to balance the lists of runs used in either year such that $||P_B|| = 0$ (c.f. equ. (F.34)). The integration involved can be over any quantity which represents the luminosity at HERMES. One could use the target information (target gas and density) as well as the beam current to calculate the luminosity. Since the target information are not very precise this would involve a rather large systematic uncertainty. The LUMI could be used which measures the rate of Bhabha or Møller scattered electrons. This is a rather precise tool to measure relative luminosities and is used in the polarized target program. There, however, the DIS rate, or better the difference in the DIS rates for different target spin states, is the subject of interest, and thus could not be used to measure the luminosity. Moreover, using the LUMI requires to fold in all the detector and trigger efficiencies in order to obtain a correct event weighting. The most practical quantity to use is the number of DIS events. With an unpolarized target the DIS rate is proportional to the luminosity.[9] In addition, detector and trigger efficiencies are already folded in - one does not have to correct for them. Thus, condition (F.34) reduces to[10]:

$$\sum_{\text{DIS 1996}} P_B + \sum_{\text{DIS 1997}} P_B = 0. \tag{4.15}$$

[9]The DIS rate is also proportional to the luminosity in the case of a polarized target. However, the constant of proportionality depends on the spin state of the target.

[10]Note that the sign of P_B changes from one year to the other.

One resulting run list (based on all the runs which pass the DQ cuts) consists of all the runs in 1996 and the required number of runs in 1997 to fulfill (4.15):

$$12756 < \quad \text{run\#} \quad < 14134 \tag{4.16}$$

$$18353 < \quad \text{run\#} \quad < 19651, \tag{4.17}$$

which results in

$$||P_B|| = 0.0000055 \approx 0. \tag{4.18}$$

One concern arising is that the DIS event set is not the best representation of the Λ event set. This can be caused by a different and changing hadron efficiency of the detector. In fact, it is known [Bern] that the chamber efficiencies are less for hadrons compared to electrons. Also, it is not guaranteed that for a period of constant tracking efficiency for electrons the tracking efficiency for hadrons will be constant too. A normalization[11] based on the 2-hadron count rate (granted the 2-hadron event is also a DIS event, i.e., two hadrons and a DIS electron are detected) is a more appropriate normalization. (Note that 2-hadron stands for 2 oppositely charged hadrons coming from the target cell.) When applied one indeed obtains a slightly modified run list:

$$12756 < \text{run\#} < 14134 \tag{4.19}$$

[11]Normalization and helicity balancing will be used in this contents and represent the same idea.

$$\left.\begin{array}{ll} \text{long tracks:} & 18342 \\ \text{short tracks:} & 18495 \\ \text{all tracks:} & 18370 \end{array}\right\} < \text{run\#} < 19651. \tag{4.20}$$

4.1.3 DIS and Λ yields

After applying all the cuts and selecting the run list one obtains the final data set which is used to extract the spin transfer coefficients. The total number of DIS events is about 4.9 million both years combined. The number of Λ's is about 1400 in 1996 and 1480 in 1997 of which around 56% come from long tracks.

Furthermore, it should be mentioned that the average beam polarization $\sqrt{||P_B^2||}$ is 51%.

4.2 Results

Using the helicity balanced event sample one can extract the spin transfer coefficient. The result can be seen in figure 4.6 which is based on a 2-hadron normalization, using all of the previously mentioned cuts. Background subtraction was done using the fit method.

Table 4.1 summarizes the results for different z bins and for data which includes lower Q^2 values ($Q^2 > 0.8GeV^2$). The average Λ polarization can be calculated by using (2.66) and $\mathcal{P}_B = 0.51$ as well as $D(y) = 0.69$, which gives $\mathcal{P}_\Lambda = 0.01 \pm 0.06$.

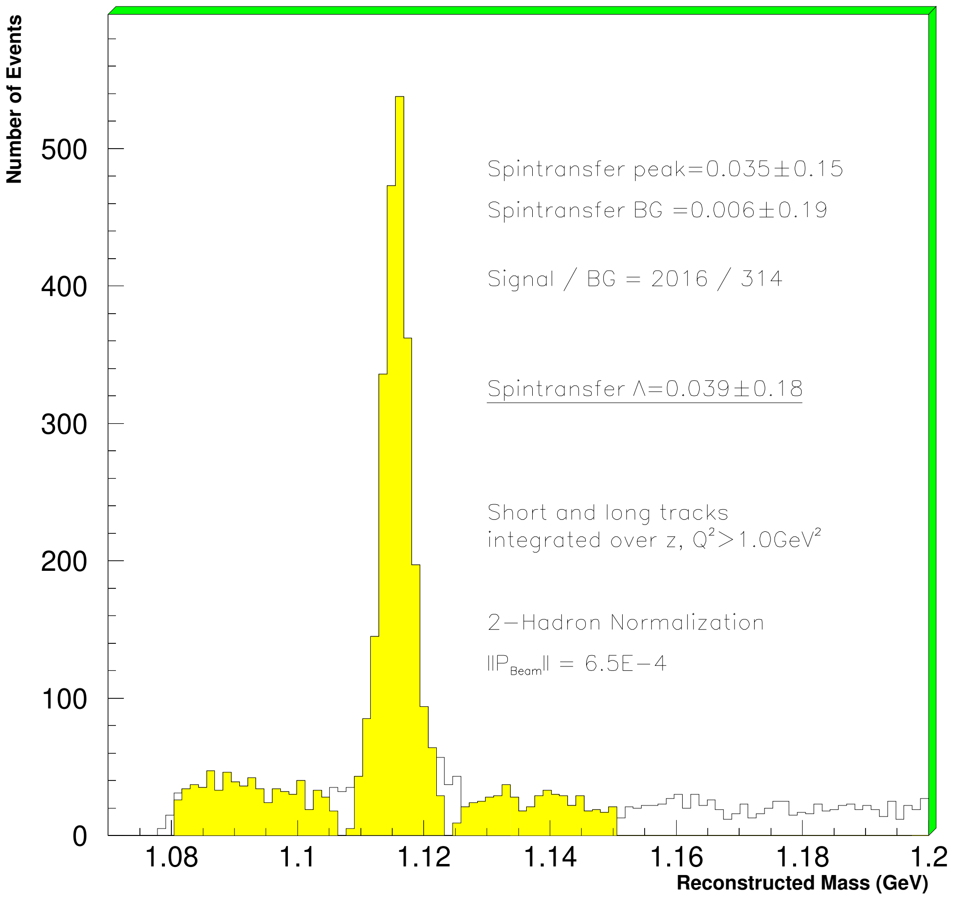

Figure 4.6: Spin transfer coefficient derived from the HERMES 1996/97 unpolarized data.

Table 4.1: Λ spin transfer averaged over z as well as for two z bins ($z < 0.4$ and $z > 0.4$. Included are all tracks, short and long, with a DIS electron of $Q^2 > 1.0(0.8) GeV^2$

		Λ spin transfer	
z	$< z >$	$Q^2 > 0.8$	$Q^2 > 1.0$
all	0.448	0.043 ± 0.165	0.039 ± 0.178
$z < 0.4$	0.314	0.071 ± 0.232	0.111 ± 0.252
$z > 0.4$	0.543	0.018 ± 0.230	-0.023 ± 0.246

4.3 Systematic Studies

It is not always wise to just trust your detector blindly and believe the result obtained is a correct picture of the physics involved. It is, therefore, appropriate to perform systematic studies to verify that the assumptions made are indeed reasonable ones. In this particular case one could look for similar (i.e., decaying) particles where the answer is known. The K_s^0 is one example; it should not be polarized. If a considerable spin transfer would be observed, the result for Λ's should be handled with care. One can also check that the result is consistent for different situations which should not have an influence on the result. Systematic checks have been done and will be summarized here.

4.3.1 Decay Length and Collinearity

As mentioned before the HERMES detector and the HERMES reconstruction only have a finite resolution. It can happen that the vector from the positron vertex to the Λ decay vertex is not collinear at all with the reconstructed momentum vector of the Λ, especially when the two vertices are close to each other. It might even happen that the Λ appears to first travel backward before it decays, according to the HRC output. This, of course, is an artifact of tracking. In those cases the event will be thrown out by the collinearity cut. One has to be careful though that one does not bias oneself towards one data sample (i.e., year) as the resolution might have changed, may it be only slightly. In particular short tracks are more sensitive to changes in the detector since less information is available for reconstruction. The cut value chosen (10 cm) proved to cut out background (i.e., particles which actually were produced at the positron vertex) and to avoid these resolution effects. In Figure 4.7 one can see that in the case of small separations between the reconstructed positron vertex and the Λ-decay vertex the Λ momentum direction is not anymore collinear to its reconstructed travel direction (shown only for short track Λ's) .

4.3.2 Polarization of the K_s^0

Similar to the Λ, the K_s^0 is a relatively long living particle. However, being a spinless particle, its angular decay distribution should be flat in the K_s^0 c.m. frame. As one can see in figure 4.8 this is not true at HERMES. This again is

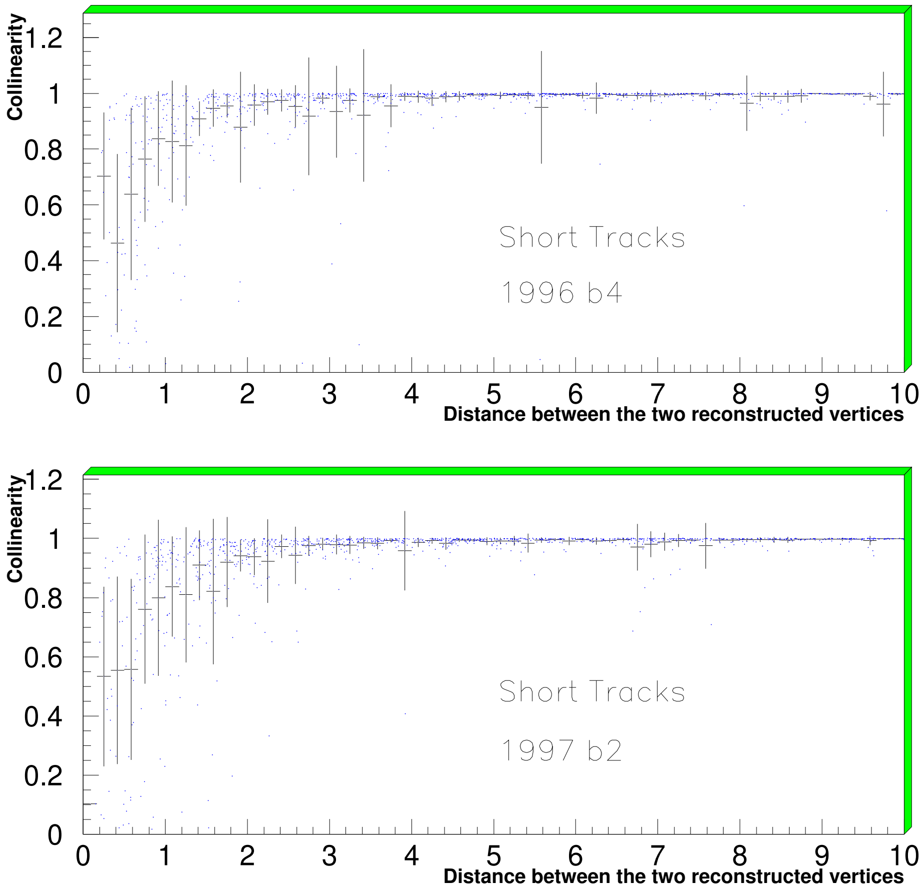

Figure 4.7: Collinearity of short track Λ's as a function of the separation of the reconstructed positron vertex and the Λ-decay vertex.

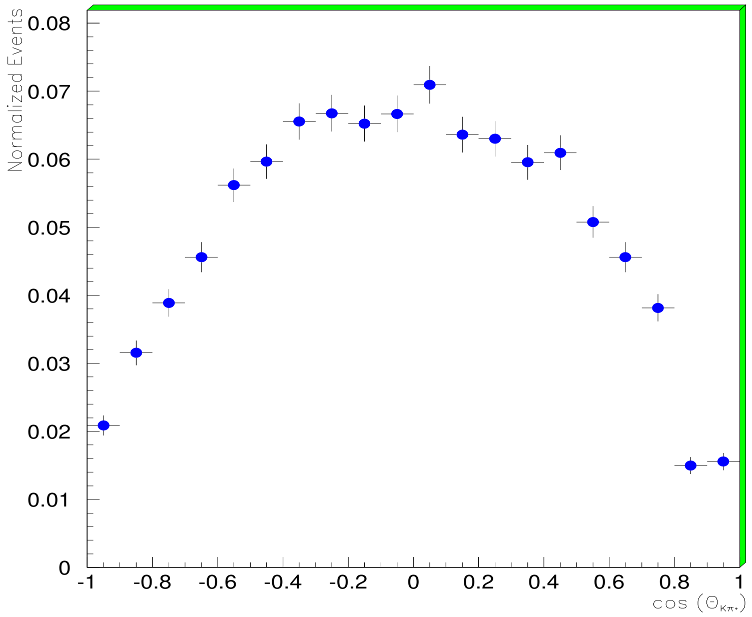

Figure 4.8: The angular decay distribution of the positive pion in the c.m. frame of the K_s^0. Data is shown for long tracks. Due to acceptance effects the distribution is not flat as expected

due to the fact that HERMES has a limited acceptance. Once again, one can apply the same apparatus used for the Λ's and eliminate acceptance effects. The resulting spin transfer term is consistent with zero as expected (figure 4.9). The same background-reducing cuts as in the case of the Λ have been applied.

One concern could arise from the fact that events under the Λ peak can be mis-identified K_s^0 events. One could cut out all events whose invariant mass $M_{\pi\pi}$ is part of the K_s^0 mass peak. However, since too many Λ's are cut out by such an approach and cutting out the K_s^0 peak leaves a gap in the angular distribution of the decaying Λ (see figure 4.10), no cut on the K_s^0 mass is applied. This is also motivated by the fact that K_s^0 are indeed unpolarized and the arising BG will be properly treated by subtracting the background.

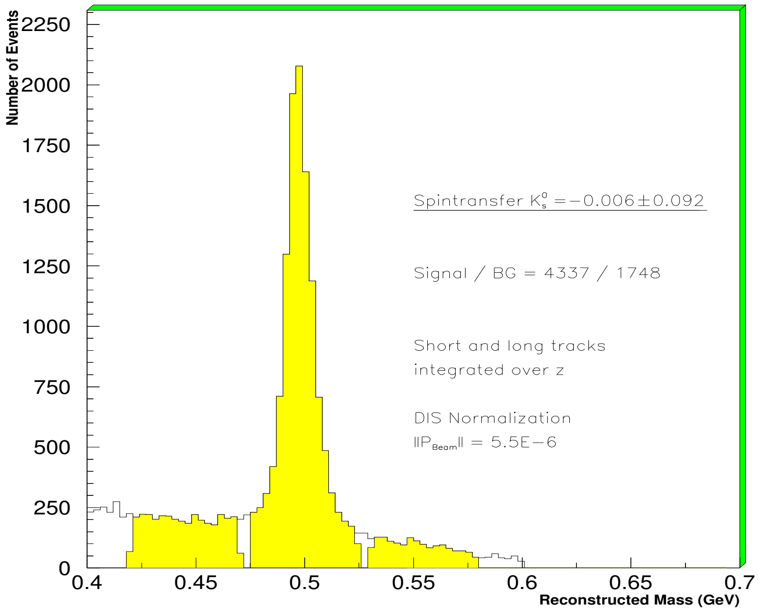

Figure 4.9: Spin transfer coefficient for K_s^0's derived from the HERMES 1996/97 unpolarized data.

4.3.3 Consistency Checks

Different consistency checks have been performed to ensure there are no systematic effects. The data set has been divided into smaller samples, i.e., Λ's in one of the two detector halves, usage of different cut values, all studies which do not change the physics involved and which should give a consistent result. No inconsistencies have been observed.

The data sample has been divided into short and long tracks as well as top and bottom, where top (bottom) stands for "π goes into top (bottom) part of the detector." The kinematic distribution (mainly z is of interest here) differ slightly for short and long tracks (short tracks have in average a lower z than long tracks). Within statistics no effect on the result can be seen (figure 4.11).

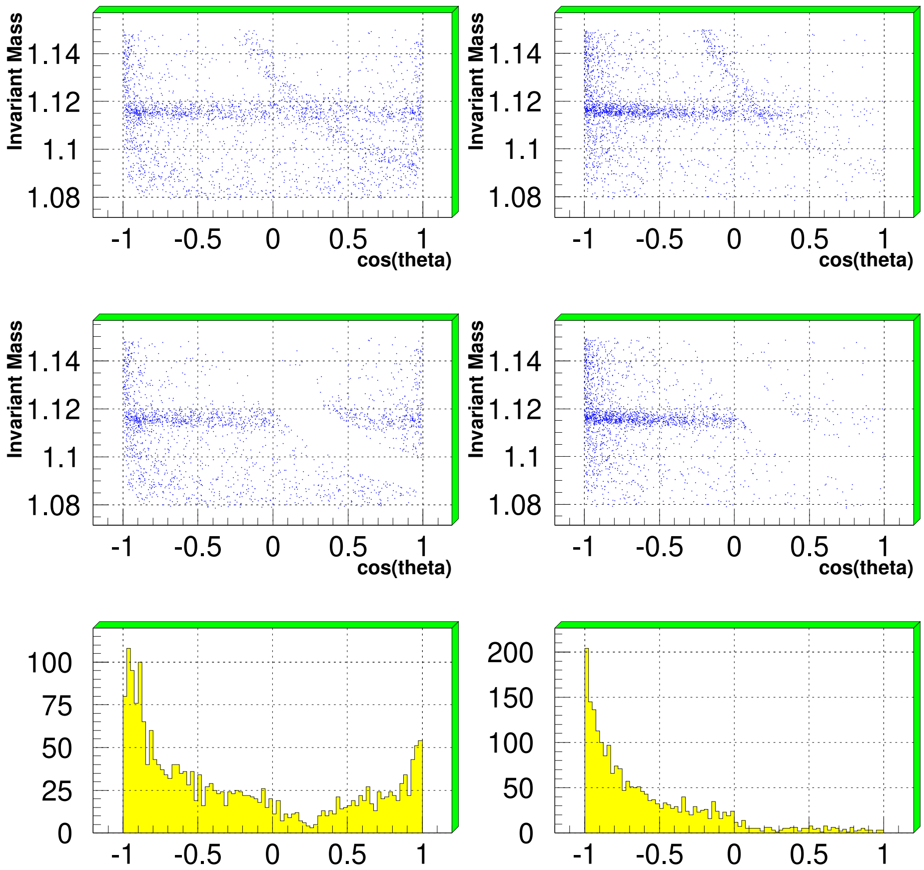

Figure 4.10: K_s^0 contamination of the Λ sample. In the upper two plots one can clearly see the K_s^0 band which is cut out in the middle two plots. This results in a dip in the angular distribution as seen in the lower two plots. There is no Cherenkov cut used, which would suppress π's in the positive hadron sample. However all the other cuts were applied. Left plots are short tracks and right plots are long tracks.

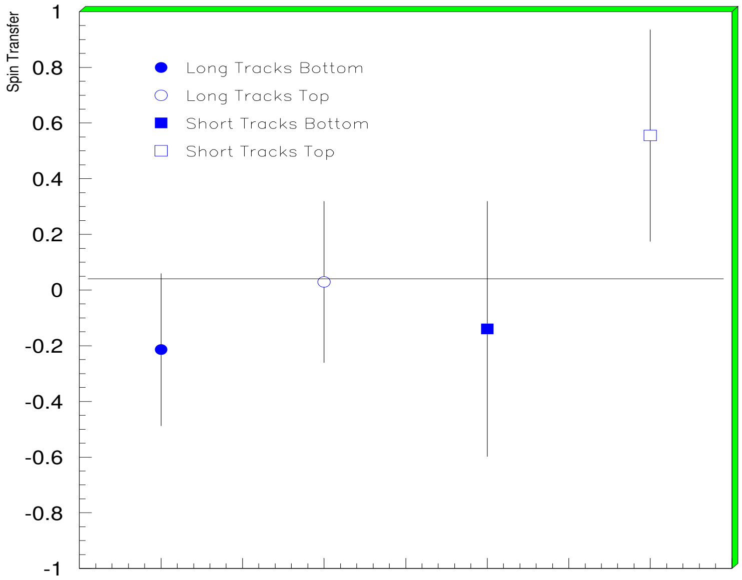

Figure 4.11: The Λ spin transfer for Top/Bottom and Short/Long tracks separately.

The collinearity cut is a cut sensitive to the tracking resolution and, hence, to any changes in the tracking resolution. Different bins in collinearity have been checked to make sure that our sample does not suffer from such changes (figure 4.12).

Although the longitudinal Λ polarization does depend on the polarization of the initial electron, the Λ spin transfer does not. This was one of the reasons to introduce this quantity. This fact can be used for another consistency check by examining only certain beam polarization bins. As can be seen in figure 4.13 the results are consistent.

The most obvious independent variable is probably time. Splitting up the data in different random (but balanced) sets also resulted in no apparent incon-

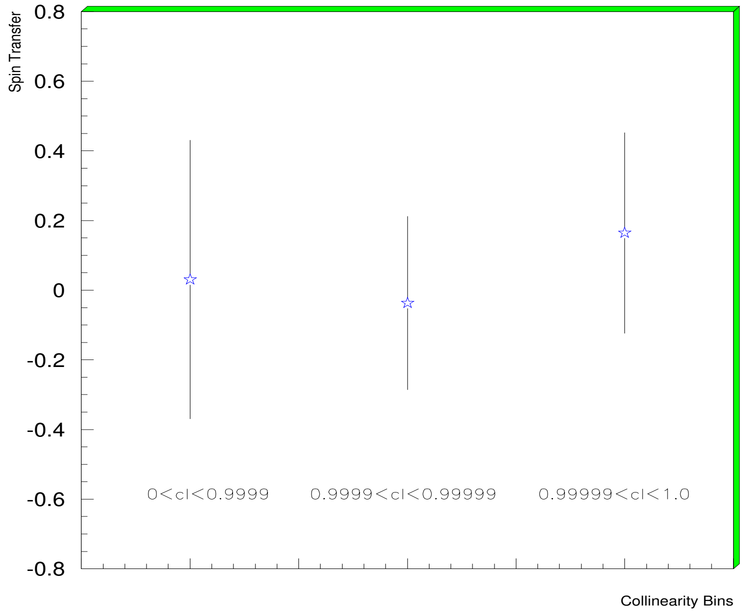

Figure 4.12: The Λ spin transfer for different collinearity bins.

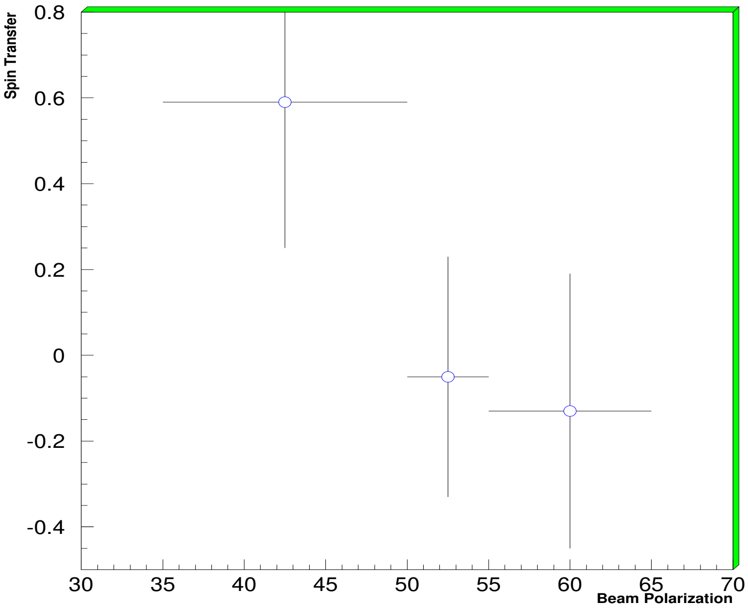

Figure 4.13: The Λ spin transfer for different beam polarization bins.

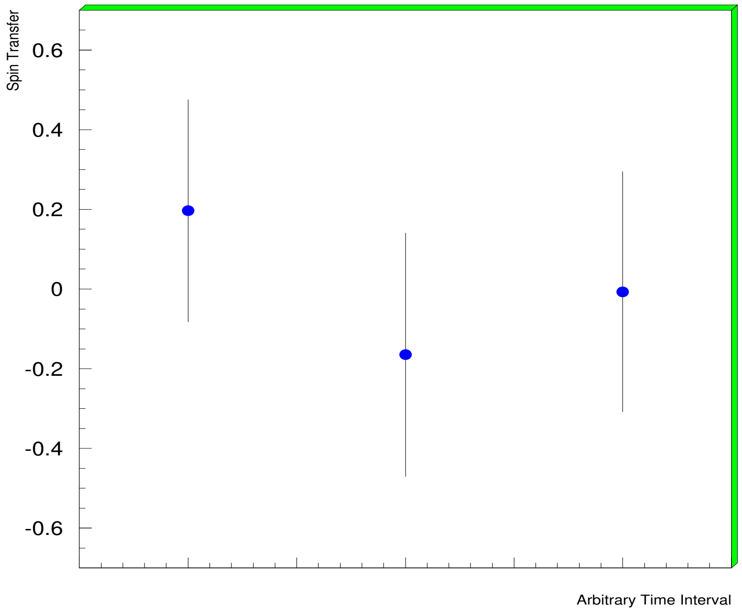

Figure 4.14: The Λ spin transfer for different (arbitrarily chosen) time bins.

sistency (figure 4.14). The running periods have been divided into 3 about equal size segments; one at the beginning, one in the middle and one at the end of either of the two running periods.

Last but not least, the result is compared using different cuts, i.e., dropping certain cuts from the list of cuts. Furthermore, the K_s^0 peak in the reconstructed $\pi^+\pi^-$ mass has been removed, as well as a cut on the coplanarity[12] has been applied. The different cuts and the results are listed in table 4.2 and also shown in figure 4.15.

[12]Similar to the collinearity, a cut on the coplanarity of the two vectors $\vec{p}_\Lambda$ and $\vec{x}$ (see section 4.1) can be applied, where the coplanarity is defined as $\frac{\vec{p}\times\vec{x}}{|p||x|}$.

Table 4.2: Λ spin transfer for different cut combinations. Results are based on a DIS normalization. Results are also plotted in figure 4.15. (If not noted otherwise, standard cuts as described in 4.1 are used.)

Cut	Description	Λ spin transfer
1	standard cuts	0.014 ± 0.176
2	$Q^2 > 0.8$	0.022 ± 0.164
3	$\frac{\vec{p}\cdot\vec{x}}{\lvert p\rvert \lvert x\rvert} > 0.998$	0.080 ± 0.174
4	K_s^0 mass peak excluded ($\lvert M_{\pi^+\pi^-} - 0.5\rvert > 0.02$)	0.021 ± 0.178
5	no cut on d	-0.006 ± 0.178
6	no cut on vertice separation	0.043 ± 0.181
7	$\frac{\vec{p}\cdot\vec{x}}{\lvert p\rvert \lvert x\rvert} > 0.0$	0.069 ± 0.175
8	no cut on Cherenkov counter, but on coplanarity	-0.043 ± 0.221

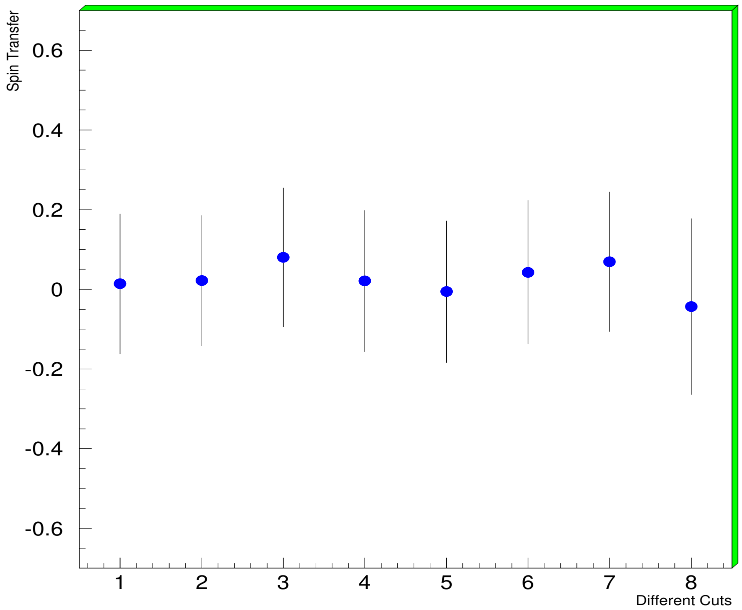

Figure 4.15: The Λ spin transfer for different applied cuts. The cuts are listed in table 4.2.

4.3.4 Comparison with Method of Direct Elimination

As already mentioned there are different methods of extracting $\hat{Q}$. Though the method using helicity balancing gives the best statistical error bar the method of direct elimination of the acceptance function gives a good cross check of the result. Using the same run list the method of direct elimination gives:

$$\hat{Q} = 0.05 \pm 0.22 \tag{4.21}$$

agreeing with the result from fig. 4.6. 30 bins in $\cos\Theta_{p\Lambda}$ are used; the χ^2 per degree of freedom for the linear fit is 0.97.

4.3.5 Random Beam Helicity Flip

To extract the spin transfer coefficient one needs to reverse the beam helicity. For systematic studies one can, however, use the data from one helicity state and artificially reverse the helicity by assigning a minus sign to the beam polarization for a part of the data. Using the 1996 data set, a false asymmetry consistent with zero was obtained:

$$\hat{Q}_{false} = 0.021 \pm 0.21. \tag{4.22}$$

CHAPTER 5

INTERPRETATION AND CONCLUSIONS

HERMES measured a Λ spin transfer consistent with zero. This might not be a surprise considering the fact that most of the Λ's produced at HERMES originate from a u quark, which is not polarized (naïve QPM) or only slightly polarized (BJ model – SU(3) rotation of proton data) within the Λ. If one assumes that the polarized quark fragmentation functions behave like their counterpart, the polarized quark distributions, then the u quark does not contribute significantly to the polarization of the produced Λ.

Nevertheless, this result gives valuable information. First of all, knowing the polarized u quark fragmentation gives a constraint on the SU(3) invariants $\hat{F}$, $\hat{D}$ and $\hat{\Sigma}$ of polarized Hyperon production (see section 2.5.2). Combining the result with the results from LEP [ALEPH, OPAL] where the Λ polarization is sizeable (>30%) or with results of polarized production of hyperons other then the Λ, one can single out the above constants and test for any SU(3) symmetry of polarized Hyperon production.

5.1 Monte Carlo Prediction

Not knowing the polarized fragmentation functions, a analysis based on a Monte Carlo simulation similar to the one performed in ref. [KBH] has be done. Here, cf., sections 2.5.2 and 2.6, one assumes the polarized fragmentation to be proportional to the polarized quark content. The studies performed in this analysis are based on the HERMES Monte Carlo package, utilizing a DIS generator to generate event kinematics. The LUND fragmentation model is used to hadronize partons generated by the DIS generator.

5.1.1 Origin of the Λ

The LUND fragmentation model not only provides a description of the final state, it also allows one to have a closer look at the "production history" of the Λ. Most of the Λ's at HERMES are produced by u-quark fragmentation (table 5.1). This is expected, since scattering off a u-quark is the dominant channel in DIS from a proton at HERMES energies. More interesting might be the production channels of the Λ's. Not all Λ's are produced directly (i.e., from string breaking in the "LUND language"). A substantial part of Λ's produced come from the decay of excited hyperons, most prominently from the decay of the $\Sigma(1385)$. Being a strong decay, this is part of the Λ fragmentation process. However, a non-negligible number of Σ^0 contribute to the Λ production as well. The most common sources of Λ's are summarized in table 5.1.

Table 5.1: Relative contributions of different sources to the Λ production

Parent	Contribution	Struck Quark	Contribution
String	51%	u	76%
$\Sigma(1385)$	29%	d	12%
Σ^0	18%	s	9%
Ξ and others	2%	other	3%

Table 5.2: LUND parameters used for modeling Λ production

Parameter	Description	LUND default	HERMES
parj(1)	$\frac{P(qq)}{P(q)}$ (di-quark suppression)	0.10	0.10
parj(2)	$\frac{P(s)}{P(u)}$ (s-quark suppression)	0.30	0.16
parj(21)	width for p_x, p_y - transverse momentum distributions for primary hadrons	0.36	0.33
parj(41)	a parameter for symmetric Lund fragmentation	0.30	0.89
parj(42)	b parameter for symmetric Lund fragmentation	0.58	0.24

All the Monte Carlo studies done use the LUND parameters tuned for the HERMES experiment. The main parameters are summarized in table 5.2.

5.1.2 Model of the Λ spin transfer

The main motivation for this Monte Carlo study is to have a consistent model of the Λ spin transfer. Various attempts to predict the Λ polarization at HERMES exist (see section 2.6) but lack consistency in their treatment of different scenarios.

In this model, a simple Ansatz is used to calculate the resulting/measured[1] spin transfer:

$$\Delta\hat{q}^{\Lambda} = c_q \hat{q}^{\Lambda}. \tag{5.1}$$

In principle, the c_q's can be functions of z; for simplicity, however, they are assumed to be constants. Moreover, assuming that the polarization transfer is proportional to the quark polarization (quark helicity conservation), one can use different scenarios for the c_q's:

- Naïve QPM – all the spin is carried by the s-quark
- BJ model (SU(3) rotation of Δq^p) – u and d are polarized as well.

The above Ansatz is only valid for Λ's produced in a strong process. Λ's coming from the decay of other hyperons have to be treated more carefully. All hyperons can, in principle, be polarized. A similar Ansatz as in the case of the Λ is made to calculate their polarization. In order to obtain the resulting Λ polarization one needs to know the polarization transfer from the parent particle to the Λ. From this the resulting polarization of the Λ can be calculated. Table 5.3 summarizes the different contributions and the expected polarization transfer. It should also be noted that the unfavored fragmentation channels, i.e., $\Delta\hat{\bar{q}}^{\Lambda}$, are assumed to not contribute to the final polarization of the Λ. This is supported by the negligible contribution to the Λ production in general (table 5.1).

[1]Note that the measured spin transfer does not completely correspond to $\hat{Q}$ introduced in section 2.6 since contributions from decaying particles are included.

Table 5.3: Polarization transfer to Λ depending on production channel. Polarization transfers from decaying hyperons are taken from [GH, Dukes].

Parent	Naïve QPM			BJ Model			Polarization transfer from parent
	c_d	c_u	c_s	c_d	c_u	c_s	
Fragmentation	0.0	0.0	1.0	-0.2	-0.2	0.58	NA
Σ^0	$\frac{2}{3}$	$\frac{2}{3}$	$-\frac{1}{3}$	0.32	0.32	-0.45	$-\frac{1}{3}$
Ξ^0	$-\frac{1}{3}$	0	$\frac{4}{3}$	-0.45	-0.16	0.79	0.9
Ξ^-	0	$-\frac{1}{3}$	$\frac{4}{3}$	-0.16	-0.45	0.79	0.9

For the event selection DIS cuts are applied. Furthermore, an x_f cut of $x_f > 0$ is used. Since it is not necessary to track the Λ (or it's decay particles) through the detector, this time intensive step is avoided. Instead, a simple box acceptance is used requiring that

$$40\text{mrad} < \quad |\Theta_{vert}| \quad < 140\text{mrad} \tag{5.2}$$

$$|\Theta_{horiz}| \quad < 170\text{mrad}. \tag{5.3}$$

Moreover, the energy of the Λ has to be bigger than 2 GeV.

Figure 5.1 shows the resulting Λ spin transfer for the two different scenarios. As expected, the Λ spin transfer is about zero for the naïve QPM scenario and negative for the BJ model, which comes from the fact that u-quarks dominate Λ production at HERMES and the only other significant contribution to the Λ

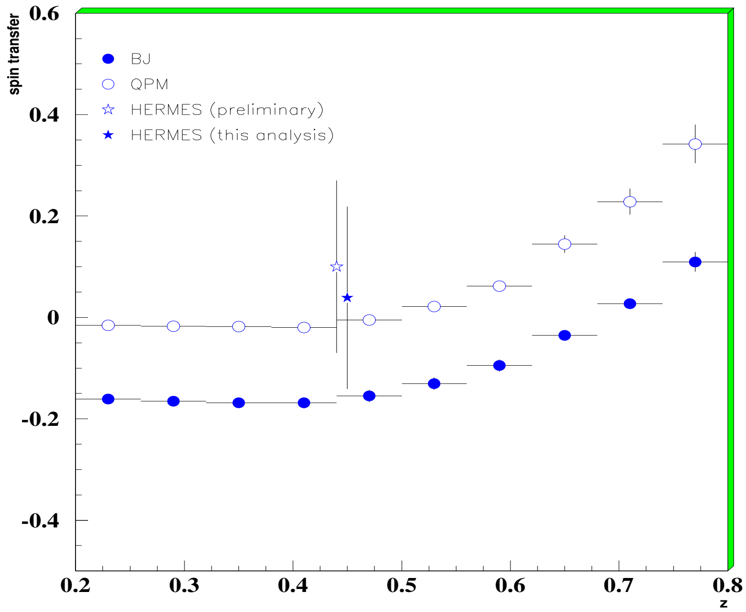

Figure 5.1: Monte Carlo prediction for the Λ spin transfer based on the assumption of helicity conservation in fragmentation and using the naïve QPM as well as the BJ model as inputs.

polarization, besides direct production, comes from the Σ^0, providing a small correction.

Last but not least an integration over z is performed based on the experimentally measured z distribution. This gives a quantity which can be compared directly to the experimental result. The values for the Λ spin transfer integrated over z as it is done at HERMES are shown in table 5.4.

One can also use a different parameterization of the polarized fragmentation functions. As mentioned in section 2.5.2, in [deFlo] a z-dependence z^α to Ansatz

Table 5.4: Integrated values of the Λ spin transfer. Shown are the values measured at HERMES and the Monte Carlo predictions using different models for the spin transfer.

Λ spin transfer		
HERMES	MC - naïve QPM	MC - BJ
0.04 ± 0.17	0.02	-0.14

(5.1) has been added. The resulting polarized fragmentation functions are thus

$$\Delta\hat{q}^{\Lambda} = z^{\alpha} c_q \hat{q}^{\Lambda}. \tag{5.4}$$

The unpolarized fragmentation functions were obtained from fits to data and α is a scenario-dependent parameter from a fit to the LEP [ALEPH, OPAL] result on Λ polarization. The description of the different scenarios can be found in section 2.5.2. One should note that in this approach decays from other hyperons were not excluded, thus, they are included in the fits for the fragmentation functions.

In this study the obtained values of α (Table 2.5) as well as the assumptions for c_q ($c_s = 1$ and $c_u = c_d = N_u$) are used. Since all the different sources of Λ's were included in the fit, it is not necessary/possible to treat decays of hyperons differently from directly produced Λ's (as done for the first MC model). One should also note that referring to the results in [deFlo] is not quite legitimate, there the favored unpolarized fragmentation functions were assumed to be equal,

$$\hat{u}^{\Lambda} = \hat{d}^{\Lambda} = \hat{s}^{\Lambda}. \tag{5.5}$$

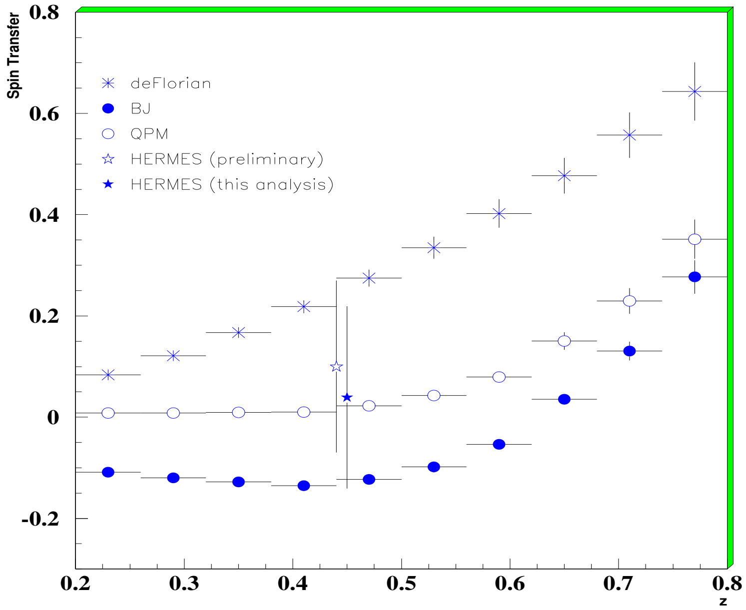

Figure 5.2: Monte Carlo prediction for the Λ spin transfer using the parameterization of the polarized fragmentation function in [deFlo]. Three scenarios are tested, one using the naïve QPM, one is inspired by the BJ and the third assumes all the three polarized quark fragmentation functions ($\Delta\hat{u}^{\Lambda}$, $\Delta\hat{d}^{\Lambda}$ and $\Delta\hat{s}^{\Lambda}$) polarized quark fragmentation functions are the same.

Whereas the first equality can probably be accepted without objection, the second equality might be a more unmotivated assumption. No attempt has been made to force the MC model to reproduce assumption 5.5. For one reason, the contribution from s-quarks in the kinematic region of HERMES is small, and secondly, the quantity of interest is independent of the unpolarized fragmentation function (assuming u-quark dominance).

Figure 5.2 shows the resulting Λ spin transfer for the different scenarios and table 5.5 shows the integrated values for the Λ spin transfer.

Apparently, more data is needed to have a conclusive answer to the question

Table 5.5: Integrated values of the Λ spin transfer using the parameterization of the polarized fragmentation functions in [deFlo] (see text for description of scenarios) and the experimentally measured z distribution.

Λ spin transfer			
HERMES	equal $\Delta\hat{q}^{\Lambda}$'s	MC - naïve QPM	MC - BJ
0.04 ± 0.17	0.26	0.04	-0.09

whether one of the models is appropriate to describe the polarized Λ production at HERMES.

5.2 SU(3) Symmetry and Polarized Fragmentation

If fragmentation behaves like the polarized quark distributions then one would expect s-fragmentation to be positively polarized and u,d fragmentation to be smaller and negatively polarized. The naïve quark model, on the other side, predicts a large polarization in s-fragmentation and none in u,d fragmentation. All this is based on the assumption that the helicity of the quark will be preserved in the fragmentation process, i.e., the polarized fragmentation function into a Λ are basically proportional to the polarized quark distributions in the Λ (latter were summarized in table 2.3).

Besides the polarization measurements in hadronic collisions, which are more difficult to relate to polarized quark fragmentation, Λ polarization has been measured at LEP [ALEPH, OPAL], where Λ's are produced at the Z^0-pole, and now at HERMES in DIS. Both the LEP experiments measured a large negative polarization of -32% and -32.9%, respectively. Thus, in a naïve approach, one could claim that u and d quarks (HERMES) do not fragment into polarized Λ's, but s quark fragmentation is highly polarized (LEP). Since in all the experiments the contribution from the decay $\Sigma^0 \to \gamma\Lambda$ was not vetoed, this picture is not quite true. Following a discussion based on SU(3) symmetry as already outlined in section 2.5.2 and appendix C.

As shown in Appendix G, the parity violating eZ^0 and qZ^0 couplings produce a polarized quark beam. The ratio between the first generation quarks and the s quarks[2] is:

$$\Delta u + \Delta d : \Delta s = 61\% : 39\%, \tag{5.6}$$

thus nearly a flavor singlet. The polarized fragmentation is therefore mostly sensitive to $\hat{\Sigma}$[3]. The observed Λ polarization of about $\frac{1}{3}$ can be explained by nearly 100% polarized s quark fragmentation and unpolarized u and d quark fragmentation which is supported by the HERMES result where one basically deals with a pure u quark beam.[4] Using the results in table 2.6 one obtains:

$$0 \approx \Delta \hat{u}_\Lambda \stackrel{SU(3)}{=} \frac{1}{3}(\hat{\Sigma} - \hat{D}) \tag{5.7}$$

[2]The u and d quark fragmentations can be combined since they are the same for the Λ as well as for the Σ^0.

[3]$0.61\Delta\hat{u}_\Lambda + 0.39\Delta\hat{s}_\Lambda \propto \hat{\Sigma} + 0.17\hat{D}$ using table 2.6

[4]Although u quarks dominate in DIS from a proton because of its charge and its abundance, there is still a considerable contribution from d quarks. Since both can be treated as being the same in Λ fragmentation due to isospin symmetry, one can just denote it to be a u quark beam.

Hence, $\hat{\Sigma} \approx \hat{D}$. This would mean that the polarized u quark fragmentation into Σ^0's, $\Delta\hat{u}^0_\Sigma = \frac{1}{3}(\hat{\Sigma} + \hat{D})$, is large and positive. Since HERMES does not distinguish Λ's produced in "real" fragmentation (meaning that only strong interaction is involved) from "fake" Λ's produced via the process $u \longrightarrow \Sigma^0 \longrightarrow \Lambda\gamma$ one has to include Σ^0's in this analysis. The polarization of the "fake" Λ's is $-\frac{1}{3}$ the polarization of the Σ^0's. What is measured at Hermes is thus

$$\begin{aligned} 0 \approx \Delta\hat{u}_\Lambda - \frac{1}{3}\Delta\hat{u}_{\Sigma^0} &\overset{SU(3)}{=} \frac{1}{3}(\hat{\Sigma} - \hat{D}) - \frac{1}{9}\left(\Delta\hat{\Sigma} + \hat{D}\right) \\ &= \frac{2}{9}\left(\Delta\hat{\Sigma} - 2\hat{D}\right). \end{aligned} \tag{5.8}$$

Therefore,

$$\Delta\hat{\Sigma} \cong 2\hat{D}. \tag{5.9}$$

One can use this result to write down the expressions for the polarization of "real" and "fake" Λ's at HERMES:

$$P_\Lambda^{\text{HERMES}} = \frac{1}{6}\frac{\hat{\Sigma}}{\hat{u}_\Lambda} \tag{5.10}$$

$$\frac{\Delta\hat{u}_{\Sigma^0}}{\hat{u}_\Lambda} = \frac{1}{2}\frac{\hat{\Sigma}}{\hat{u}_\Lambda} \tag{5.11}$$

The LEP experiments measure a different linear combination of the polarized quark fragmentation functions (see also Appendix G):

$$\begin{aligned} P_\Lambda^{\text{ALEPH}} \equiv 0.32 &= \frac{N_u P_u \Delta\hat{u}_\Lambda + N_d P_d \Delta\hat{d}_\Lambda + N_s P_s \Delta\hat{s}_\Lambda}{N_u \hat{u}_\Lambda + N_d \hat{d}_\Lambda + N_s \hat{s}_\Lambda} \\ &= \frac{0.51\Delta\hat{u}_\Lambda + 0.94\Delta\hat{d}_\Lambda + 0.94\Delta\hat{s}_\Lambda}{0.78\hat{u}_\Lambda + \hat{d}_\Lambda + \hat{s}_\Lambda} \end{aligned}$$

$$= \frac{0.80\hat{\Sigma}+0.14\hat{D}}{1.78\hat{u}_\Lambda+\hat{s}_\Lambda} \tag{5.12}$$

$$< \frac{0.80\hat{\Sigma}+0.14\frac{1}{2}\hat{\Sigma}}{1.78\hat{u}_\Lambda} = 0.49\frac{\hat{\Sigma}}{\hat{u}_\Lambda}. \tag{5.13}$$

Hence,

$$\frac{\hat{\Sigma}}{\hat{u}_\Lambda} > 0.65. \tag{5.14}$$

Making use of equ. (5.10), The polarization of the "true" Λ's at HERMES is expected to be

$$P_\Lambda^{\text{HERMES}} = 0.11. \tag{5.15}$$

A more precise treatment requires the inclusion of Σ^0's in the calculation for the LEP result and the normalization at HERMES:

$$\begin{aligned}
P_{\text{“}\Lambda\text{''}}^{\text{ALEPH}} \equiv 0.32 &= \frac{N_u P_u \Delta\hat{u}_\Lambda + N_d P_d \Delta\hat{d}_\Lambda + N_s P_s \Delta\hat{s}_\Lambda}{N_u\left(\hat{u}_\Lambda+\hat{u}_{\Sigma^0}\right)+N_d\left(\hat{d}_\Lambda+\hat{d}_{\Sigma^0}\right)+N_s\left(\hat{s}_\Lambda+\hat{s}_{\Sigma^0}\right)} \\
&\quad -\frac{1}{3}\frac{N_u P_u \Delta\hat{u}_{\Sigma^0} + N_d P_d \Delta\hat{d}_{\Sigma^0} + N_s P_s \Delta\hat{s}_{\Sigma^0}}{N_u\left(\hat{u}_\Lambda+\hat{u}_{\Sigma^0}\right)+N_d\left(\hat{d}_\Lambda+\hat{d}_{\Sigma^0}\right)+N_s\left(\hat{s}_\Lambda+\hat{s}_{\Sigma^0}\right)} \\
&= \frac{0.51\Delta\hat{u}_\Lambda + 0.94\Delta\hat{d}_\Lambda + .94\Delta\hat{s}_\Lambda}{0.78\left(\hat{u}_\Lambda+\hat{u}_{\Sigma^0}\right)+\left(\hat{d}_\Lambda+\hat{d}_{\Sigma^0}\right)+\left(\hat{s}_\Lambda+\hat{s}_{\Sigma^0}\right)} \\
&\quad -\frac{1}{3}\frac{0.51\Delta\hat{u}_{\Sigma^0} + 0.94\Delta\hat{d}_{\Sigma^0} + 0.94\Delta\hat{s}_{\Sigma^0}}{0.78\left(\hat{u}_\Lambda+\hat{u}_{\Sigma^0}\right)+\left(\hat{d}_\Lambda+\hat{d}_{\Sigma^0}\right)+\left(\hat{s}_\Lambda+\hat{s}_{\Sigma^0}\right)} \\
&= \frac{0.80\hat{\Sigma}+0.14\hat{D}}{1.78\left(\hat{u}_\Lambda+\hat{u}_{\Sigma^0}\right)+\left(\hat{s}_\Lambda+\hat{s}_{\Sigma^0}\right)} \\
&\quad -\frac{1}{3}\frac{0.80\hat{\Sigma}-0.14\hat{D}}{1.78\left(\hat{u}_\Lambda+\hat{u}_{\Sigma^0}\right)+\left(\hat{s}_\Lambda+\hat{s}_{\Sigma^0}\right)} \\
&= \frac{0.53\hat{\Sigma}+\frac{1}{2}0.19\hat{\Sigma}}{1.78\left(\hat{u}_\Lambda+\hat{u}_{\Sigma^0}\right)+\left(\hat{s}_\Lambda+\hat{s}_{\Sigma^0}\right)} &(5.16) \\
&< \frac{0.63\hat{\Sigma}}{1.78\left(\hat{u}_\Lambda+\hat{u}_{\Sigma^0}\right)} < 0.35\frac{\hat{\Sigma}}{\hat{u}_\Lambda+\hat{u}_{\Sigma^0}}. &(5.17)
\end{aligned}$$

Therefore,

$$\frac{\hat{\Sigma}}{\hat{u}_\Lambda + \hat{u}_{\Sigma^0}} > 0.91 \tag{5.18}$$

and

$$\frac{\Delta \hat{u}_\Lambda}{\hat{u}_\Lambda + \hat{u}_{\Sigma^0}} = \frac{1}{6}\frac{\hat{\Sigma}}{\hat{u}_\Lambda + \hat{u}_{\Sigma^0}} \geq 0.15, \tag{5.19}$$

the correction due to Σ^0's is now even larger! However the number of Σ^0's, $\hat{u}_{\Sigma^0}$, produced at HERMES is too large:

$$\frac{\Delta \hat{u}_{\Sigma^0}}{\hat{u}_\Lambda + \hat{u}_{\Sigma^0}} = \frac{1}{2}\frac{\hat{\Sigma}}{\hat{u}_\Lambda + \hat{u}_{\Sigma^0}} \geq 0.45, \tag{5.20}$$

meaning that there are about at least as many Λ's coming from Σ^0's as there are Λ's coming from "real" fragmentation[5] This, however, is in contradiction from what one expects, i.e., from the LUND model or from other experiments. This might be due to the simplifying assumptions made (see below) or maybe a hint that that SU(3)might not be a good symmetry for polarized fragmentation functions.

There are a few points which should be taken into account when discussing above result. For one thing, Q^2-evolution has been neglected in this analysis as well as contributions from other particles, i.e., Ξ. Furthermore, exact SU(3) has been assumed, which might not be such a good approximation. Since fragmentation involves pair creation, i.e., when creating an s quark one also has to produce a $\bar{s}$ quark, the symmetry-breaking mass differences between the light quarks become even more important. However, the trend should be clear: The "true" Λ

[5] Using the constraint (2.56) one gets $\frac{\hat{u}_{\Sigma^0}}{\hat{u}_\Lambda+\hat{u}_{\Sigma^0}} \geq \frac{\Delta\hat{u}_{\Sigma^0}}{\hat{u}_\Lambda+\hat{u}_{\Sigma^0}} \geq 0.45$ or $\frac{\hat{u}_\Lambda}{\hat{u}_{\Sigma^0}} \leq \frac{0.55}{0.45} \approx 1$.

polarization, meaning the polarization of the Λ's produced in fragmentation, is probably larger than what has been measured at HERMES, i.e., the correction for the Σ^0's is positive. It is a pity that the contribution from the Σ^0's can not be singled out.

5.3 Conclusion

As mentioned before, there is not enough data available yet to draw a complete picture of polarized fragmentation, neither can we exclude the phenomenological models based on helicity conservation in the fragmentation process. More statistics is needed to be able to discriminate between the different scenarios. It would also useful to look for other hyperons and perform a similar analysis as it done for the Λ. This would give a more constraint picture of polarized fragmentation. Given such a possibility one can perform a complete SU(3) analysis of polarized fragmentation functions and extract $\hat{\Sigma}$, $\hat{F}$ and $\hat{D}$, the SU(3) invariants of polarized fragmentation. This would give an answer whether SU(3) is a good symmetry in polarized fragmentation or whether it is broken. However, already the large number of Σ^0's in the SU(3) analysis suggests that flavor symmetry is broken. How badly? – more data will give the answer.

One conclusion, however, is probably valid already. Polarized fragmentation does not (yet) result in a new "spin crisis": In contrast to DIS, the flavor singlet fragmentation appears to be large, whereas the contribution to the Λ polarization from u and d quarks seems to be small.

APPENDIX A

CALLAN GROSS RELATION

In the QPM the proton is made of spin-1/2 partons (quarks). One therefore could derive the structure functions of the proton from the "structure functions" of Dirac particles. For parton i with fractional charge e_i one has

$$W_1^i = e_i^2 \frac{Q^2}{4m^2} \delta \left(\nu - \frac{Q^2}{2m} \right) \tag{A.1}$$

$$W_2^i = e_i^2 \delta \left(\nu - \frac{Q^2}{2m} \right). \tag{A.2}$$

Making use of $\delta(ax) = \frac{1}{a}\delta(x)$ and $m = \xi M$ this can be rewritten as

$$W_1^i = e_i^2 \frac{x}{\xi} \frac{1}{2M} \delta(\xi - x) \tag{A.3}$$

$$W_2^i = e_i^2 \frac{\xi}{\nu} \delta(\xi - x). \tag{A.4}$$

Summing over all quark flavours and integrating over ξ (including the probability, $q_i(\xi)$, to find a quark of flavour i with momentum fraction ξ) one obtains

$$\begin{aligned} F_1(x) &= MW_1 \\ &= \frac{1}{2} \int d\xi \sum_i e_i^2 q_i(\xi) \frac{x}{\xi} \delta(\xi - x) \end{aligned}$$

$$
\begin{aligned}
&= \frac{1}{2}\sum_i e_i^2 q_i(x) && \text{(A.5)} \\
F_2(x) &= \nu W_2 \\
&= \int d\xi \sum_i e_i^2 q_i(\xi)\xi\delta\left(\xi - x\right) \\
&= \sum_i e_i^2 x q_i(x), && \text{(A.6)}
\end{aligned}
$$

from which follows the Callan Gross Relation (2.35).

APPENDIX B

NON-RELATIVISTIC QUARK MODEL SPIN WAVE FUNCTIONS

In the non-relativistic quark parton model baryons are built from the three quarks u, d and s (baryons which include the heavy quarks c, b and t will not be considered here since they fall outside the scope of interest and are not expected to play a large role at HERMES energies). The masses of those quarks are assumed to be negligible (at least compared to the relevant energy scales involved) and thus $SU(3)$ flavor symmetry can be applied.

Because quarks are fermions there can not be quarks with the same quantum numbers or, in other words, the total wave function has to be antisymmetric. The combined flavor, spin and space wave function, however, has to be symmetric since the baryon forms a color singlet state which is antisymmetric. Furthermore, ground state wave functions have zero angular momentum and thus are symmetric:

$$P\Phi(\vec{x}) = (-1)^l \Phi(\vec{x}) \tag{B.1}$$

Therefore, the spin flavor wave function has to be symmetric.

Table B.1: Permutation symmetries of the baryon spin-flavor wave functions (S-symmetric, M-mixed, A-antisymmetric)

Spin SU(2)	Flavor SU(3)	Spin-flavor SU(6)
S	S	S
S	M	M
S	A	A
M	S	M
M	M	S,M,A
M	A	M

Though in the case of two quarks (i.e., mesons) the spin wave function can be antisymmetric, this is not true for a system of three particles (cf., [Fla 82]). Here, only symmetric (spin-3/2) or mixed (spin-1/2) states are possible. From table (B.1) one can see that in order to have a totally symmetric (in flavor and spin and thus also in flavor, spin and space) state one needs either a symmetric or a mixed flavor combination.

In the following only the baryon octet with mixed spin and mixed flavor symmetries is considered. This will give the wave function of the baryons of interest (i.e., p, Λ, Σ^0 and Ξ). A simple *recipe* to form the spin flavor wave function is taken from [Fla 82] and applied to the case of the Λ:

1. write down the correct three quark combination:

   uds

2. if the three quarks do not have definite isospin add a term where u and d are permuted with the appropriate sign:

   $uds - dus$

3. if there is still no antisymmetric pair of two quarks antisymmetrize an s quark with either an u or a d quark:

   (still) $uds - dus$

4. assign an S=1/2 spin wave function in such a way that the pair which is antisymmetric in flavor is antisymmetric in spin as well:

$$(uds - dus) \times (\uparrow\downarrow\uparrow - \downarrow\uparrow\uparrow) = u\uparrow d\downarrow s\uparrow - u\downarrow d\uparrow s\uparrow$$
$$- d\uparrow u\downarrow s\uparrow + d\downarrow u\uparrow s\uparrow$$

5. add the even permutations of the quarks to make the total expression symmetric under simultaneous interchange of spin and isospin:

$$u\uparrow d\downarrow s\uparrow - u\downarrow d\uparrow s\uparrow - d\uparrow u\downarrow s\uparrow + d\downarrow u\uparrow s\uparrow +$$
$$d\downarrow s\uparrow u\uparrow - d\uparrow s\uparrow u\downarrow - u\downarrow s\uparrow d\uparrow + u\uparrow s\uparrow d\downarrow +$$
$$s\uparrow u\uparrow d\downarrow - s\uparrow u\downarrow d\uparrow - s\uparrow d\uparrow u\downarrow + s\uparrow d\downarrow u\uparrow$$

6. normalize the wave function appropriately:

$$|\Phi_\Lambda>=\frac{1}{\sqrt{12}}|u\uparrow d\downarrow s\uparrow - u\downarrow d\uparrow s\uparrow - d\uparrow u\downarrow s\uparrow + d\downarrow u\uparrow s\uparrow$$
$$+d\downarrow s\uparrow u\uparrow - d\uparrow s\uparrow u\downarrow - u\downarrow s\uparrow d\uparrow + u\uparrow s\uparrow d\downarrow$$
$$+s\uparrow u\uparrow d\downarrow - s\uparrow u\downarrow d\uparrow - s\uparrow d\uparrow u\downarrow + s\uparrow d\downarrow u\uparrow> \tag{B.2}$$

The wavefunctions of the all the octet states are listed in table B.2. From above result one can easily compute Δu, Δd and Δs for Λ:

$$\begin{aligned}\Delta u_\Lambda &= u\uparrow - u\downarrow \\ &= \frac{1}{12}[1-1-1+1+1-1-1+1+1-1-1+1] \\ &= 0 \\ \Delta d_\Lambda &= d\uparrow - d\downarrow \\ &= \frac{1}{12}[-1+1+1-1-1+1+1-1-1+1+1-1] \\ &= 0 \\ \Delta s_\Lambda &= s\uparrow - s\downarrow \\ &= \frac{1}{12}[1+1+1+1+1+1+1+1+1+1+1+1] \\ &= 1\end{aligned}$$

Similarly, one obtains Δu, Δd and Δs for all the other octet members (table B.3).

Table B.2: Spin flavor wave functions for the members of the baryon octet

$$
\begin{aligned}
|\Phi_p> &= \frac{1}{\sqrt{18}}|2u{\uparrow}u{\uparrow}d{\downarrow}+2d{\downarrow}u{\uparrow}u{\uparrow}+2u{\uparrow}d{\downarrow}u{\uparrow}-u{\downarrow}d{\uparrow}u{\uparrow}-u{\uparrow}u{\downarrow}d{\uparrow} \\
&\qquad -u{\downarrow}u{\uparrow}d{\uparrow}-d{\uparrow}u{\downarrow}u{\uparrow}-u{\uparrow}d{\uparrow}u{\downarrow}-d{\uparrow}u{\uparrow}u{\downarrow}> \\
|\Phi_n> &= -\frac{1}{\sqrt{18}}|2d{\uparrow}d{\uparrow}u{\downarrow}+2u{\downarrow}d{\uparrow}d{\uparrow}+2d{\uparrow}u{\downarrow}d{\uparrow}-d{\downarrow}u{\uparrow}d{\uparrow}-d{\uparrow}d{\downarrow}u{\uparrow} \\
&\qquad -d{\downarrow}d{\uparrow}u{\uparrow}-u{\uparrow}d{\downarrow}d{\uparrow}-d{\uparrow}u{\uparrow}d{\downarrow}-u{\uparrow}d{\uparrow}d{\downarrow}> \\
|\Phi_{\Sigma^+}> &= \frac{1}{\sqrt{18}}|(2u{\uparrow}u{\uparrow}s{\downarrow}+2s{\downarrow}u{\uparrow}u{\uparrow}+2u{\uparrow}s{\downarrow}u{\uparrow}-u{\downarrow}s{\uparrow}u{\uparrow}-u{\uparrow}u{\downarrow}s{\uparrow} \\
&\qquad -u{\downarrow}u{\uparrow}s{\uparrow}-s{\uparrow}u{\downarrow}u{\uparrow}-u{\uparrow}s{\uparrow}u{\downarrow}-s{\uparrow}u{\uparrow}u{\downarrow}> \\
|\Phi_{\Sigma^0}> &= -\frac{1}{\sqrt{36}}|2d{\uparrow}s{\downarrow}u{\uparrow}+2s{\downarrow}d{\uparrow}u{\uparrow}+2u{\uparrow}d{\uparrow}s{\downarrow}+2u{\uparrow}s{\downarrow}d{\uparrow}+2s{\downarrow}u{\uparrow}d{\uparrow}+2d{\uparrow}u{\uparrow}s{\downarrow} \\
&\qquad -d{\downarrow}s{\uparrow}u{\uparrow}-s{\uparrow}d{\downarrow}u{\uparrow}-u{\uparrow}d{\downarrow}s{\uparrow}-u{\uparrow}s{\uparrow}d{\downarrow}-s{\uparrow}u{\uparrow}d{\downarrow}-d{\downarrow}u{\uparrow}s{\uparrow} \\
&\qquad -s{\uparrow}u{\downarrow}d{\uparrow}-u{\downarrow}s{\uparrow}d{\uparrow}-d{\uparrow}s{\uparrow}u{\downarrow}-d{\uparrow}u{\downarrow}s{\uparrow}-u{\downarrow}d{\uparrow}s{\uparrow}-s{\uparrow}d{\uparrow}u{\downarrow}> \\
|\Phi_{\Sigma^-}> &= -\frac{1}{\sqrt{18}}|2d{\uparrow}d{\uparrow}s{\downarrow}+2s{\downarrow}d{\uparrow}d{\uparrow}+2d{\uparrow}s{\downarrow}d{\uparrow}-d{\downarrow}s{\uparrow}d{\uparrow}-d{\uparrow}d{\downarrow}s{\uparrow} \\
&\qquad -d{\downarrow}d{\uparrow}s{\uparrow}-s{\uparrow}d{\downarrow}d{\uparrow}-d{\uparrow}s{\uparrow}d{\downarrow}-s{\uparrow}d{\uparrow}d{\downarrow}> \\
|\Phi_\Lambda> &= \frac{1}{\sqrt{12}}|u{\uparrow}d{\downarrow}s{\uparrow}-u{\downarrow}d{\uparrow}s{\uparrow}-d{\uparrow}u{\downarrow}s{\uparrow}+d{\downarrow}u{\uparrow}s{\uparrow}+d{\downarrow}s{\uparrow}u{\uparrow}-d{\uparrow}s{\uparrow}u{\downarrow} \\
&\qquad -u{\downarrow}s{\uparrow}d{\uparrow}+u{\uparrow}s{\uparrow}d{\downarrow}+s{\uparrow}u{\uparrow}d{\downarrow}-s{\uparrow}u{\downarrow}d{\uparrow}-s{\uparrow}d{\uparrow}u{\downarrow}+s{\uparrow}d{\downarrow}u{\uparrow}> \\
|\Phi_{\Xi^0}> &= \frac{1}{\sqrt{18}}|2s{\uparrow}s{\uparrow}u{\downarrow}+2u{\downarrow}s{\uparrow}s{\uparrow}+2s{\uparrow}u{\downarrow}s{\uparrow}-s{\downarrow}u{\uparrow}s{\uparrow}-s{\uparrow}s{\downarrow}u{\uparrow} \\
&\qquad -s{\downarrow}s{\uparrow}u{\uparrow}-u{\uparrow}s{\downarrow}s{\uparrow}-s{\uparrow}u{\uparrow}s{\downarrow}-u{\uparrow}s{\uparrow}s{\downarrow}> \\
|\Phi_{\Xi^-}> &= \frac{1}{\sqrt{18}}|2s{\uparrow}s{\uparrow}d{\downarrow}+2d{\downarrow}s{\uparrow}s{\uparrow}+2s{\uparrow}d{\downarrow}s{\uparrow}-s{\downarrow}d{\uparrow}s{\uparrow}-s{\uparrow}s{\downarrow}d{\uparrow} \\
&\qquad -s{\downarrow}s{\uparrow}d{\uparrow}-d{\uparrow}s{\downarrow}s{\uparrow}-s{\uparrow}d{\uparrow}s{\downarrow}-d{\uparrow}s{\uparrow}s{\downarrow}>
\end{aligned}
$$

Table B.3: Polarized quark distribution in the members of the baryon octet

Baryon	Δu	Δd	Δs
p	$\frac{4}{3}$	$-\frac{1}{3}$	0
n	$-\frac{1}{3}$	$\frac{4}{3}$	0
Σ^+	$\frac{4}{3}$	0	$-\frac{1}{3}$
Σ^0	$\frac{2}{3}$	$\frac{2}{3}$	$-\frac{1}{3}$
Σ^-	0	$\frac{4}{3}$	$-\frac{1}{3}$
Λ	0	0	1
Ξ^0	$-\frac{1}{3}$	0	$\frac{4}{3}$
Ξ^-	0	$-\frac{1}{3}$	$\frac{4}{3}$

APPENDIX C

POLARIZED QUARK DISTRIBUTIONS OF THE HYPERON OCTET

The naïve QPM fails to describe the spin structure of nucleons. Therefore, one does not expect it to be a good model for the spin structure of the remaining members of the hyperon octet. One can, however, use the present data on the proton (neutron) spin structure in conjunction with data from the semi-leptonic hyperon decay amplitudes to calculate the spin structure of the members in the hyperon octet. This procedure is outlined in this appendix.

The main assumption entering the calculation is that the octet is indeed a SU(3) flavor octet. This is assumed to be nearly correct (there are mass differences especially when involving strange quarks but symmetry breaking is assumed to be small). The spin structure is characterized by the polarized quark distributions.[1] The first moment of the spin structure function g_1 is related to the polarized quark distributions through g_1

$$\Gamma_1 \;=\; \int_0^1 dx g_1(x) \tag{C.1}$$

[1]Though other contributions,e.g., gluons, exist, but are not of interest in this calculation.

$$= \frac{1}{2}\left(\frac{4}{9}\Delta u + \frac{1}{9}\Delta d + \frac{1}{9}\Delta s\right). \tag{C.2}$$

Γ_1 can also be written in terms of the hadronic matrix elements of the octet of quark SU(3) axial-vector currents and the flavor singlet axial current a_0, a_3 and a_8:

$$\Gamma_1 = \frac{1}{12}\left(a_3 + \frac{1}{\sqrt{3}}a_8 + \frac{4}{3}a_0\right), \tag{C.3}$$

where

$$\begin{aligned} a^0 &= \Delta u + \Delta d + \Delta s \\ a^3 &= \Delta u - \Delta d \\ a^8 &= \frac{1}{\sqrt{3}}\left(\Delta u + \Delta d - 2\Delta s\right). \end{aligned} \tag{C.4}$$

In general, the octet axial-vector currents are

$$J_\mu^i = \bar{\psi}\gamma_\mu\gamma_5\left(\frac{\lambda_i}{2}\right)\psi \qquad (i = 1, 2, \ldots, 8) \tag{C.5}$$

with λ_i being the usual Gell-Mann matrices and ψ a column vector in the SU(3) flavor space. The singlet current is just

$$J_\mu^0 = \bar{\psi}\gamma_\mu\gamma_5\psi. \tag{C.6}$$

(Note, that the singlet current matrix element a_0 is often referred to as $\Delta\Sigma$ or the spin carried by the quarks. In the naïve QPM it is assumed to be 1. $a_3^P = g_A$ is also known as the axial coupling which governs the neutron β-decay.) The hadronic matrix element for a specific baryon with spin S, mass m_B and momentum p is

[BT, AEL]:

$$2m_B S_\mu a^0 = \langle p, S | J^0_\mu | p, S \rangle \tag{C.7}$$

$$m_B S_\mu a^i = \langle p, S | J^i_\mu | p, S \rangle. \tag{C.8}$$

One can relate those matrix elements to the SU(3) flavor structure constants F and D which are available from the hyperon β-decay data. To do so one should remember that all the hyperon β-decays are also described by F and D and that for two baryons B_j and B_k the matrix element of the octet of axial currents is [Bai]:

$$\langle B_j; p, S | J^i_\mu | B_k; p, S \rangle = 2m_B S_\mu \{ D d_{ijk} - iF f_{ijk} \} \tag{C.9}$$

where d_{ijk} and f_{ijk} are the usual SU(3) group structure functions (cf. table C.1), the B_i can be calculated similarly to the λ_i from the octet representation, i.e.

$$\begin{array}{ll} B_1 = \frac{1}{\sqrt{2}}(B_{12} + B_{21}) & B_2 = \frac{-i}{\sqrt{2}}(B_{12} - B_{21}) \\ B_4 = \frac{1}{\sqrt{2}}(B_{31} + B_{13}) & B_5 = \frac{i}{\sqrt{2}}(B_{31} - B_{13}) \\ B_6 = \frac{1}{\sqrt{2}}(B_{23} + B_{32}) & B_7 = \frac{-i}{\sqrt{2}}(B_{23} - B_{32}) \\ B_3 = \frac{1}{\sqrt{2}}(B_{11} - B_{22}) & B_8 = \sqrt{\frac{3}{2}}(B_{11} + B_{22}) \end{array}$$

where [Georgi]

$$B_{ij} = \begin{pmatrix} \frac{\Sigma^0}{\sqrt{2}} + \frac{\Lambda}{\sqrt{6}} & \Sigma^+ & P \\ \Sigma^- & -\frac{\Sigma^0}{\sqrt{2}} + \frac{\Lambda}{\sqrt{6}} & N \\ \Xi^- & \Xi^0 & -\frac{2\Lambda}{\sqrt{6}} \end{pmatrix}, \tag{C.10}$$

thus

Table C.1: The non-zero elements of the symmetric (d_{ijk}) and antisymmetric (f_{ijk}) structure functions [Bai]

ijk	f_{ijk}	ijk	d_{ijk}	ijk	d_{ijk}
123	1	118	$\frac{1}{\sqrt{3}}$	146	$\frac{1}{2}$
147	$\frac{1}{2}$	157	$\frac{1}{2}$	228	$\frac{1}{\sqrt{3}}$
156	$-\frac{1}{2}$	247	$-\frac{1}{2}$	256	$\frac{1}{2}$
246	$\frac{1}{2}$	338	$\frac{1}{\sqrt{3}}$	344	$\frac{1}{2}$
257	$\frac{1}{2}$	355	$\frac{1}{2}$	366	$-\frac{1}{2}$
345	$\frac{1}{2}$	377	$-\frac{1}{2}$	448	$-\frac{1}{2\sqrt{3}}$
367	$-\frac{1}{2}$	558	$-\frac{1}{2\sqrt{3}}$	668	$-\frac{1}{2\sqrt{3}}$
458	$\frac{\sqrt{3}}{2}$	778	$-\frac{1}{2\sqrt{3}}$	888	$-\frac{1}{\sqrt{3}}$
678	$\frac{\sqrt{3}}{2}$				

$$
\begin{aligned}
B_1 &= \tfrac{1}{\sqrt{2}}(\Sigma^+ + \Sigma^-) & B_2 &= -\tfrac{i}{\sqrt{2}}(\Sigma^+ - \Sigma^-) \\
B_4 &= \tfrac{1}{\sqrt{2}}(\Xi^- + p) & B_5 &= \tfrac{i}{\sqrt{2}}(\Xi^- - p) \\
B_6 &= \tfrac{1}{\sqrt{2}}(N + \Xi^0) & B_7 &= -\tfrac{i}{\sqrt{2}}(N - \Xi^0) \\
B_3 &= \Sigma^0 & B_8 &= \Lambda
\end{aligned}
$$

Eq. (C.9) can be easily obtained by following the argumentation in [Georgi]: In order to build an SU(3) invariant out of matrices one has to contract all indices. If one considers an operator $\hat{O}$ between two baryon states B_i and B_j, i.e.,

$$\langle B_i|\hat{O}|B_j\rangle, \tag{C.11}$$

this can be realized by taking the traces of the product of the three matrices.[2]

[2]Note, that one has to take the Hermitian conjugate of B_i since it appears in a bra.

Only two permutations are independent[3] combinations:

$$\mathrm{tr}(\hat{O}B_jB_i^\dagger) \quad \text{and} \quad \mathrm{tr}(\hat{O}B_i^\dagger B_j). \tag{C.12}$$

However, it became customary to use the commutator and the anti-commutator instead, leading to

$$\langle B_i|\hat{O}|B_j\rangle = D\mathrm{tr}(\hat{O}\{B_j, B_i^\dagger\}) + F\mathrm{tr}(\hat{O}[B_i^\dagger, B_j]). \tag{C.13}$$

F and D are constants which depend only on the operator one is interested in but not on the specific baryon. This feature allows one to relate the expectation values of an operator for different baryons which makes it vital to the whole argumentation in this calculation.

From our definition of B_i and $\hat{O}$ one can see following resemblance to the λ-matrices:

$$B_i \sim \frac{\lambda_i}{\sqrt{2}} \tag{C.14}$$

$$\hat{O}_i \sim \frac{\lambda_i}{2}, \tag{C.15}$$

which leads to

$$\mathrm{tr}(\hat{O}_i\{B_k, B_j^\dagger\}) \sim \frac{1}{4}\mathrm{tr}(\lambda_i\{\lambda_k, \lambda_j\}) = -if_{ijk} \tag{C.16}$$

$$\mathrm{tr}(\hat{O}_i[B_k, B_j^\dagger]) \sim \frac{1}{4}\mathrm{tr}(\lambda_i[\lambda_k, \lambda_j]) = d_{ijk}, \tag{C.17}$$

and thus gives equ. (C.9).

[3]The other permutations result the same since the trace is invariant under cyclic permutations of its arguments.

F and D can be obtained from the hyperon β-decay since the same currents are involved. An analysis of the current data [WA2] results in

$$F = 0.477 \pm 0.012 \tag{C.18}$$

$$D = 0.756 \pm 0.011 \tag{C.19}$$

In order to calculate Γ_1 and, hence, Δq one needs to calculate the matrix elements a_3 and a_8. For example, let us calculate the the matrix elements of the proton:

$$|P\rangle = \frac{1}{\sqrt{2}}(|B_4\rangle + i|B_5\rangle) \tag{C.20}$$

$$\langle P| = \frac{1}{\sqrt{2}}(\langle B_4| - i\langle B_5|). \tag{C.21}$$

Thus, using the (anti)symmetry properties of d_{ijk} (f_{ijk}) and (C.9),

$$m_P S_\mu a_P^i \equiv \langle P; p, S|J_\mu^i|P; p, S\rangle \tag{C.22}$$

$$= \frac{1}{2}\langle B_4| - i\langle B_5|J_\mu^i|B_4\rangle + i|B_5\rangle$$

$$= m_P S_\mu \{D(d_{i44} + d_{i55}) + 2F f_{i45}\}. \tag{C.23}$$

More specific,

$$a_P^3 = D + F \tag{C.24}$$

$$a_P^8 = \frac{1}{\sqrt{3}}(3F - D). \tag{C.25}$$

From this it follows readily that

$$\Gamma_1^P = \frac{1}{18}\left(D + 3F + 2\Delta\Sigma\right). \tag{C.26}$$

(Note, that the neutron case can be related to the proton by simply exchanging Δu and Δd, thus, $\Delta d^N = \Delta u^P$ and vice versa. This only changes a_3:

$$a_N^3 = -a_P^3 \tag{C.27}$$

$$a_N^8 = a_P^8 \tag{C.28}$$

from which the Bjørken sum rule follows:

$$\begin{aligned} \Gamma_1^P - \Gamma_1^N &= \frac{2}{12} a_3^P && \text{(C.29)} \\ &= \frac{1}{6}(D + F), && \text{(C.30)} \end{aligned}$$

which agrees with the experimental value.)

The Λ (B_8) and the Σ^0 (B_3) cases are straight-forward:

$$\begin{aligned} m_B S_\mu a_B^i &\equiv \langle B^j | J_\mu^i | B^j \rangle \qquad (j = 3, 8) \\ &= m_B S_\mu \{ D d_{ijj} - iF f_{ijj} \} \\ &= m_B S_\mu D d_{ijj} && \text{(C.31)} \end{aligned}$$

and therefore,

$$a_\Lambda^3 = a_{\Sigma^0}^3 = 0 \tag{C.32}$$

$$a_\Lambda^8 = -a_{\Sigma^0}^8 = -\frac{2}{\sqrt{3}} D \tag{C.33}$$

To calculate Γ_1 one needs to make use of the proton (or the neutron) data in order to extract the singlet term $(\Delta\Sigma)$.

$$\frac{1}{9}\Delta\Sigma = \Gamma_1^P - \frac{1}{18}(D+3F) \tag{C.34}$$

Thus,

$$\begin{aligned} \Gamma_1^\Lambda &= \frac{1}{18}(2\Sigma - D) && \text{(C.35)} \\ &= \Gamma_1^P - \frac{1}{18}(2D+3F). && \text{(C.36)} \end{aligned}$$

Not only the first moment is accessible but also the quark polarization. Inverting C.4 gives

$$\begin{aligned} \Delta u &= \frac{1}{6}(2\Sigma + 3a_3 + \sqrt{3}a_8) \\ \Delta d &= \frac{1}{6}(2\Sigma - 3a_3 + \sqrt{3}a_8) \\ \Delta s &= \frac{1}{3}(\Sigma - \sqrt{3}a_8) && \text{(C.37)} \end{aligned}$$

Table C.2 summarizes the polarized quark distributions and table C.3 the first moments of g_1.

Table C.2: Polarized quark distributions using SU(3) and the available nucleon data [ADA]. $\Delta\Sigma$ has been extracted from Γ_1^P and where applicable $D+F$ has been replaced by the more precisely known value $g_A = 1.2573 \pm 0.0028$ for the calculation

	Δu		Δd		Δs	
p	$\frac{1}{3}(\Delta\Sigma + D + 3F)$	0.79 ± 0.04	$\frac{1}{3}(\Delta\Sigma - 2D)$	-0.45 ± 0.04	$\frac{1}{3}(\Delta\Sigma + D - 3F)$	-0.16 ± 0.05
n	$\frac{1}{3}(\Delta\Sigma - 2D)$	-0.45 ± 0.04	$\frac{1}{3}(\Delta\Sigma + D + 3F)$	0.79 ± 0.04	$\frac{1}{3}(\Delta\Sigma + D - 3F)$	-0.16 ± 0.05
Σ^+	$\frac{1}{3}(\Delta\Sigma + D + 3F)$	0.79 ± 0.04	$\frac{1}{3}(\Delta\Sigma + D - 3F)$	-0.16 ± 0.05	$\frac{1}{3}(\Delta\Sigma - 2D)$	-0.45 ± 0.04
Σ^0	$\frac{1}{3}(\Delta\Sigma + D)$	0.32 ± 0.04	$\frac{1}{3}(\Delta\Sigma + D)$	0.32 ± 0.04	$\frac{1}{3}(\Delta\Sigma - 2D)$	-0.45 ± 0.04
Σ^-	$\frac{1}{3}(\Delta\Sigma + D - 3F)$	-0.16 ± 0.05	$\frac{1}{3}(\Delta\Sigma + D + 3F)$	0.79 ± 0.04	$\frac{1}{3}(\Delta\Sigma - 2D)$	-0.45 ± 0.04
Λ	$\frac{1}{3}(\Delta\Sigma - D)$	-0.20 ± 0.04	$\frac{1}{3}(\Delta\Sigma - D)$	-0.20 ± 0.04	$\frac{1}{3}(\Delta\Sigma + 2D)$	0.58 ± 0.04
Ξ^0	$\frac{1}{3}(\Delta\Sigma - 2D)$	-0.45 ± 0.04	$\frac{1}{3}(\Delta\Sigma + D - 3F)$	-0.16 ± 0.05	$\frac{1}{3}(\Delta\Sigma + D + 3F)$	0.79 ± 0.04
Ξ^-	$\frac{1}{3}(\Delta\Sigma + D - 3F)$	-0.16 ± 0.05	$\frac{1}{3}(\Delta\Sigma - 2D)$	-0.45 ± 0.04	$\frac{1}{3}(\Delta\Sigma + D + 3F)$	0.79 ± 0.04

Table C.3: First moment of g_1 using SU(3) and the available nucleon data. $\Gamma_1^P(Q^2 = 10GeV^2) = 0.142 \pm 0.008 \pm 0.011$ [ADA] has been inserted for $\Delta\Sigma$ and where applicable $D+F$ has been replaced by the more precisely known value $g_A = 1.2573 \pm 0.0028$ for the calculation

Baryon	Γ_1	$\Gamma_1(\Gamma_1^P)$	value
p	$\frac{1}{18}(2\Delta\Sigma + 3F + D)$	Γ_1^P	0.142 ± 0.014
n	$\frac{1}{9}(\Delta\Sigma - D)$	$\Gamma_1^P - \frac{1}{6}g_A$	-0.068 ± 0.014
Σ^+	$\frac{1}{18}(2\Delta\Sigma + 3F + D)$	Γ_1^P	0.142 ± 0.014
Σ^0	$\frac{1}{18}(2\Delta\Sigma + D)$	$\Gamma_1^P - \frac{1}{6}F$	0.062 ± 0.014
Σ^-	$\frac{1}{18}(2\Delta\Sigma - 3F + D)$	$\Gamma_1^P - \frac{1}{3}F$	-0.017 ± 0.014
Λ	$\frac{1}{18}(2\Delta\Sigma - D)$	$\Gamma_1^P - \frac{1}{18}(2g_A + F)$	-0.024 ± 0.014
Ξ^0	$\frac{1}{9}(\Delta\Sigma - D)$	$\Gamma_1^P - \frac{1}{6}g_A$	-0.068 ± 0.014
Ξ^-	$\frac{1}{18}(2\Delta\Sigma - 3F + D)$	$\Gamma_1^P - \frac{1}{3}F$	-0.017 ± 0.014

APPENDIX D

SPIN AS A 4-VECTOR

The polarization of Λ's can be extracted from its decay $\Lambda \to p\pi$:

$$\frac{d\sigma}{d\Theta} = \sigma_0(1 + \beta P \cos \Theta_{p\vec{s}}), \tag{D.1}$$

where $\beta = 0.642$, $\Theta_{p\vec{s}}$ is the angle between the direction of the outgoing proton and the quantization axis in the center of momentum frame of the Λ and P is the polarization along this axis (latter quantity is the one of interest). In principle, one just needs to measure this decay distribution in the c.m. frame and the polarization can be easily extracted. In practice, however, one usually has only the decay distribution in the laboratory frame available, hence one has to do a Lorentz transformation into the c.m. frame. The question is then: What happens to the polarization axis (or quantization axis, respectively)? One has to transform it as well. The spin is a 4-vector which obeys the familiar transformation rules. One, however, has to find the 4 components of the spin in the lab frame. One condition on the spin 4-vector is that it is perpendicular to the momentum 4-

vector:

$$s^\mu p_\mu = 0. \tag{D.2}$$

Since $p^k = 0$ in the c.m. frame and $p^0 = M_\Lambda$ it follows from (D.2) that the zeroth component of the spin 4-vector must vanish. Then, the space components are just the *familiar* spin components (s_x, s_y, s_z). Hence, in the c.m. frame one can easily contract the spin 4-vector s^μ:

$$\begin{aligned} s^\mu s_\mu &= -(s_x^2 + s_y^2 + s_z^2) && \text{(D.3)} \\ &= -s(s+1) && \text{(D.4)} \\ &= -\frac{3}{4}. && \text{(D.5)} \end{aligned}$$

Now, one has basically all tools to obtain the spin 4-vector in the laboratory frame. Let $\vec{P}$ be the polarization vector ($\vec{s} \propto \vec{P}$) and introduce the unit vector in this direction

$$\vec{e}_P = \frac{\vec{P}}{\mid \vec{P} \mid}, \tag{D.6}$$

Then, the spin four-vector can formally be written as

$$s^\mu = (a, b\vec{P}). \tag{D.7}$$

Therefore,

$$s^2 \equiv s^\mu s_\mu = a^2 - P^2 b^2. \tag{D.8}$$

In the laboratory frame the particle's four momentum is

$$p^\mu = (\sqrt{m^2 + p^2}, \vec{p}) \tag{D.9}$$

and its contraction with the s_μ

$$\begin{aligned} p^\mu s_\mu &= a\sqrt{m^2 + p^2} - b\vec{P}\vec{p} && \text{(D.10)} \\ &= 0. && \text{(D.11)} \end{aligned}$$

Using (D.8) and doing some algebra one can solve for a and b:

$$\begin{aligned} b^2 &= -\frac{(m^2 + p^2)}{P^2(m^2 + p^2 \sin^2\theta)} s^2 && \text{(D.12)} \\ &= -\frac{E^2}{P^2(m^2 + p^2 \sin^2\theta)} s^2 && \text{(D.13)} \\ a^2 &= -\frac{p^2 \cos^2\theta}{m^2 + p^2 \sin^2\theta} s^2 && \text{(D.14)} \end{aligned}$$

where θ is the angle between the momentum and the polarization vectors in the laboratory frame (of course the whole expression is not limited to the laboratory frame, hence any frame is fine as long as the variables used are all in the same frame). Using above expressions in (D.7) one obtains the spin four-vector s^μ as a function of the observables p, E and θ:

$$s^\mu = \frac{\sqrt{-s^2}}{\sqrt{m^2 + p^2 \sin^2\theta}} (p\cos\theta, E\vec{e}_P), \tag{D.15}$$

which can be boosted into the frame of choice. In most cases one is interested in the c.m. frame, thus in a boost along the momentum direction of the particle. For practical reasons, choose a coordinate system where the momentum direction coincides with the z direction. Then one can write down (D.15) in terms of the spherical coordinates θ and ϕ:

$$s^\mu = \frac{\sqrt{-s^2}}{\sqrt{m^2 + p^2 \sin^2\theta}}(p\cos\theta, E\sin\theta\cos\phi, E\sin\theta\sin\phi, E\cos\theta) \tag{D.16}$$

and

$$p^\mu = (E, 0, 0, p). \tag{D.17}$$

As it is realized readily the spin four-vector in the c.m. frame is then

$$s^\mu = \frac{\sqrt{-s^2}}{\sqrt{m^2 + p^2 \sin^2\theta}}(0, E\sin\theta\cos\phi, E\sin\theta\sin\phi, m) \tag{D.18}$$

(where all the angles and kinematics are the ones measured in the previous, i.e., laboratory, frame).

APPENDIX E

DATA QUALITY CUTS

For this analysis the burst list provided by Stefan Bernreuther is used. In addition to the cuts applied in Stefan's burst list an additional cut on the beam polarization is applied:

$$0.35 < |P_{beam}| < 0.65 \tag{E.1}$$

Following a description of the burst level list (Version 08.98):

```
All runs of the 96c1 and 97b2 DST production are used
(including all targets).

The following cuts were applied :

1) To select unpolarized data :

    96c1: g1Quality.bDQTop & 0xa000
          &&g1Quality.bDQBot & 0xa000

          valve settings indicates unpol gassystem operating and
          Mark Sutters offline analysis indicates unpol running

    97b2: g1Quality.bDQTop & 0x8000
          &&g1Quality.bDQBot & 0x8000

          valve settings indicates unpol gassystem operating

2) Cuts:
```

```
96c1: NOT( g1Quality.bDQTop & 0x21e13dc
           || g1Quality.bDQBot & 0x21e13dc )

97b2: NOT( g1Quality.bDQTop & 0x21e03dc
           || g1Quality.bDQBot & 0x21e03dc )


1 - 0x00000004 - the deadtime cut, average DAQ deadtime outside
                  of the range [0.50,1.00),
2 - 0x00000008 - burst length outside of range [0.00,11.0)
3 - 0x00000010 - the MDM beam current outside of range (5.0,50.0)
4 - 0x00000040 - this record is part of the first burst in a
                  run (iuDSTbad & 0x00004000)
5 - 0x00000080 - this record is part of last burst of the run and
                  should be cut because either:
                   (a) there was a burst number jump at the
                       end of the run (iuDSTbad & 0x000001000),
                    or
                   (b) this record is part of the last burst
                       in a fill which contained at least
                       one reconstructed event
                       (iuDSTbad & 0x10000000)
6 - 0x00000100 - all other uDST bad bit cuts, i.e. this bit is set
                  if any of the following uDST bad bits are set:
                   0x00000001 = event and slow data out of sync
                                 at spinflip
                   0x00000008 = (VME2 clock==0)
                   0x00000010 = missing 1203 detected in slow data
                   0x00000020 = (a VME clock==0)
                   0x00000040 = event and slow data out of sync by
                                 1 usec at end of record
                   0x00000080 = event and slow data out of sync by
                                 1 usec at start of record
                   0x00000100 = burst number jump in the event data
                                 at the end of this record
                   0x00000200 = burst number jump in the event data
                                 at the start of this record
                   0x00000400 = burst number jump in the slow data
                                 at the end of this record
                   0x00000800 = burst number jump in the slow data
                                 at the start of this record
```

```
                    0x00080000 = this record has a table overflow
                    0x02000000 = the previous burst had an event
                                  backjump
                    0x04000000 = this burst had an event backjump
                    0x08000000 = next burst had an event backjump


  7 - 0x00000200 - the logbook data quality (as determined from the
                   logrun.new file maintained by the shifts)
                   indicates that the run is unanalyseable or, for
                   the bottom detector, the VC plate was in.

  8 - 0x00001000 - beampol data quality rejects this burst

  9 - 0x00020000 - the GMS indicates one or more dead blocks in the
                   TOP calorimeter or two or more dead blocks in
                   the bottom calorimeter
 10 - 0x00040000 - the GMS indicates one or more dead paddles in the
                   preshower (H2) or blocks in the lumi
 11 - 0x00080000 - the TRD group data quality rejects this record
 12 - 0x00100000 - the CAEN system detected a trip in the FCs or BCs
 13 - 0x02000000 - the Cerenkov group DQ rejects this record


3) HV-Trip cuts (created by Andreas Gute)

       If there is a trip in one of the following detectors,
       the burst is thrown away:

           FC, BC1/2, CE, BC3/4 ,TRD

4)   Short(Magnet-)Tracks :

        For analysis of  short tracks, a flag is set if:

         -there was a trip or a PCOS initialization (96c1)
         -there was a trip in the MCs
  (97b2, no PCOS info available in DSTs)
```

APPENDIX F

EXTRACTION FORMALISM

F.1 Extraction of Quark Spin Transfer Term

Two methods have been proposed to extract the quark spin transfer term, $\hat{Q}$, from the accumulated Λ events. One, based on count rates, cancels out the acceptance directly. Another method has been proposed by the HERMES St. Petersburg group and uses a helicity balanced run list to eliminate acceptance effects.

F.1.1 Helicity Balance

This method has been proposed by the St. Petersburg group. Starting with the following expression for the number of Λ's detected at a given time and with a given set of kinematic conditions

$$\frac{dN_\Lambda}{d\epsilon d\lambda d\Omega_p dt} = L(t)\frac{d\sigma(\epsilon,\lambda)}{d\epsilon d\lambda}\alpha(\epsilon,\lambda,\vec{k_p})\left(1 + P_B(t)\vec{S_\Lambda}\cdot\vec{k_p}\right) \tag{F.1}$$

where

$$\epsilon \;=\; \text{kinematic variables of the positron} \tag{F.2}$$

$$\lambda \;=\; \text{kinematic variables of the } \Lambda \tag{F.3}$$

$$\vec{k_p} = \text{proton momentum unit vector} \tag{F.4}$$

$$t = \text{time} \tag{F.5}$$

$$L(t) = \text{instantaneous luminosity} \tag{F.6}$$

$$\frac{d\sigma(\epsilon,\lambda)}{d\epsilon d\lambda} = \Lambda \text{ electroproduction cross section} \tag{F.7}$$

$$\alpha(\epsilon,\lambda,\vec{k_p}) = \text{detector acceptance} \tag{F.8}$$

$$P_B(t) = \text{positron beam polarization} \tag{F.9}$$

$$\vec{S_\Lambda} = \text{defined by } \beta\vec{P_\Lambda} = P_B\vec{S_\Lambda} \tag{F.10}$$

$$\beta = 0.642 \pm 0.013,\ \text{decay asymmetry in } \Lambda \text{ c.m. system} \tag{F.11}$$

the total number of detected Λ's can be written as the integral of the expression for the production rate:

$$\begin{aligned} N_\Lambda &= \int dN_\Lambda &\text{(F.12)}\\ &= \int L(t)\frac{d\sigma(\epsilon,\lambda)}{d\epsilon d\lambda}\alpha(\epsilon,\lambda,\vec{k_p})\left(1+P_B(t)\vec{S_\Lambda}\cdot\vec{k_p}\right)d\epsilon d\lambda d\Omega_p dt &\text{(F.13)}\\ &= N_\Lambda^0\left(1+||P_B||\left\langle\vec{S_\Lambda}\cdot\vec{k_p}\right\rangle\right) &\text{(F.14)}\end{aligned}$$

where

$$\begin{aligned} N_\Lambda^0 &= L\int\frac{d\sigma(\epsilon,\lambda)}{d\epsilon d\lambda}\alpha(\epsilon,\lambda,\vec{k_p})d\epsilon d\lambda d\Omega_p &\text{(F.15)}\\ L &= \int L(t)dt &\text{(F.16)}\\ ||P_B|| &= \frac{1}{L}\int L(t)P_B(t)dt &\text{(F.17)}\\ \left\langle\vec{S_\Lambda}\cdot\vec{k_p}\right\rangle &= \frac{L}{N_\Lambda^0}\int\frac{d\sigma(\epsilon,\lambda)}{d\epsilon d\lambda}\alpha(\epsilon,\lambda,\vec{k_p})\vec{S_\Lambda}\cdot\vec{k_p}d\epsilon d\lambda d\Omega_p &\text{(F.18)}\end{aligned}$$

The brackets "|| ||" define a luminosity–weighted average of any quantity that depends only on the time, while the brackets "⟨ ⟩" define an average over the production cross section and detector acceptance of any quantity that depends on the kinematics.

If one divides the expression for $\frac{dN_\Lambda}{d\epsilon d\lambda d\Omega_p dt}$ by N_Λ, one obtains a normalized probability function for detecting a Λ as a function of time:

$$\frac{dw(t)}{d\epsilon d\lambda d\Omega_p dt} = \frac{1}{N_\Lambda}\frac{dN_\Lambda}{d\epsilon d\lambda d\Omega_p dt} \tag{F.19}$$

$$= \frac{L(t)\frac{d\sigma(\epsilon,\lambda)}{d\epsilon d\lambda}\alpha(\epsilon,\lambda,k_p)\left(1+P_B(t)\vec{S_\Lambda}\cdot\vec{k_p}\right)}{N_\Lambda^0\left(1+||P_B||\left\langle\vec{S_\Lambda}\cdot\vec{k_p}\right\rangle\right)} \tag{F.20}$$

One can use $dw(t)$ to perform averages over the experimental data of any quantity, say X, which depends on the time and/or the kinematics. Such an average will be represented with the brackets "{ }", thus:

$$\left\{X(\epsilon,\lambda,\vec{k_p},t)\right\} = \int dw(t)X = \frac{1}{N_\Lambda}\sum_{i=1}^{N_\Lambda}X_i \tag{F.21}$$

where X_i is the value of X in the ith Λ event. An important special case occurs when $X(\epsilon,\lambda,\vec{k_p},t) = P_B^n(t)F(\epsilon,\lambda,\vec{k_p})$, where F is any quantity which only depends on the kinematics. Then

$$\{P_B^n F\} = \frac{||P_B^n||\langle F\rangle + ||P_B^{n+1}||\left\langle F\vec{S_\Lambda}\cdot\vec{k_p}\right\rangle}{1+||P_B||\left\langle\vec{S_\Lambda}\cdot\vec{k_p}\right\rangle} \tag{F.22}$$

From this equation comes the most significant result: If one picked a data set for which the luminosity–weighted average beam polarization is zero, that is

$||P_B|| = 0$, then one would get:

$$\{F\} = \langle F\rangle \tag{F.23}$$

$$\text{and} \tag{F.24}$$

$$\{P_B F\} = ||P_B^2|| \left\langle F\vec{S_\Lambda}\cdot\vec{k_p}\right\rangle \tag{F.25}$$

for any quantity F which only depends on the kinematics. Hence the name "helicity balance" for this method. This result allows one to proceed without knowing what the acceptance function is. However, one is forced to rely on the assumption that the acceptance function does not depend on the time.

Let F be $\cos\Theta_{p\Lambda}$, that is the cosine of the angle between the proton and Λ momenta, in the Λ c.m. frame, then

$$\begin{aligned}
\{P_B\cos\theta_p\} &= ||P_B^2|| \left\langle \cos\theta_p\vec{S_\Lambda}\cdot\vec{k_p}\right\rangle && \text{(F.26)}\\
&= ||P_B^2|| \left\{ \cos\theta_p\vec{S_\Lambda}\cdot\vec{k_p}\right\} && \text{(F.27)}\\
&= ||P_B^2|| \{\cos\theta_p S_\Lambda\cos\theta_p\} && \text{(F.28)}\\
&= ||P_B^2|| \left\{S_\Lambda\cos^2\theta_p\right\} && \text{(F.29)}
\end{aligned}$$

Since $S_\Lambda = \beta\hat{Q}D(y)$, and if one takes $\hat{Q}$ to be a slow function of the kinematic variables of the Λ, then

$$\begin{aligned}
\{P_B\cos\theta_p\} &= ||P_B^2|| \left\{\beta\hat{Q}D(y)\cos^2\theta_p\right\} && \text{(F.30)}\\
&= \beta\hat{Q}||P_B^2|| \left\{D(y)\cos^2\theta_p\right\} && \text{(F.31)}
\end{aligned}$$

or

$$\frac{1}{N_\Lambda}\sum_{i=1}^{N_\Lambda} P_{B,i}\cos\theta_{p,i} = \beta\hat{Q}||P_B^2||\frac{1}{N_\Lambda}\sum_{i=1}^{N_\Lambda} D(y_i)\cos^2\theta_{p,i} \tag{F.32}$$

and therefore

$$\hat{Q} = \frac{\left(\sum_{i=1}^{N_\Lambda} P_{B,i}\cos\theta_{p,i}\right)}{\left(\beta||P_B^2||\sum_{i=1}^{N_\Lambda} D(y_i)\cos^2\theta_{p,i}\right)} \tag{F.33}$$

if

$$||P_B|| = 0 \tag{F.34}$$

Note that this is a sum over events and does not involve any histograms. The uncertainty in $\hat{Q}$ can be computed by first getting the uncertainty on the numerator and denominator *via* a sum over the squares of the weights (recall the numerator and denominator are each an average of some quantity), and then calculating the uncertainty in the ratio in the usual way.

F.1.2 Direct Elimination of the Acceptance Function

Starting with the same description of the yield of Λ's as a function of time and kinematic conditions

$$\frac{dN_\Lambda}{d\epsilon d\lambda d\Omega_p dt} = L(t)\frac{d\sigma(\epsilon,\lambda)}{d\epsilon d\lambda}\alpha(\epsilon,\lambda,\vec{k_p})\left(1 + P_B(t)\vec{S_\Lambda}\cdot\vec{k_p}\right) \tag{F.35}$$

and integrating this with respect to ϵ, λ and time, one obtains:

$$\begin{aligned} \frac{dN_\Lambda}{d\Omega_p} &= L\sigma^0\alpha(\vec{k_p})\left(1 + ||P_B||\vec{S_\Lambda}\cdot\vec{k_p}\right) && \text{(F.36)} \\ &= L\sigma^0\alpha(\vec{k_p})\left(1 + ||P_B||S_\Lambda\cos\theta_p\right) && \text{(F.37)} \end{aligned}$$

where

$$\sigma^0\alpha(\vec{k_p}) = \int \frac{d\sigma(\epsilon,\lambda)}{d\epsilon d\lambda}\alpha(\epsilon,\lambda,\vec{k_p})d\epsilon d\lambda. \tag{F.38}$$

One then bins the yield of Λ's in $\cos\Theta_{p\Lambda}$. To simplify things a little, let $N(\cos\theta_p) = \frac{dN_\Lambda}{d\Omega_p}$ be the histogram for the yield of Λ's, already including subtraction of background. Then one can express that for each beam helicity state as

$$N^{\pm}(\cos\Theta_{p\Lambda}) = L^{\pm}\sigma_0\alpha(\cos\Theta_{p\Lambda})(1 \pm ||P_B^{\pm}||S_\Lambda\cos\Theta_{p\Lambda}) \tag{F.39}$$

or

$$N^{\pm}(x) = L^{\pm}\sigma_0\alpha(x)(1 \pm ||P_B^{\pm}||S_\Lambda x) \tag{F.40}$$

where $x = \cos\Theta_{p\Lambda}$, and the plus or minus sign refers to the sense of the beam helicity.

Assuming that the acceptance $\alpha(x)$ does not depend on the helicity, one can form the asymmetry

$$A(x) = \frac{\left(L^-||P_B^-||N^+ - L^+||P_B^+||N^-\right)}{\left(L^-||P_B^-||N^+ + L^+||P_B^+||N^-\right)} \tag{F.41}$$

$$= \frac{\left(||P_B^-|| - ||P_B^+|| + 2||P_B^+||||P_B^-||S_\Lambda x\right)}{\left(||P_B^-|| + ||P_B^+||\right)} \tag{F.42}$$

in which the acceptance function has canceled out.

Taking $S_\Lambda = \beta\hat{Q}D(y)$, then the quantity of interest, $\hat{Q}$, is extracted in one of two ways:

- By integrating the asymmetry $A(x)$ against xdx:

$$\hat{Q} = \frac{||P_B^-|| + ||P_B^+||}{2\beta D(y)||P_B^+||||P_B^-||}\left(\int_{-1}^{1} A(x)xdx\right)$$

  Note that this is exactly equivalent to fitting the asymmetry $A(x)$ to a straight line as a function of x.

- By integrating the "forward" and "backward" hemispheres of the asymmetry and subtracting them:

$$\hat{Q} = \frac{3(||P_B^-|| + ||P_B^+||)}{4\beta D(y)||P_B^+||||P_B^-||}\left(\int_{0}^{1} A(x)dx - \int_{-1}^{0} A(x)dx\right)$$

In both the Helicity Balance and Direct Elimination methods, the acceptance α does not affect the extracted value of $\hat{Q}$ to the extent that it does not change with the beam helicity change. Both methods have the characteristic that the quantity of interest, $\hat{Q}(z, Q^2)$, has been factored out of all integrals, so we really only measure an average value of $\hat{Q}$ over some range of z and Q^2. Dividing the events into a few bins in z and Q^2 can reveal the dependence of $\hat{Q}$ on these variables, however this kind of study is severely limited by statistics at present. In the Helicity Balance method, the exact value of the depolarization $D(y)$ is used for each event, while in the Direct Elimination method, one must use an event averaged value for $D(y)$ in the final step.

F.2 Background Subtraction

Though the background is relatively small one still has to take it into account. There are different methods of background subtraction available. A fast way (mainly used for cut studies) is to assume a linear background and simply subtract an equal number of mass bins next to the peak from the distributions under the peak. An example for the mass bins can be seen in fig. 4.3.

Another method is based on a dilution calculation. Here, one assumes that the background has a constant asymmetry (which does not have to be zero). One then can fit signal and background and calculate the corrected asymmetry.

$$N^{tot} A_{\Lambda}^{meas} = N^{\Lambda} A_{\Lambda} + N^{BG} A_{BG} \tag{F.43}$$

$$A_{\Lambda} = \frac{1}{N^{\Lambda}} (N^{tot} A_{\Lambda}^{meas} - N^{BG} * A_{BG}) \tag{F.44}$$

where

$$
\begin{aligned}
A_{\Lambda} &= \text{real } \Lambda \text{ asymmetry} \\
A_{\Lambda}^{meas} &= \text{measured } \Lambda \text{ asymmetry} \\
A_{BG} &= \text{Background asymmetry} \\
N^{tot} &= \text{total number of events under peak} \\
N^{\Lambda} &= \text{total number of } \Lambda\text{s under peak (fitted)} \\
N^{BG} &= \text{total number of BG events under peak (fitted)}
\end{aligned}
$$

.

Using the fact that

$$N^{tot} = N^{\Lambda} + N^{BG} \tag{F.45}$$

one obtains

$$A_{\Lambda} = A_{\Lambda}^{meas} + \frac{N^{BG}}{N^{\Lambda}}(A_{\Lambda}^{meas} - A_{BG}). \tag{F.46}$$

The statistical error is simply

$$\Delta A_{\Lambda} = \sqrt{(\frac{N^{tot}}{N^{\Lambda}}\Delta A_{\Lambda}^{meas})^2 + (\frac{N^{BG}}{N^{\Lambda}}\Delta A_{BG})^2} \tag{F.47}$$

To minimize the correction term one obviously has to minimize $\frac{N^{BG}}{N^{\Lambda}}$. For the error on the asymmetry one has to include errors from the fit as well as the errors on A_{Λ}^{meas} and A_{BG}. The advantage of this method compared to the simpler method involving only a simple subtraction of BG events is that statistical fluctuations in the BG are less important since one could, in principle, include all the background bins. The disadvantage is that one has to do more restrictive assumptions about the BG asymmetry (namely being constant over the considered mass range). Any derivation from this does not change the statistical uncertainty but increases the systematic uncertainty.

In the analysis presented in this thesis, this method of background subtraction is used.

APPENDIX G

THE PARITY-VIOLATING qZ^0-COUPLING

Quarks produced at the Z^0 pole are polarized due to the electro-weak coupling. In the standard model it can be written as (cf., [PDG]):

$$\bar{\Psi}_i \gamma^\mu (g_V^i - g_A^i \gamma^5) \Psi_i Z_\mu. \tag{G.1}$$

Ψ and Z denote the fermion fields and the neutral weak boson field, g_V^i and g_A^i are the axial and vector couplings and can be calculated from

$$g_V^i = t_i - 2q_i \sin^2 \Theta_W \tag{G.2}$$

$$g_A^i = t_i, \tag{G.3}$$

where t_i is the weak isospin of fermion i (1/2 for u-type quarks and -1/2 for d-type quarks), q_i are the fractional charges and Θ_W is the weak angle ($\sin^2 \Theta_W = 0.2319 \pm 0.0005$). The relative coupling strength to a right(left)-handed quark is

$$g_R^i = (g_V^i - g_A^i) \frac{1 + \gamma^5}{2} \tag{G.4}$$

$$g_L^i = (g_V^i + g_A^i) \frac{1 - \gamma^5}{2}, \tag{G.5}$$

yielding a relative probability to produce a right(left)-handed quark

$$(g_R^i)^2 = (g_V^i - g_A^i)^2 = (2q_i \sin^2\Theta_W)^2 \tag{G.6}$$

$$(g_L^i)^2 = (g_V^i + g_A^i)^2 = (2t_i - 2q_i \sin^2\Theta_W)^2. \tag{G.7}$$

From this one can easily calculate the polarization of a quark with flavor i and its relative contribution to the quark beam:

$$\Delta q_i \sim (g_R^i)^2 - (g_L^i)^2 \tag{G.8}$$

$$q_i \sim (g_R^i)^2 + (g_L^i)^2 \tag{G.9}$$

$$P_i \equiv \frac{\Delta q_i}{q_i} = \frac{(g_R^i)^2 - (g_L^i)^2}{(g_R^i)^2 + (g_L^i)^2} \tag{G.10}$$

The values for the different quark flavors are summarized in table G.1.

Table G.1: Relative production strengths and polarizations of the light quark flavors at the Z^0-pole

	Quark flavor		
Quantity	Up	Down	Strange
t_i	$\frac{1}{2}$	$-\frac{1}{2}$	$-\frac{1}{2}$
q_i	$\frac{2}{3}$	$-\frac{1}{3}$	$-\frac{1}{3}$
P_i	-66.4%	-93.5%	-93.5%
$N_i = \frac{q_i}{q_s}$	0.775	1.0	1.0

BIBLIOGRAPHY

[ADA] D. Adams et al., Phys. Lett. **B329**, 399 (1994).

[ADAMO] *ADAMO – Entity-Relationship Programming System, Version 3.3*, Programming Techniques Group, ECP Division, CERN Geneva (1994).

[AEL] M. Anselmino, A. Efremov, E. Leader, Phys. Rept. **261**, 1 (1995).

[ALEPH] D. Buskulic et al. [ALEPH Collaboration], Phys. Lett. **B374**, 319 (1996).

[AP] G. Altarelli, G. Parisi, Nucl. Phys. **B126**, 298 (1977).

[Assaf] F. Assaf, Master's Thesis, New Mexico State University (1999).

[Bai] D. Bailin, in "Weak Interactions," Sussex University Press (1982).

[Bass] S.D. Bass, hep-ph/9902280.

[Ben 92] C. Bennhold, B. K. Jennings, L. Tiator, and S. S. Kamalov, Nucl. Phys. **A540**, 621 (1992).

[Benisch] T. Benisch, Diploma Thesis, Univ. Erlangen-Nürnberg (1994).

[Bern] S. Bernreuther et al. Nucl. Instrum. Meth. **A416**, 45 (1998).

[BHHL] R. Brun, R. Hagelberg, M. Hansroul and J.C. Lassalle, "Geant: Simulation Program For Particle Physics Experiments. User Guide And Reference Manual," CERN-DD/78/2; R.Brun et al., "GEANT-*Detector Description and Simulation Tool*," CERN Application Software Group, Geneva (1993).

[BJ] M. Burkardt, R.L. Jaffe, Phys. Rev. Lett. **70**, 2537 (1993).

[Bjør] J. Bjørken, Phys. Rev. **D1**, 1376 (1970).

[BT] S. D. Bass, A. W. Thomas, Prog. Part. Nucl.Phys. **33**, 449-476 (1994).

[Che 96] H.-Y. Cheng, Int. J. Mod. Phys. **A11**, 5109 (1996).

[deFlo] D. de Florian, M. Stratmann and W. Vogelsang, Phys. Rev. **D57**, 5811 (1998).

[Dukes] E.C. Dukes, Ph.D. Dissertation, University of Michigan (1984).

[Düren] M Düren, *"The HERMES Experiment: From the design to the first results,"* DESY Int. Rep. HERMES-95-02(95/07) (1995).

[E142] P.L. Anthony et al. [E142 Collaboration] Phys. Rev. **D54**, 6620 (1996).

[E143] K.Abe et al. [E143 Collaboration] Phys. Rev. Lett. **76**, 587 (1996).

[E154] K.Abe et al. [E154 Collaboration] Phys. Lett. **B404**, 377 (1997).

[EJ] J. Ellis and R.L. Jaffe, Phys. Rev. **D9**, 1444 (1974); Phys. Rev. **D10**, 1669 (1974).

[EKK] J. Ellis, D. Kharzeev and A. Kotzinian, Z. Phys. **C69**, 467 (1996).

[EMC 88] J. Ashman et al. [EMC Collaboration] Phys. Lett. **B 206**, 364 (1988).

[Feyn] R.P. Feynman, Phys. Rev. Lett. **23**, 1415 (1969).

[FF] R.D. Field and R.P. Feynman, Nucl. Phys. **B136**, 1 (1978).

[Fla 82] D. Flamm, F. Schoeberl, in "Introduction to the QUARK MODEL OF ELEMENTARY PARTICLES," Gordon and Breach Science Publishers (1982).

[Georgi] H. Georgi, in "Weak interactions and modern particle theory," Benjamin/Cummings Publishing Company (1984).

[GH] G. Gustafson and J. Hakkinen, Phys. Lett. **B303**, 350 (1993).

[GKV] C. Gerthsen, H. O. Kneser, H. Vogel, in "Physik," Springer-Verlag (1989).

[GRV] M. Gluck, E. Reya and A. Vogt, Z. Phys. **C67**, 433 (1995).

[GWS] S. Weinberg, Phys. Rev. Lett. **19**, 1264 (1967); Phys. Rev. **D5**, 1412 (1972); A. Salam, in "Elementary Particle Theory: Relativistic Groups and Analyticity" Nobel Symposium No. 8, ed. N. Svartholm, Almqvist and Wiksell, Stockholm (1968); S. Glashow, Nucl. Phys. **22**, 579 (1961).

[GZ] M. Gell-Mann, Phys. Lett. **8**, 214 (1964), G. Zweig, *CERN* report **TH401**, **TH412** (1964).

[H1] T. Ahmed et al. [H1 Collaboration], Nucl. Phys. **B439**, 471 (1995).

[He3] D. DeSchepper et al. Nucl. Instrum. Meth. **A419**, 16 (1998).

[Heller] K. Heller, in "SPIN 96 – Proceedings," World Scientific (1997).

[HER 97] K. Ackerstaff et al. [HERMES Collaboration] Phys. Lett. **B404**, 383 (1997).

[HER 98a] A. Airapetian et al. [HERMES Collaboration], Phys. Lett. **B442**, 484 (1998).

[HER 98b] K. Ackerstaff et al. [HERMES Collaboration] Phys. Rev. Lett. **82**, 1164 (1999).

[HERMES] K. Ackerstaff et al. [HERMES Collaboration], Nucl. Instrum. Meth. **A417**, 230 (1998).

[HERWIG] B.R. Webber et al., Comp. Phys. Comm. **67**, 465 (1992).

[Hew] J.L. Hewett, SLAC-PUB-7930 (1997).

[IMR] D. Indumathi, H.S. Mani and A. Rastogi, Phys. Rev. **D58**, 094014 (1998).

[Jaffe] R.L. Jaffe, Phys. Rev. **D54**, 6581 (1996).

[Kaiser] R.B. Kaiser, PhD thesis, Simon Fraser University (1997).

[KBH] A. Kotzinian, A. Bravar and D. von Harrach, Eur. Phys. J. **C2**, 329 (1997).

[LUND] B. Anderson, G. Gustafson, et.al., Z. Phys. **C9**, 233 (1981).

[MCG] G. Ingelman, A. Edin and J. Rathsman, Comput. Phys. Commun. **101**, 108 (1997); B. Andersson, G. Gustafson, G. Ingelman and T. Sjostrand, Phys. Rept. **97**, 31 (1983).

[MRST] A.D. Martin, R.G. Roberts, W.J. Stirling, R.S. Thorne Eur. Phys. J. **C4** 463-496 (1998).

[MT] P.J. Mulders and R.D. Tangerman, Nucl. Phys. **B461**, 197 (1996).

[OPAL] K. Ackerstaff et al. [OPAL Collaboration], Eur. Phys. J. **C2**, 49 (1997).

[PDG] C. Caso et al. [Particle Data Group], in "Review of particle physics," Eur. Phys. J. **C3**, 1 (1998).

[Rob] R. G. Roberts, in "The Structure of the Proton," Cambridge University Press (1990).

[Ruth] E. Rutherford, Phil. Mag. **21**, 669 (1911).

[SMC] B. Adeva et al. [SMC Collaboration] Phys. Lett. **B302**, 533 (1993).

[ST] A.A. Sokolov and I.M. Ternov, Sov. Phys. Doklady **8**, 1203 (1964).

[WA2] WA2 Group, Z. Phys. **C21**, 27 (1983).

[Wander] W. Wander, Doktorarbeit, Univ. Erlangen-Nürnberg (1995).